EUROPEAN ORGANIZATION FOR NUCLEAR RESEARCH

CERN/LHC/98-02 (EET)

A HIGH RESOLUTION SPALLATION DRIVEN FACILITY AT THE CERN-PS TO MEASURE NEUTRON CROSS SECTIONS IN THE INTERVAL FROM 1 eV TO 250 MeV.

C. Rubbia, S. Andriamonje[1], D. Bouvet-Bensimon[1], S. Buono[2], R. Cappi, P. Cennini, C. Gelès, I. Goulas, Y. Kadi, P. Pavlopoulos[3], J.P. Revol, A. Tzima[4], V. Vlachoudis[4]

Abstract

The design of innovative Accelerator-Driven Systems (ADS) for incineration of nuclear waste, energy production and radio-isotope activation for medical applications as well as many other subjects in Nuclear Physics, requires a knowledge as complete and as precise as possible of cross sections for neutron induced processes.

The spallation mechanism is a remarkably powerful source of neutrons: in a Lead spallation target, one 24 GeV proton may produce as many as 760 neutrons. The CERN PS accelerator is capable of accelerating $2 \div 3 \times 10^{13}$ ppp, resulting in as many as 2×10^{16} neutrons at each pulse. This extraordinarily prolific source can be concentrated in short time pulses which are typically of the order of $\pm$ 10 ns, offering the added feature of a tremendous potential accuracy in the time of flight (TOF) determination of the neutron energy.

To the very small time uncertainty of the source one has to add the fluctuations in the moderating time needed to produce a wide initial neutron spectrum capable of covering the full extent of the energy domain in which cross sections need to be measured. It is a fortunate circumstance that the moderation in a high A material (the spallation target) occurs in a large number of steps in which the energy loss is small ($\leq 1\%$). Hence the time fluctuations in the slowing-down process are also small, since the moderation time is strongly correlated with the energy of the outgoing neutron.

These features, already exploited in the TARC experiment, permit a very accurate TOF measurement of the incoming neutron energy. The rich initial source offers, at a measuring station located at the distance L, a flux of $2.8 \times 10^5/L^2$(km) n/cm^2/pulse.

The facility allows to study systematically and with excellent resolution neutron cross sections of almost any element using targets of very modest mass (even few milligrams), as needed for unstable or otherwise expensive materials, like for instance transuranics, in the interval from 1 eV to 250 MeV.

Geneva, May 30, 1998

[1]On leave from CEN-Bordeaux
[2]CRS4 Cagliari
[3]University of Basel
[4]University of Thessaloniki

TABLE OF CONTENTS

1.— GENERAL CONSIDERATIONS.

1.1. - Need for new data on Cross Sections. The experimental determination of neutron cross sections, elastic and inelastic across the whole Mendeleiev Table has always been of primary importance in Nuclear Physics. Many of the salient features of nuclear levels can be determined from the resonant structure of such cross sections and of their decay schemes. These cross sections have many different channels and exhibit a complex phenomenology with very many resonances over a very wide energy spectrum, extending from a fraction of eV to many MeV of neutron kinetic energy.

In addition to such a primary interest, recent developments at CERN and elsewhere have raised the practical need for better known cross sections aimed specifically at the design and understanding of the behaviour of Accelerator Driven Systems (ADS). In such devices, a charged particle beam is used to produce intense neutron fluxes which, in turn, can be used for incineration of nuclear waste [1], energy production (EA) [2] and radio-isotopes activation [3] for medical and other applications. A new, promising method of nuclear propulsion for deep space travel has also been considered [4].

These practical studies make massive use of Montecarlo techniques in order to predict ADS behaviour in a variety of possible configurations and running conditions. In contrast with the conventional multi-group methods used in Reactor studies, the sub critical nature of the device, in which all fundamental modes are excited following a high energy cascade, can be best studied primarily with a Montecarlo simulation of the complex nuclear phenomena. The relatively high energies involved require that not only neutron capture and fission, but also a larger variety of channels, like for instance (n,2n), (n,3n), (n,np), etc. should be taken into consideration. The presence of a high energy cascade implies extending the exploration to higher energies ($\approx$ 250 MeV for our programme).

A fundamental pre-requisite of any computing method is the availability of reliable cross section data for many channels and at the appropriate energies. Unfortunately, the available Compilation Databases [5] — in general based on a mix of experimental measurements and of theoretical

prejudices — present many "holes" and substantial differences amongst them, most likely due to the different fitting procedures used and the reliance on different theoretical models. They cannot be considered today as a totally reliable basis for planning in detail for instance the Energy Amplifier (EA) [6] prototype unit and simulating with the required accuracy the behaviour of the machine with a variety of different fuels, as required for instance when planning the incineration of radioactive waste from LWR's. Indeed, while the Thorium and Uranium related cross sections are relatively well known, there are sometimes gigantic differences between Databases [5] when it comes to Americium and Curium, or more generally to higher Actinides (see also Appendix I).

The comprehensive elimination of LWR Waste implies consideration for the transmutation of several long-lived Fission Fragments into stable species as well. For such elements, the information is even more lacunary and in many important cases, like for instance ^{90}Sr, there are orders of magnitude discrepancies in the experimental data [7], mostly confined to the region of thermal or epi-thermal neutrons. Instead, the most promising transmutation method, the TARC [8] requires precise information on the resonances and specifically their widths.

1.2.- Neutrons from spallation. Existing data are coming from compilations of many different experiments, often not in perfect agreement and generally each dedicated to specific energy domains and elements. They are currently mostly performed in association with a time of flight measurement of the incoming neutron (TOF). This technique has been generally limited by the strength of the primary neutron source used which conditions the length of the flight-path and therefore the energy resolution vs. counting rate.

Powerful spallation sources are being considered for a variety of applications, from slow neutron sources (as alternative to Reactors) to the EA. These sources make use of the specifically high flux of neutrons attainable using the spallation process in the many GeV range for the incoming proton. The preferred target is Lead which has a large neutron yield ($\approx$ 30 n/proton at 1 GeV and linearly growing for higher energies) and a high transparency for neutrons of energy $\leq$ 1 MeV.

Spallation as a powerful neutron producer can be coupled with the remarkable longitudinal beam density which can be produced by large, modern Proton-Synchrotrons like for instance the CERN-PS, which can generate high intensities (peak current of several hundred mA) of 24 GeV (kinetic energy) protons — high enough to produce a vast number of neutrons by spallation — in the form of short (≤ 20 ns) pulses which can eventually be a train of bunches separately extracted during the flat top at a few milliseconds distance. The total proton intensity is thus of the order of $2 \div 3 \times 10^{13}$ ppp (protons per pulse) for instance in the form of four separate intense bunches of 10 ns r.m.s duration with a repetition rate of a few seconds, depending on the sharing between users. In the future, the CERN-PS will be mostly used as injector for the SPS and therefore spare time is generally available for additional physics at 24 GeV. The development of the antiproton source[5] has further improved over the years the longitudinal phase space of the extracted beam and the four bunch operation.

Let us consider for instance the CERN-PS operated like for antiproton production with an intensity of 2.5×10^{13} ppp and an energy of 24 GeV on a Lead spallation target. We will produce $24 \times 30 \times 2.5 \times 10^{13} = 1.8\ 10^{16}$ neutrons/pulse. Assuming they become isotropic[6] within the spallation volume, we have a source strength of 1.43×10^{15} n/ster/pulse. If we wish to have at the end of the flight-path a flux of 10^5 n/cm^2/pulse, acceptable for most cross section measurements, the flight path is :

$$\sqrt{1.43 \times 10^{15} / 10^{5}} = 1.19 \times 10^{5}\ \ cm = 1.19\ \ km\ \ !!$$

With such a flight-path L, the TOF energy resolution ΔE for a neutron of kinetic energy E due to a beam time uncertainty Δt is given by

$$\left.\frac{\Delta E}{E}\right|_{BEAM} = 2\frac{\Delta t}{t} \approx \frac{2c}{L}\frac{\sqrt{2(E/m_n)}}{1+(E/m_n)}\Delta t$$

where c is the light speed and m_n = 939.56 MeV is the neutron mass. For Δt = 10^{-8} s, E = 100 keV and L = 1 km the expected resolution is given in Figure 1. The energy resolution is, as expected, quite good over the whole energy interval. It should be however remarked that this is only the contribution due to the beam time uncertainty. Additional contributions have to be added due

---

[5]Such a tremendous time density of particles is required in order to produce the necessary number of antiprotons (> 10^{11}/day) which are injected in one turn in the AA-ACOL complex.

[6]A more precise angular distribution will be computed later on with the help of a detailed Montecarlo calculation.

to (1) the thermalisation process and (2) the detector resolution, which are discussed next.

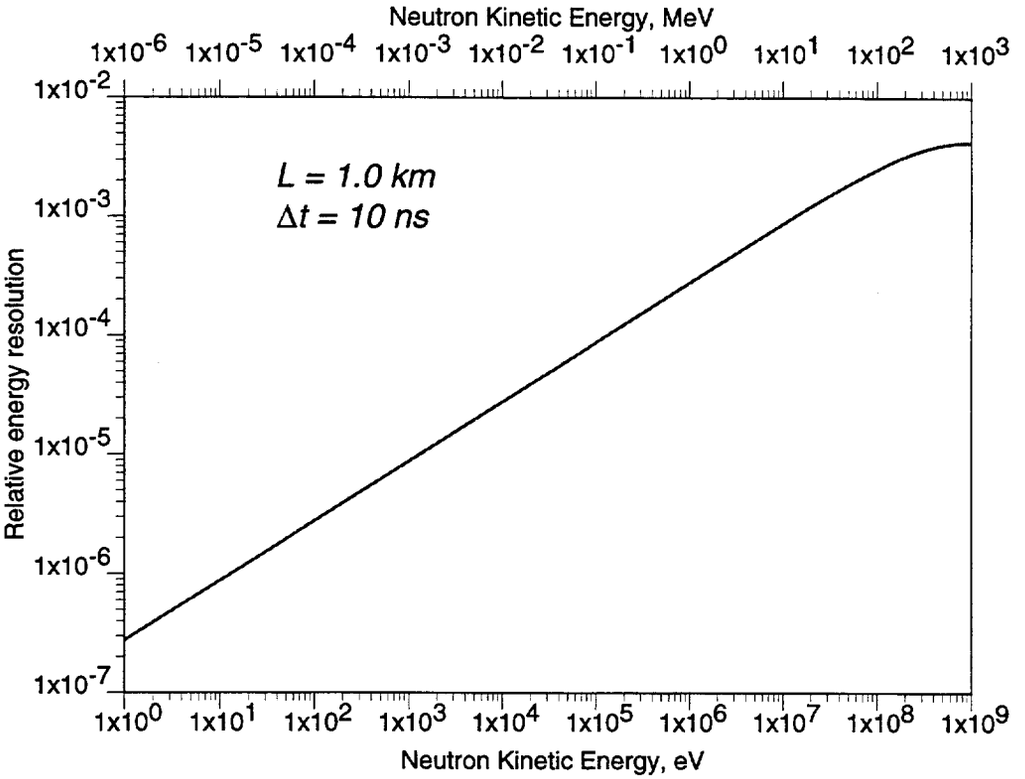

Figure 1. *Neutron energy relative uncertainty after 1 km of flight path due to 10 ns beam time spread.*

1.3.- Neutron moderation with a small time spread. A time of flight selection of the neutron energy requires the shortest initial neutron pulse, in principle of duration of the order of the precision timing of the detectors used to observe the reactions, which is currently of several nanoseconds. As we have already pointed out, the accelerator is generating a sharp initial pulse, for which however one has to add the moderation time in the absorber. The spallation source of a large A material has the remarkable property, already exploited in the TARC [8] experiment of sharply correlating the slowing down time and energy of the resulting neutrons. This property, already noticed in 1944 by E.L. Feinberg [9] is due to the averaging effect of the very large number of elastic collisions, with a tiny energy loss at each step because of the high A and therefore the smallness of the recoil energy at each step.

It is a fortunate circumstance that, for high A, moderation introduces a relatively small time spread, once the energy of the outgoing neutron is defined. This has been explored in great detail by the TARC experiment [8], where it has been shown that a sharp correlation exists between the time of

moderation t and the kinetic energy E of the neutron. This correlation is valid only in the energy region in which elastic scattering dominates. As we shall see later on this is the case for $E \leq 10^4$ eV.

More precisely, for a large block of Lead, energy E and moderation time t are directly correlated [10], with a simple empirical law of the form:

$$E(eV) = \frac{1.72\ 10^5}{[t(\mu s) + 0.4]^2} \qquad [1]$$

Neglecting the generally small 0.4 μs term, one can interpret this formula by saying that it is as if the neutron path inside the moderator, evaluated at the energy of observation[7], had been λ = 5.74 m. The energy spread ΔE for a given time of moderation has been calculated [11]. The distribution around the mean speed v for a fixed moderation time is in a very good approximation a gaussian, with a r.m.s. spread Δv, essentially energy independent and given by

$$\frac{\Delta v}{v} = \sqrt{\frac{\xi}{3} + \frac{kT}{4E}}$$

where T is the temperature of the moderator, k the Boltzmann constant and ξ the average, logarithmic energy decrement (lethargy) given by

$$\xi = 1 - \frac{(A-1)^2}{2A} \ln\left(\frac{A+1}{A-1}\right)$$

The logarithmic energy decrement for Lead is $\xi = 9.54 \times 10^{-3}$. In this case, the r.m.s. energy spread is

$$\frac{2\Delta v}{v} = \frac{\Delta E}{E} \approx 0.114\left[1 + \frac{2}{E(eV)}\right]^{1/2}$$

Such time spread has been currently measured in the TARC experiment [8] and found to be essentially energy independent and in excellent agreement with the above formula. Such a time spread induces an apparent source length $\Delta\lambda$ in the direction of the flight-path which is also energy independent for E >> 2 eV and t >> 0.4 μs. As already pointed out, the average delay for moderation is known and can be corrected for instance with formula [1] given above. The value of $\Delta\lambda$ is

$$\Delta\lambda = \Delta v\, t = 0.057 v\, t =$$

$$= 0.057\sqrt{\frac{2Ec^2}{(Mc^2)}}\sqrt{\frac{1.72\ 10^{-7}(eV)}{E}} = 0.057\sqrt{\frac{2 \times 1.72\ 10^{-7} c^2}{939.56 \times 10^6}} = 0.327\ m \qquad [2]$$

---

[7] Of course, in reality the diffusive path is much longer because of the higher energies. An analytic calculation would give $\lambda = A\,\delta$, where A is relating to the moderating nuclei and δ = 2.8 cm is the average mean free path of diffusion for the neutron.

which is a very small number. This feature is specifically due to the properties of the high A moderator.

To conclude, in the region in which the elastic scattering dominates — as confirmed by a more detailed Montecarlo calculation described later on — the slowing-down process accounts for an artificial lengthening of the path length of about 5.7 metres, corresponding to an extra time evaluated at the speed of the outgoing neutron. But, because of the strong energy-time correlation, the corresponding gaussian spread is reflected in a (energy independent) longitudinal uncertainty of the flight path of a mere ≈ 33 cm r.m.s. Above this region the spread in $\Delta\lambda$ grows significantly, to narrow again for energies above a few MeV (Figure 2) around the prompt time $\lambda = 0$. We notice that narrowly spaced resonances are not expected at such energies.

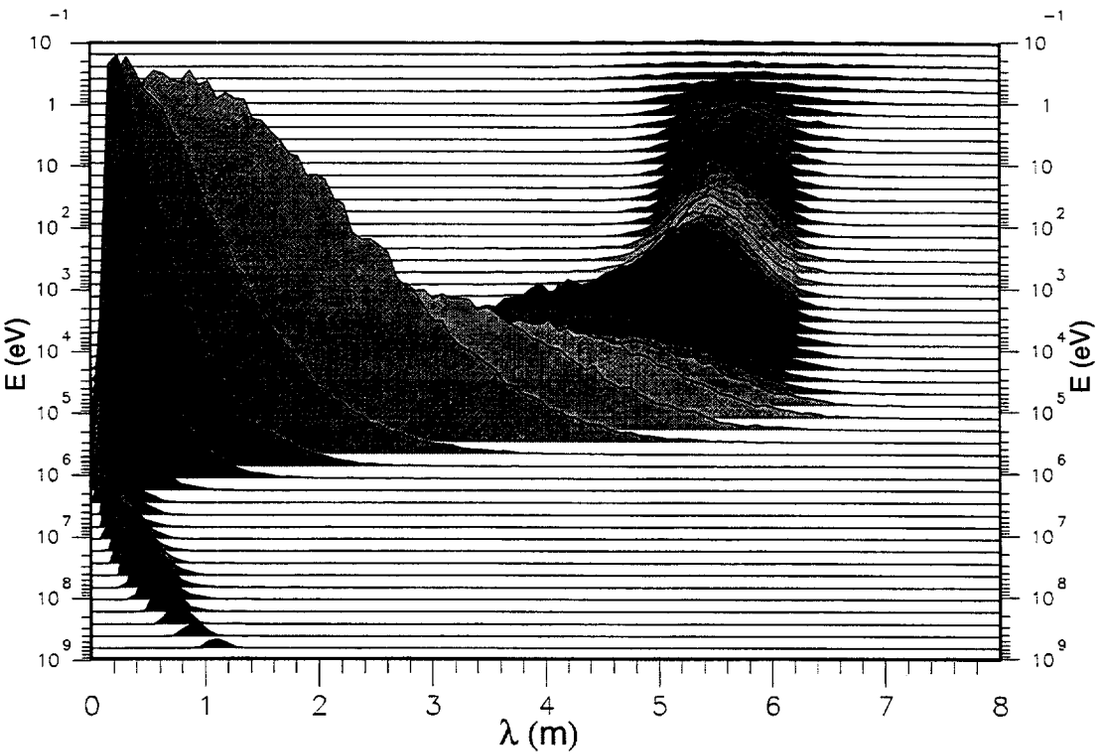

Figure 2. *Montecarlo distribution of the equivalent neutron path inside the moderator, evaluated at the energy of observation. The narrow clustering for energies ≤ 10^4 eV is evident. For higher energy the iso-lethargic model breaks down due to emergence of inelastic channels and the distribution broadens up. At high energies it narrows again.*

The energy uncertainty due to the thermalisation process can be easily evaluated with the help of λ and of its variance $\Delta\lambda$, for instance extracted from Figure 2. The thermalisation time is replaced by a displacement of a "virtual" neutron source which emits the neutron already at the final energy.

The source is located on a plane parallel to the outer face of the spallation target (normal to the TOF direction) at a distance λ and with an uncertainty $\Delta\lambda$ from it:

$$\left.\frac{\Delta E}{E}\right|_{TOF} = 2\frac{\Delta t}{t} = 2\frac{\Delta\lambda}{\lambda + L}$$

Setting for instance L = 1 km, λ = 5.7 m, $\Delta\lambda$ = 0.33 m valid for E < 10^4 eV we find $\Delta E/E|_{TOF} = 6.56 \times 10^{-4}$, energy independent.

1.4.- General outline of the facility. The existing CERN-PS beam dump could be modified in order to become the spallation target for the facility. At the present location it is possible to realise an unobstructed time of flight of about 230 m, making use of existing tunnels in the direction of the ISR. While the position at such distance is a good compromise between rates and resolution, it would seem reasonable to foresee a second station at about 1 km, for which a "sewer pipe" tube is required. The existing tunnel sets to about 10 degrees the direction of the neutron beam, referred to the incoming proton beam direction.

The geometry of the Lead spallation target has been optimised in order to get a neutron spectrum which provides an appropriate "illumination" of the whole energy spectrum from 1 eV to about 250 MeV (Figure 3). Taking into account the fact that cross sections are generally decreasing with energy and aiming at roughly comparable statistics over the full spectrum, the neutron spectrum should not be iso-lethargic but with a peak in the region around about 0.3 MeV. This implies a target thickness of about 60 cm in the direction of the beam.

The time of flight (230 m) as a function of the energy is shown in Figure 4 for the close position. It appears that an acquisition time of the order of a few milliseconds is sufficient to accumulate most of the data. Slower neutrons will of course continue to accumulate at longer times. An appropriate filter may be required in order to eliminate these events if several bunches are recorded in close succession. The bunch separation in this case could be typically of the order of 30 ÷ 50 ms. The very slow neutrons (thermal neutrons) which travel with the speed of some 2200 m/s will actually resent of the gravitational fall. Taking an extreme case, over the 1.0 km of the longest path, their time of flight is as large as 1.0/2.2 ≈ 0.45 sec! Over this time

the free fall path is $dz = 1/2\,gt^2 \approx 1.0$ m and they will be probably spontaneously cleared by the geometry of the pipe.

The amount of beam energy to be dissipated in the target is (2.5×10^{13})$\times$ 24 10^9 $\times$ 1.6 10^{-19} = 96 kJoule/pulse. Even at the rate of a pulse every 6 sec, this represents an average power of 16 kWatt, which is relatively modest. However, the peak power is astronomical. Fortunately the cascade is spread out over a large volume. The initial beam can be suitably defocused in order to avoid a pin-hole effect in correspondence to the entry point of the target.

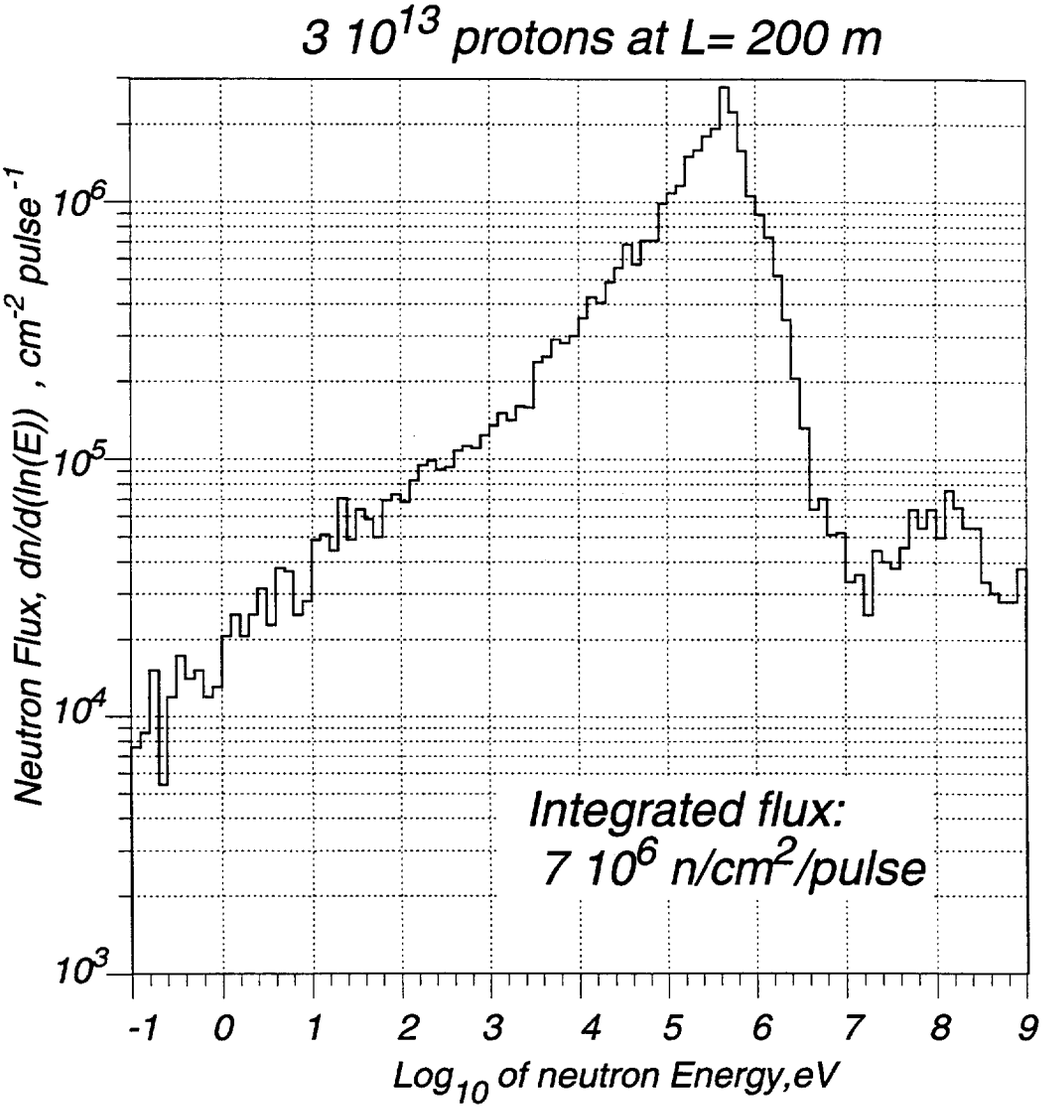

Figure 3. *Typical neutron spectrum at 200 m distance from target for a single proton pulse. The integrated neutron flux is 7 $\times$ 10^6 n/cm^2. The spectrum is deviating from iso-lethargic in order to compensate for the general drop of cross sections with increasing energy.*

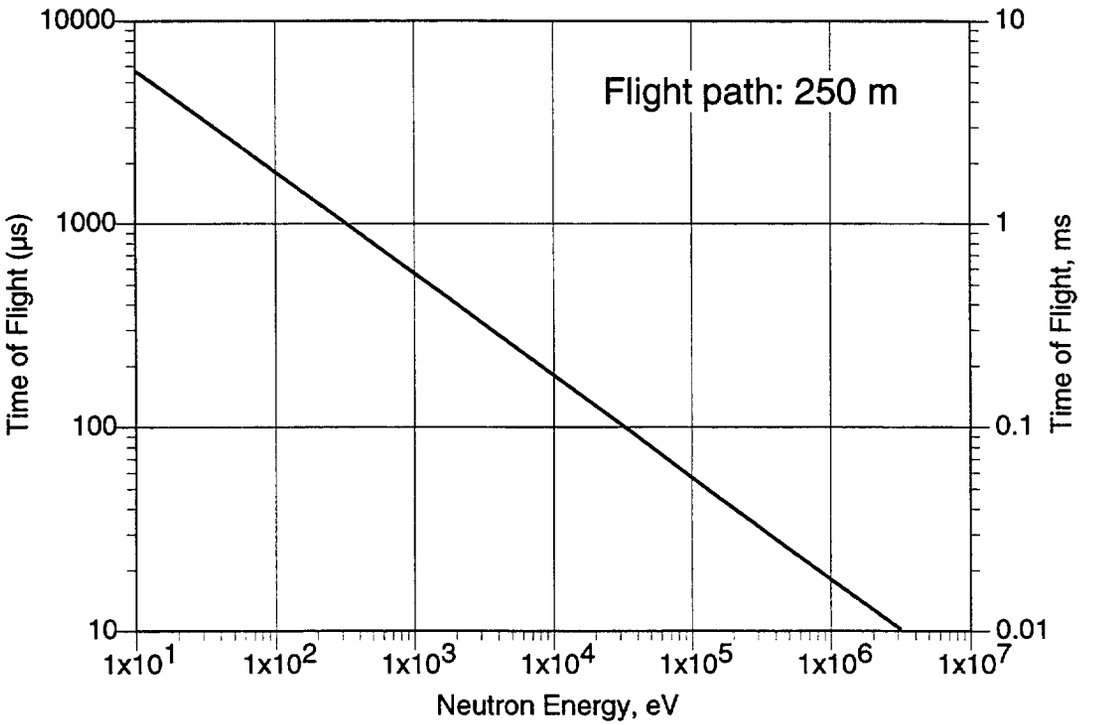

Figure 4. *Time of Flight as a function of the neutron kinetic energy for a flight-path of 0.250 km.*

Therefore there will be no vaporisation of Lead, for which the requirement is of 177.8 kJ/mole, but some partial melting could occur after many pulses in the central part in view of the low melting point of Lead (327 C°) and of the small specific heat 0.13 kJ/kg/K and conductivity, 35 W/m/K. However, since the block is of considerable size ($2\times2\times1.6$ m^3) there will be no consecutive loss of liquid or other inconveniences. The total power of 16 kWatt, incidentally not different from the case of all thick targets used at CERN-PS, for instance for neutrino or antiproton operation, can be dissipated with conventional methods already in use at CERN. The activation of the target is presumably comparable to (if not less than) the one used for neutrino beams and in a beam dump.

The target is followed by a long drift length over which the time of flight is measured by the time of occurrence of the event. As pointed out a sweeping magnet could be of advantage in order to remove charged particle contamination. The pipe must be obviously evacuated. There is substantial experience in this field at CERN, since a similar arrangement, though of much larger diameter is used as neutrino beam decay path.

Other neutral particles (a clearing magnet might be of help to eliminate the protons and the other charged particles) are γ's[8], K^o's, etc. and they are prompt. The anti-neutron contamination is very small at these energies and strongly absorbed by the Lead.

The detection set-up is also conventional. We assume that targets are prefabricated in the form of thin deposits on a plastic backing, like it is customary for β-spectrometry. They can be relatively large in size and therefore very thin, since the beam diameter can be substantial, as determined by collimators. Thin targets are needed since the fission products as well as low energy γ's must be generally detected. The detectors must be of such a kind as to provide a good timing measurement ($\approx$ 10 ns), in order to match the time spread of the initial neutron pulse. Since a large number of events will be collected at each pulse, it is necessary that they are finely segmented in order to minimise counting losses and pile-ups. The data acquisition must be capable of recording both the event characteristics and the time of occurrence, related to the sharp prompt timing of relativistic particles.

It should be possible to run the detector as a highly standardised facility, in which different targets and different detectors are used in a variety of configurations according to the requirements of each, specific measurement. The beam flux can be monitored with He^3 counters.

In general the measuring station is introducing a modest beam loss: therefore several targets could be cascaded at appropriate distances in order to make the best use of the beam time.

1.5.- Resonance spacing and widths. The energy resolution of the detection device must be somehow matched to the expected resonance spacing, since the energy resolution must be sufficient to resolve them. There is a vast literature on level density in nuclei, and it is beyond the scope of this paper to discuss them. In order to have some qualitative indication on the performance of the detector, we have therefore simply considered the list of resolved resonances given in Ref. [5] which are generally relative to an energy domain $E \leq 10^4$ eV, where the resolution of the spectrometer is roughly constant and dominated by $\Delta E/E|_{TOF} \approx 6.56 \times 10^{-4}$ at L = 1 km and about five

[8] The gamma flux is expected to be modest, since the Lead constitutes a strong shield. Eventually a local Lead filter could be added, not to affect the TOF measurement.

times larger at L = 230 m, $\Delta E/E|_{TOF} \approx 2.8 \times 10^{-3}$. Since substantial differences are known to exist between the databases [5] an experimental verification of such data is certainly one of the primary tasks of the experiment. In Figures 5a and 5b we display the relative resonance distances $\Delta E/E|_{nearest}$ (e.g. for each resonance the difference of energy to the nearest resonance) against the natural resonance width, $\Gamma/E|_{nat}$. It should be pointed out that for the narrowest $\Gamma/E|_{nat}$ the actual experimental width will be determined by the Doppler broadening due to thermal motion.

The first, essential requirement of the experimental resolution is the one of separating resonance states, and hence that $\Delta E/E|_{nearest} \leq \Delta E/E|_{TOF}$. We see that this is generally the case for medium A nuclei, at least for those resonances which are the basis of the present information [5]. The level spacing is however much narrower for instance in the case of the Actinides, which fully justifies the extension of the flight path to 1 km and eventually beyond.

The true resonance widths $\Gamma/E|_{nat}$ are generally much smaller than the experimental resolution, though the actual width may be affected by the Doppler broadening, especially at low energies. An infinitely narrow resonance of a nucleus of atomic number A >>1 at the temperature T acquires a relative width

$$\left.\frac{\Delta E}{E}\right|_{TH} = 2.27 \times 10^{-2} \sqrt{\frac{T(^\circ K)}{A\ E(eV)}}$$

For instance for E = 10^3 eV, A = 238 and T = 300°K, we find $\Delta E/E|_{TH} = 8.07 \times 10^{-4}$, which is about our TOF energy resolution for L = 1 km. We remark that $\Delta E/E|_{TH} \approx E^{-1/2}$ and that in practice for most of the resonances in Figure 5 the actual width is masked by the thermal motion of the target.

An experimental determination of the resonance width can also be performed by observing the self-absorption for instance as a function of the target thickness. Such a parameter can be easily varied for instance by changing the inclination of the target foil with respect to the beam. Though the separation of the resonance levels and the experimental determination of the width is of capital importance for Nuclear Physics related studies, it should also be remarked that the utilisation of the measured cross section for instance as an input to the Montecarlo simulation may not require resolving single resonances, since an "effective" cross section can be directly derived from the experimental data, including the relevant "screening" factor.

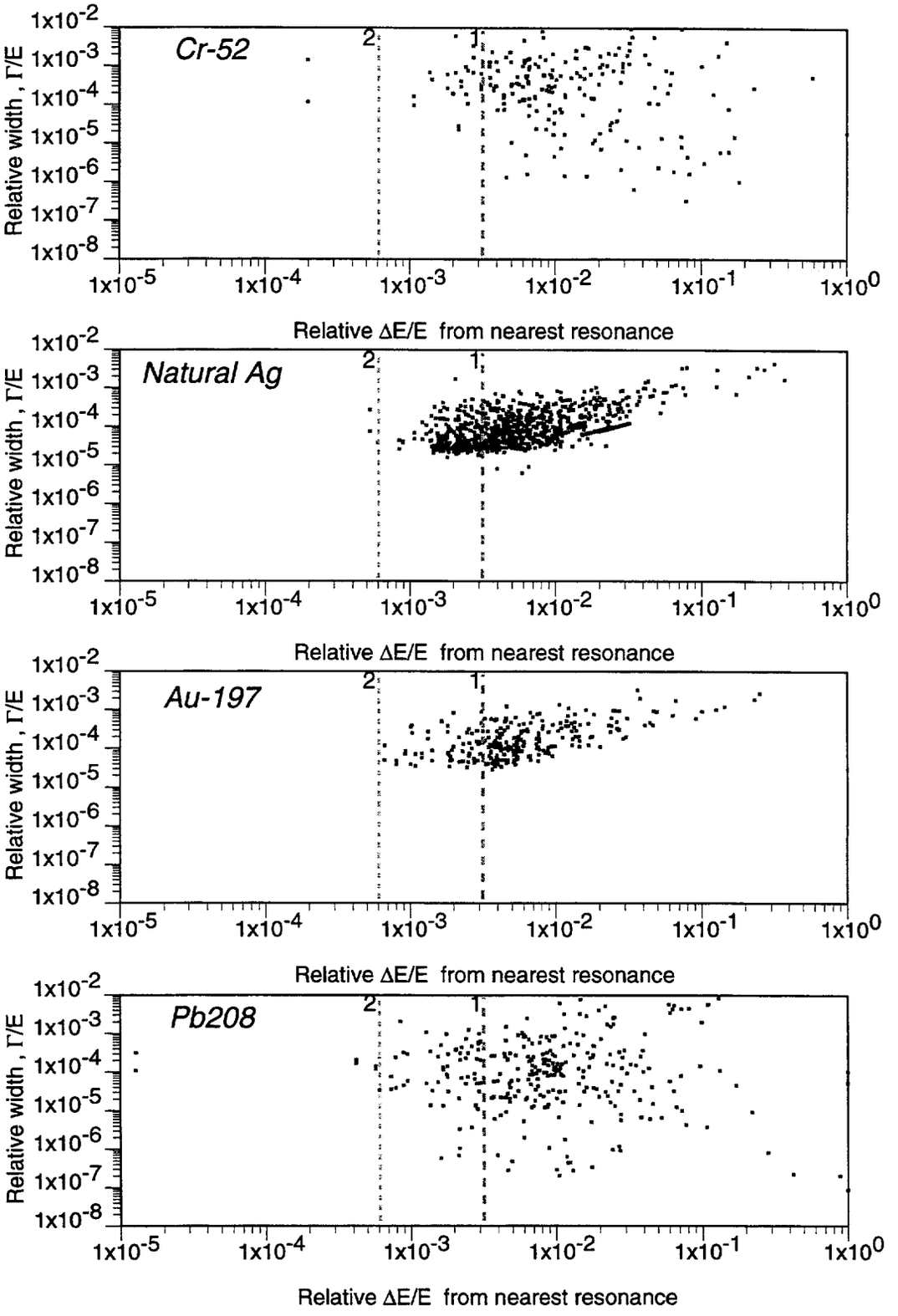

Figure 5a. *Nuclear level density and theoretical natural width for resolved levels according to Ref. [5] for typical medium and high A nuclei. The lines 1 and 2 represent the expected resolution of the 200 m and 1 km TOF configurations.*

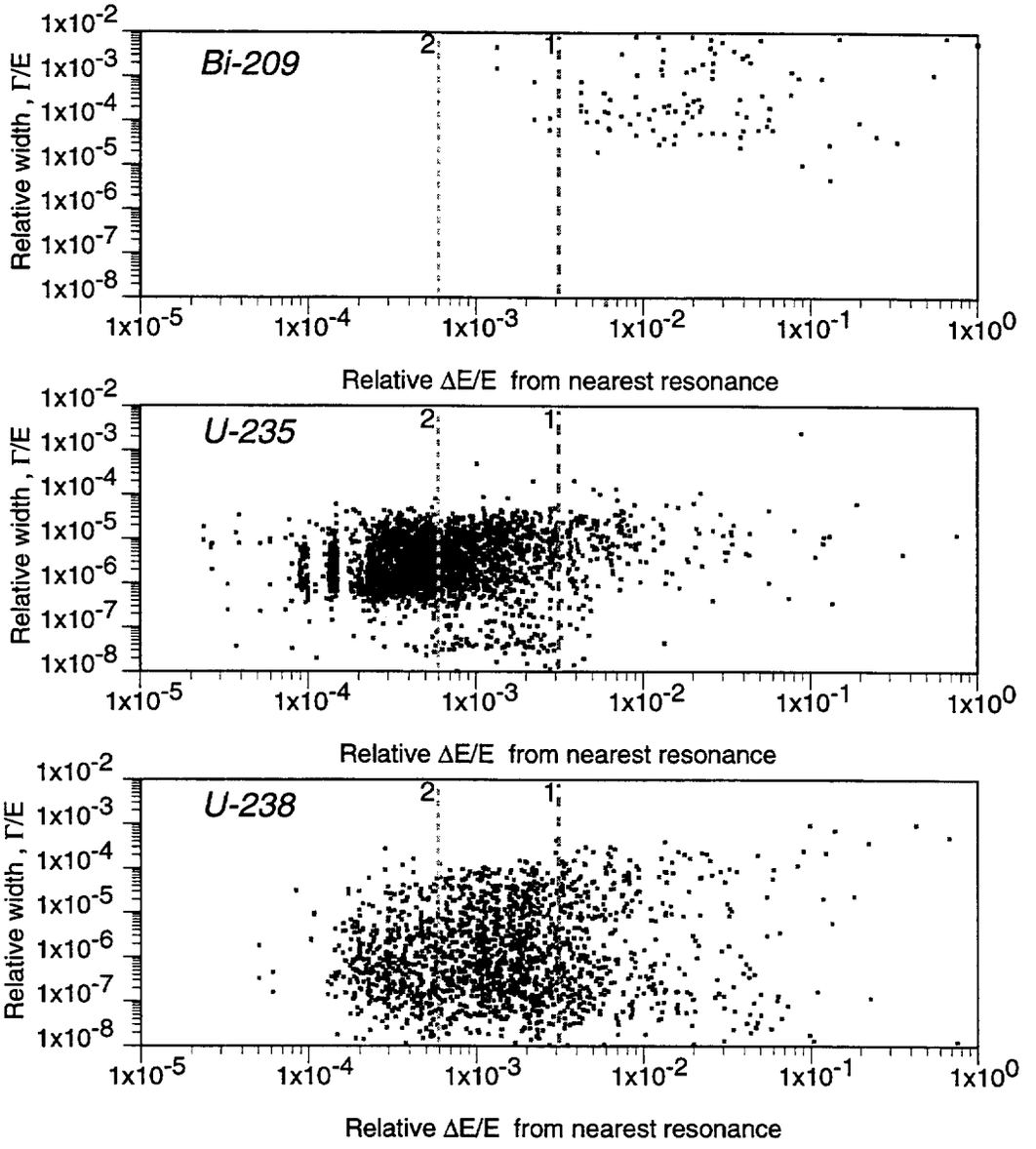

Figure 5b. *Nuclear level density and theoretical natural width for resolved levels according to Ref. [5] for high A nuclei and two well measured Actinides. The lines 1 and 2 represent the expected resolution of the 200 m and 1 km TOF configurations.*

1.6.- A facility with the CERN-SPS ?. A potential request for even higher energy resolution would imply longer TOF distances, which require higher neutron fluxes in order to preserve the attractive feature of using thin targets. It is generally known that the neutron yield grows linearly with the proton energy. We have therefore briefly speculated on the possibility of a major increase of the energy of the proton beam, using, instead of the PS, the 450 GeV/c proton beam from the CERN SPS.

An efficient neutron production from a spallation source suggests a lead block of a size commensurate with the extent of spallation cascade. Fortunately, the dimensions of the spallation cascade grows only logarithmically with higher proton energies. In turn, a larger distance between the beam interaction point and the exit surface of the block implies a reduction of the outgoing neutron flux density due to the smaller solid angle. Therefore the effective neutron flux for high proton energies is determined from the interplay between parameters implying a new optimisation procedure.

In order to get a first estimate of the effects, we have simulated the neutron flux and energy spectrum induced from 450 GeV/c protons on a lead block of rectangular shape (2 x 2 x 1.8 m^3) by means of the FLUKA [12] and TARC Montecarlo [13] programs. The maximum neutron flux coming out of the lead block corresponds to 80 cm distance between the beam interaction point and the exit surface of the lead block and shows an increase by a factor of 10 as compared to the flux obtained from 24 GeV protons, although the neutron production at 450 GeV/c is ~ 19 times higher than at 24 GeV/c. The resulting neutron energy spectrum and energy resolution at 450 GeV/c proton energy have a very similar shape to those at 24 GeV (Figure 2 and Figure 3). Therefore the basic features of the method, though not yet optimised, are generally preserved.

Since the flux decreases quadratically and the resolution improves linearly with the TOF length, the SPS proton beam would allow for instance a TOF length of 3-6 times, improving the neutron energy resolution by a corresponding factor as compared to the 1 km. The general layout of such a long flight path needs further studies. For the moment we would simply remark that such a possibility for a second generation experiment looks promising in a distant future.

2. — THE EXPERIMENTAL LAYOUT.

2.1.- Opportunities offered by the CERN site. The CERN strategy of an accelerator complex evolution where each new accelerator uses the previous machines as injectors, has the advantage of offering many potential options which can be exploited in the most cost effective way. Our project requires a high intensity, high energy, fast extracted proton beam which can be directed onto a neutron producing target. In addition, a long flight-path tunnel pointing to the target at a convenient angle, away from the proton beam direction is required in order to collect and direct neutrons towards the detectors. This tunnel must be absolutely straight, capable of housing the evacuated beam pipe without interfering with other CERN activities and must be essentially free from radiation. It is fortunate that such a configuration already exists, though limited to 230 metres flight-path, as the TT2A beam line from the CERN PS used to inject protons into the West Hall. The tunnel has ample size as to permit the installation of the measuring station and it is well shielded, since it was used to transfer the primary proton beam. It also allows to use the present main PS beam dump as a target station. If one takes into account the vast experience developed by the CERN staff, this makes this choice of location the most obvious one, for both technical and economical reasons.

We propose to make use of the extracted proton beam line from the PS, TT2 (Figure 6) which has several functions: (1) it is used to inject protons into the SPS through the TT10 line. (2) It serves for the production of antiprotons and (3) it is used to send the protons to the beam dump situated immediately after the bifurcation with TT10. By simply replacing the concrete block, at present used as beam dump, with the Lead Target we can achieve a high intensity neutron source, *still maintaining the full functionality of fundamental beam dump facility*. This is possible, since the Target Station requires no access and no specific instrumentation. All magnets and all beam optics elements are already operational in situ, as well as the shielding necessary for the radio protection safety. The tunnel TT2A line connects in a straight line the beam dump area with the experimental area of the former ISR (Intersecting Storage Rings). The length of the TT2A tunnel is ~230 m, adequate for the first phase of the project. The TT2A tunnel construction is sufficient for the radio-protection shielding from the neutron flux.

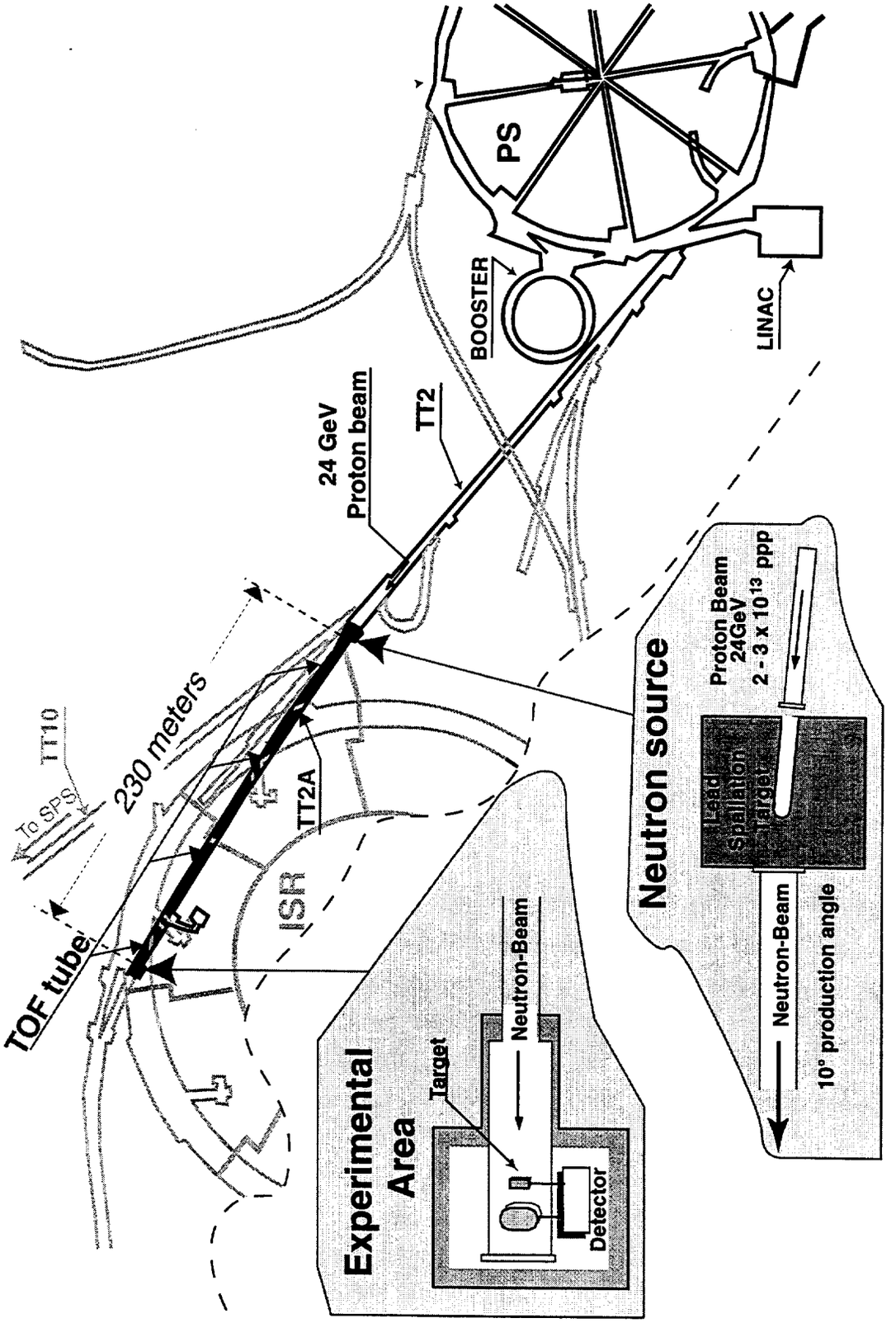

Figure 6. *General layout of the experiment. The proton beam is extracted through TT2 and hits the modified beam dump (Neutron source). After the TOF tunnel (TT2A) neutrons are detected in the Experimental Area at about 230 m from the primary target.*

On the other hand, the large surface area in the ISR ring at the end of the TT2A tunnel provides all necessary infrastructure and services required in the running of various experiments.

The 1000 metre TOF Tunnel must be constructed ex-novo, pointing directly to the same beam dump. The detailed layout of this facility is under study. At this moment we can only say that we see sufficient space within the CERN site to extend the TOF well beyond 1 km.

2.2.- *The proton beam.* The LINAC and PS Booster system supply up to 3×10^{13} ppp at 1 GeV every 1.2 s. The PS machine accelerates these beams up to 26 GeV/c and tailors their longitudinal characteristics to the specific needs of the programme. Bunch lengths and number of bunches may be modified with standard debunching/rebunching techniques, using the wide frequency range of the RF systems and the flexibility of their controls. Ultimately, a large variety of proton beams is routinely available at CERN. We plan to use the same PS fast extracted beam presently used to produce antiprotons on the AAC conversion target, replacing the beam dump for this line with our own Lead target.

This proton beam is generated in the form of several short ($\sigma \approx 10$ ns) pulses, few tens (50) milliseconds apart, repeated several times during the flat top, providing a total of $2 \div 3 \times 10^{13}$ protons per PS super cycle. A "super-cycle" made of various magnetic cycles is constructed out of several cycles during normal operation. Under these assumptions, a minimum of 6000 pulses can be collected on our target per day, with a 14.4 s super-cycle and without significant interferences with the remainder of the CERN experimental programmes.

2.3.- *Optimisation of the neutron source.* We consider the CERN-PS proton beam with an intensity of 3×10^{13} ppp and a kinetic energy of 24 GeV incident on a large Lead spallation target of rectangular shape (Figure 7). The generally preferred spallation material is Lead, which has a large neutron yield (30 n/proton at 1 GeV) linearly growing for higher energies and a high transparency for neutrons of energy < 1 MeV. Let us consider for instance the lateral (x-y plane) and upstream size of the target as infinite and the proton beam penetrating the Lead block through a pipe with an inclination of 10° with respect to the z-axis, as determined by the existing tunnel geometry. The

proton beam interacts with the Lead at a distance d from the downstream "exit" surface of the block. The outer face of the block is perpendicular to the direction of the TOF tunnel, in order to minimise the time spread of exiting neutrons.

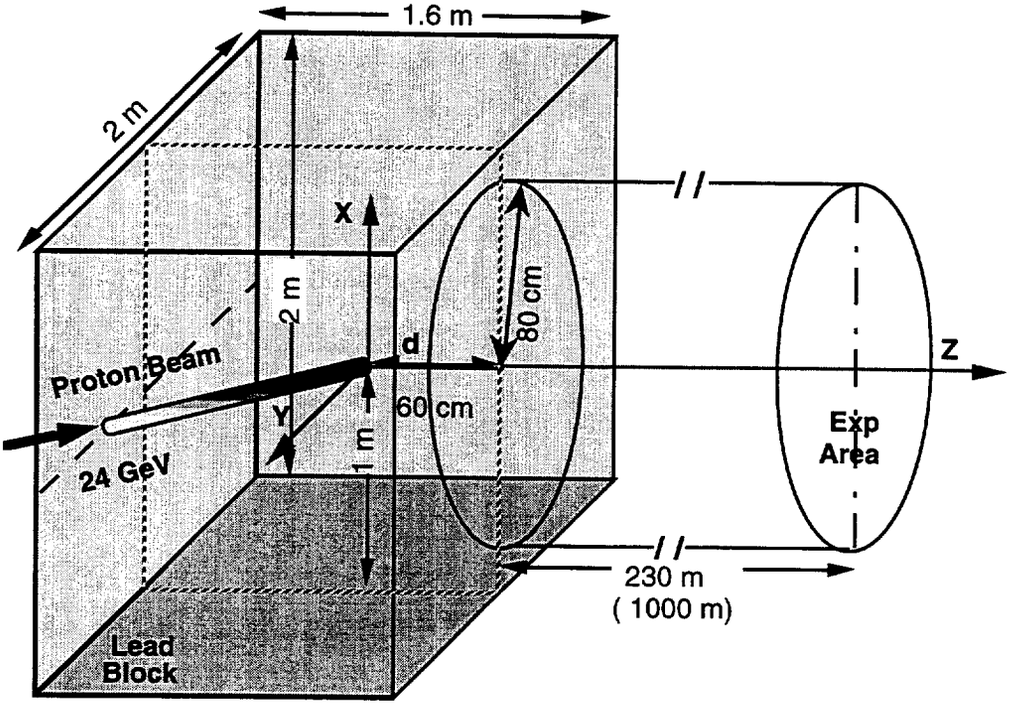

Figure 7. A schematic view of the neutron source.

Neutrons are generated mainly by high energy interactions described by the FLUKA programme [12], which we used to simulate the interaction of the proton beam with the Lead, following the neutrons down to a threshold energy of 20 MeV. Then all physical processes through the Lead block are simulated with the TARC Montecarlo programme [13], where the cross sections for energies below 20 MeV are obtained from a selection of the four known Nuclear Databases [5].

The spallation cascade is directed forward and spreads out over a large volume. Spallation neutrons emanating from the cascade volume with large angles become isotropic through iso-lethargic moderation naturally achieved within the infinite lateral and backward lead volume. The spallation neutrons in the forward direction can either exit directly the target or undergo also iso-lethargic moderation, depending on the amount of Lead between the production point and the exit face of the lead block. Therefore the distance d between the neutron production point and the exit face of the lead block determines the "hardness" of the neutron spectrum.

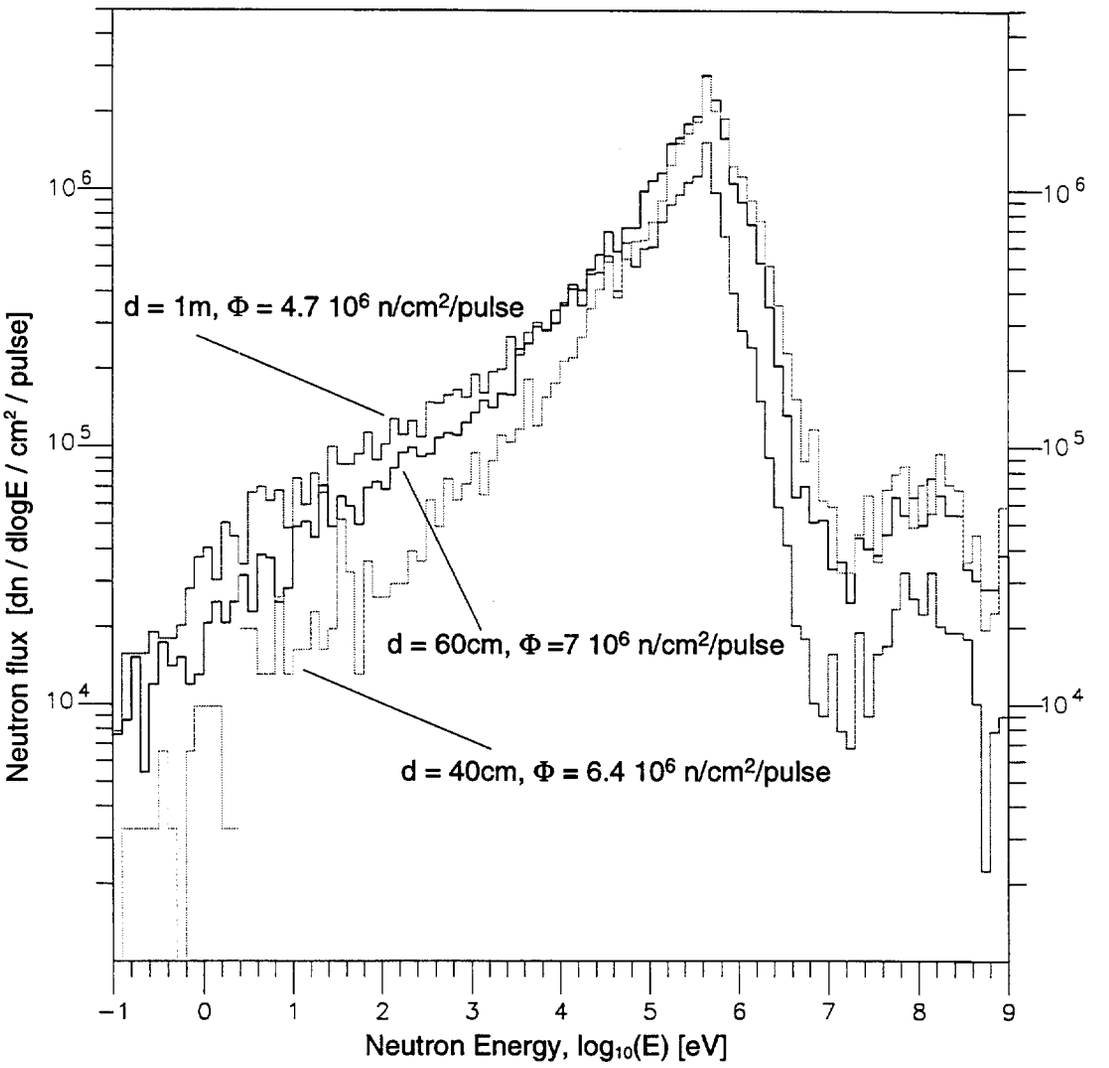

Figure 8. *Neutron energy spectra for different distances d.*

The neutron spectrum has to be optimised such as to be as close as possible to the neutron energy spectrum of the EA and to provide uniform illumination of the energy interval of interest for potential measurements. By means of the FLUKA and the TARC Montecarlo programs, we simulated all physics processes as a function of the distance d for the case of an infinitely large Lead block and we studied the neutron energy spectrum at the exit surface. Figure 8 shows the spectrum of the neutrons emanating from the downstream surface of the target for different distances d. This neutron spectrum becomes harder as the distance d decreases. The corresponding variation of the integral of the neutron flux as function of distance d is shown in Figure 9. For a maximal flux and taking into account the general trend of neutron cross-sections decreasing with energy, we opted for the optimal distance $d \approx 60$ cm.

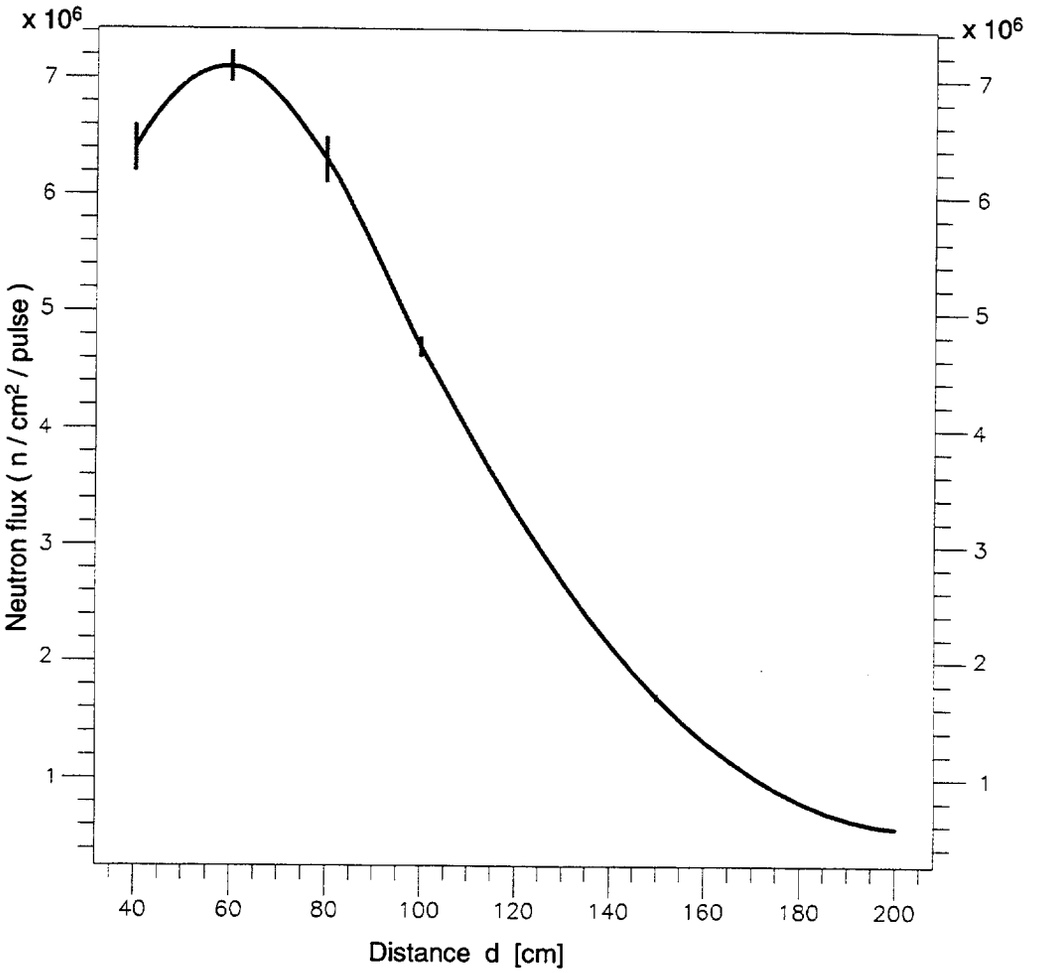

Figure 9. *The integral of the neutron flux as function of distance d.*

Having determined the optimum position of the beam interaction point, we have studied the effect of the lateral and backward dimensions of the Lead block on the neutron energy spectrum and the flux. Both the flux and the energy spectrum of neutrons coming out of the downstream surface of the Lead target are practically unaltered down to a block size of 2 m.

The neutron flux at the downstream exit surface of the target has a radial dependence forward peaked at small radii. The neutron transport through the TOF tunnel collects neutrons enclosed in a radius of 80 cm, representing a fraction of more than 80% of the total number of neutrons reaching the downstream surface of the target, in turn 40% of the produced neutrons. These neutrons projected to a distance of 200 m (1000 m) represent a homogeneous flux of 7×10^6 (2.8×10^5) $n/cm^2/pulse$[9]. Their energy spectrum is shown in Figure 10.

[9]The value L = 200 m is taken as a reference value. For different lengths of the TOF, fluxes and consequently rates must be scaled as the inverse of the square of the distance.

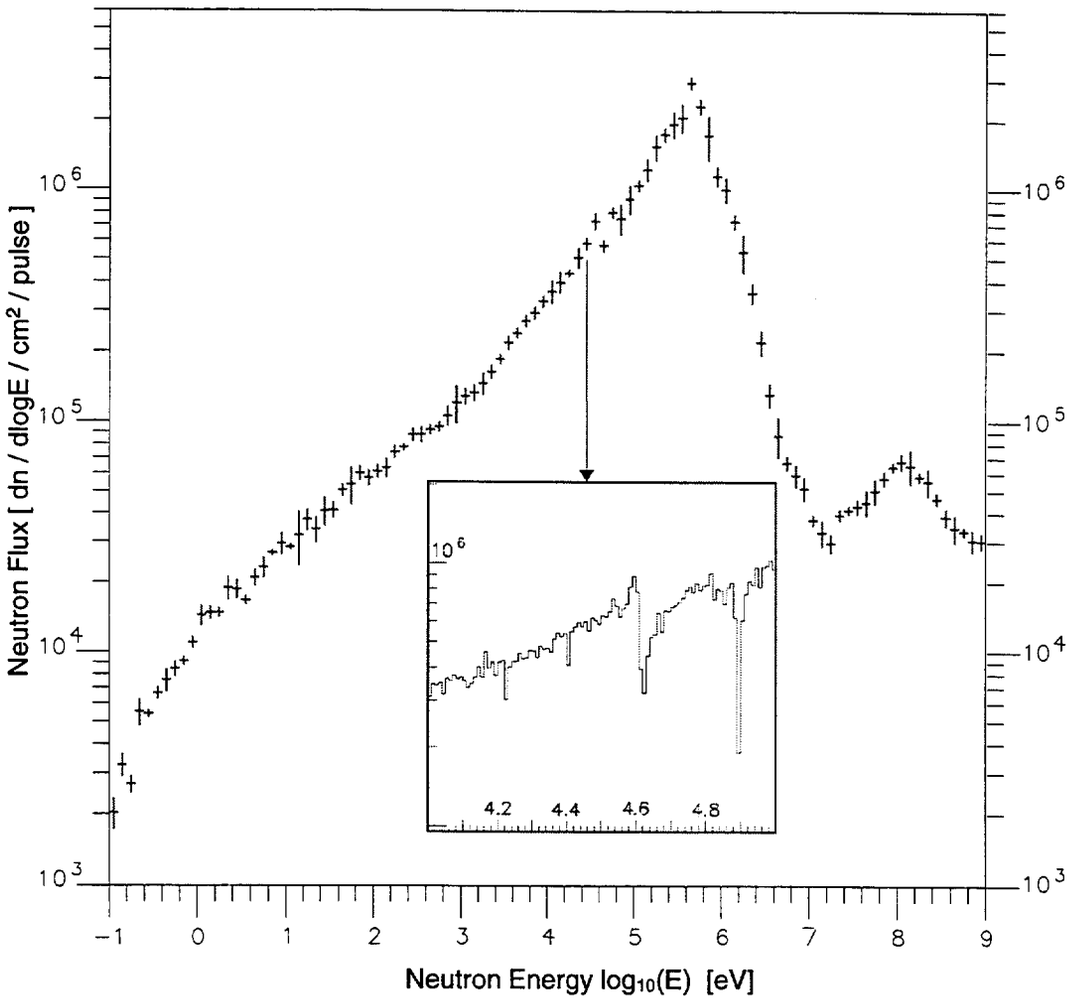

Figure 10. *The energy dependence of the neutron flux at the reference distance of 200 m (for different lengths, fluxes must be scaled as the inverse of the square of the distance). The insert shows the details of the region between 10 keV and 100 keV.*

The neutron spectrum has some dispersive "glitches" at 17.4 keV, 42.6 keV and 77.6 keV, in correspondence to the strong capture resonances of the Lead moderator, having the natural isotopic composition. In order to remove this fine structure from the source, a "scrambler" layer can be added at the surface of the target. The lethargy of this material must be preferably very close to the Lead lethargy, in order not to degrade the time to energy correlation. The best candidate material is ^{208}Pb, which is an element with practically no resonances in the energy range of the "glitches". We could envisage to replace the natural Lead in the last ~15 cm layer of the Lead block with Lead isotopically enriched with ^{208}Pb. In this way, the additional scattering in the ^{208}Pb "scrambler" would erase the "memory" of these resonance structures.

The TARC experiment [8] has shown, that the energy of the neutrons and their moderation time t are directly correlated with the simple empirical law of Equation [1]. This property is due to the averaging effect of the very large number of elastic collisions, with a tiny energy loss at each step. Using the TARC Montecarlo simulation, we have calculated the neutron path, $\lambda = vt$ inside the moderator, evaluated from the time t elapsed since its creation and from its velocity v, *when exiting the Lead surface* (Figure 2). In Figure 11a, showing the mean path λ as a function of the neutron energy, three regions can be recognised, corresponding to three different physical processes.

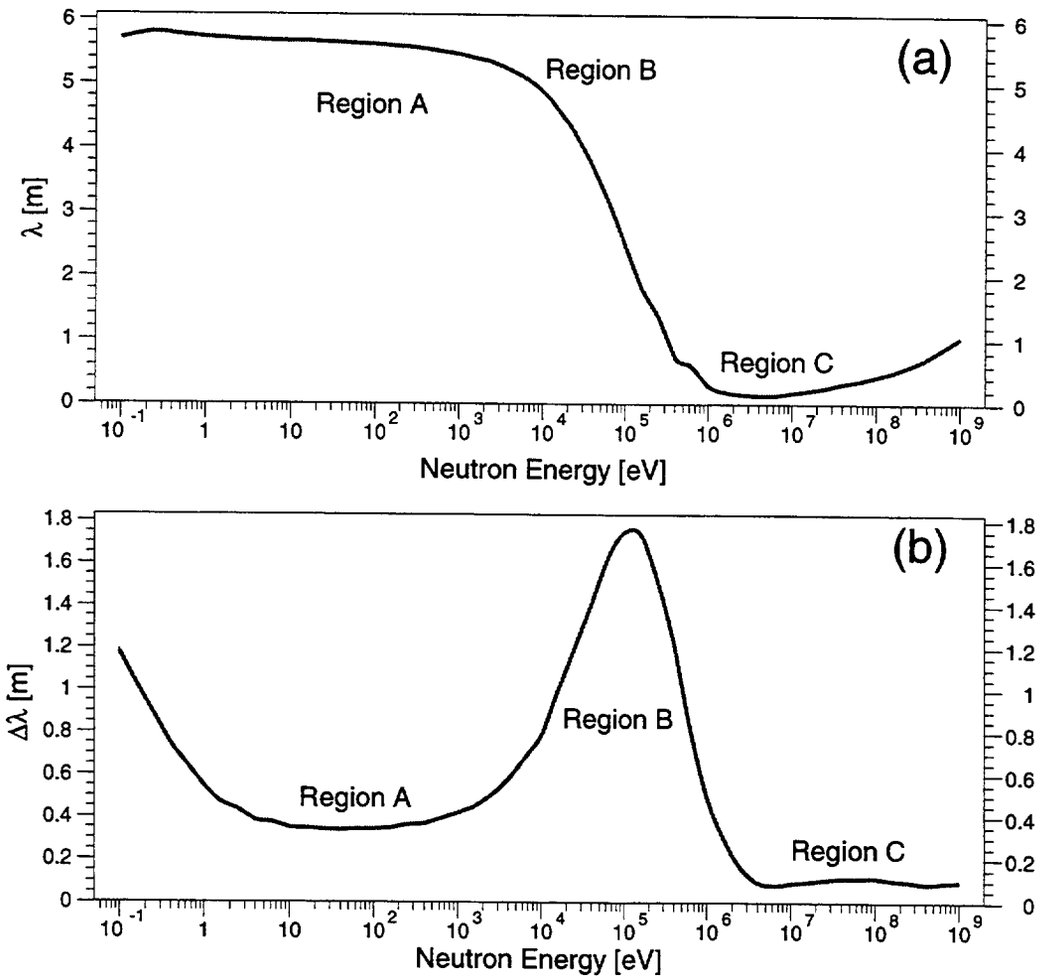

Figure 11. *Montecarlo results at the downstream surface of the Lead target as a function of neutron energy for a) The mean path λ and b) The uncertainty in the path λ as a function of neutron energies .*

The region A extending up to few times 10^4 eV, corresponds to the fully iso-lethargic moderation and the path λ is independent of the neutron energy. Equation [1] can then be interpreted by saying that it is as if the neutron path inside the target, evaluated at the energy of observation, had

been λ = 5.7 m , independently from the energy of the neutron. In the region B, neutrons originate mainly from non-elastic reactions of the spallation neutrons and in region C we find the fast unmoderated neutrons themselves, which obviously travel much smaller paths.

Due to the averaging effect of the very large number of elastic collisions, the moderation process introduces a time uncertainty translated into an uncertainty in the neutron's path inside the target. The accelerator is generating sharp pulses ($\sigma \approx 10$ ns), for which however one has to add this moderation time uncertainty.

Using the TARC Montecarlo simulation program, we have calculated the slowing down time spread, which reflects into an energy independent uncertainty in the neutron's path inside the target of $\Delta\lambda = \pm 33$ cm, in full agreement with Equation [2]. Figure 11b shows the uncertainty in the path $\Delta\lambda$ as a function of the neutron energy, where the three above regions, corresponding to the three different physical processes, can be again recognised. The increase of $\Delta\lambda$ in the thermal energy region (Figure 11b) originates from the thermal motion of the Lead nuclei, which is described by the term proportional to the temperature of the Lead. Indicatevely after 1000 m flight path the resolution in the determination of the neutron energy is as precise as 6.6×10^{-4} in the region A and is always better than 2×10^{-3} up to 20 keV. In regions B and C it never exceeds the value of 3.6×10^{-3}, although we notice that in region B and C narrowly spaced resonances are not expected.

2.4.- Thermal effects of the proton beam. The CERN PS accelerator is accelerating typically up to 3×10^{13} protons per pulse, with a cycle of 14.4 seconds, which correspond to a current of 0.33 μA at 24 GeV.

The heat deposition of such a proton beam in the Lead target has been accurately calculated using FLUKA [12]. The beam size has been taken as a circular spot of 1 cm diameter distributed as a parabola. A contour map of the power deposited in $W/cm^3/\mu A$ is given in Figure 12. The total heat released in the target is 14.7 kW/μA, of which only about 7 W/μA are released in the window. Window cooling does not therefore represent a problem in this application.

In order to study the thermal effects of the heat released in the target we have used the finite volumes numerical code StarCD [14] which allows to

cope with the complexity of the heat distribution and the dependence of the Lead physical properties on the temperature.

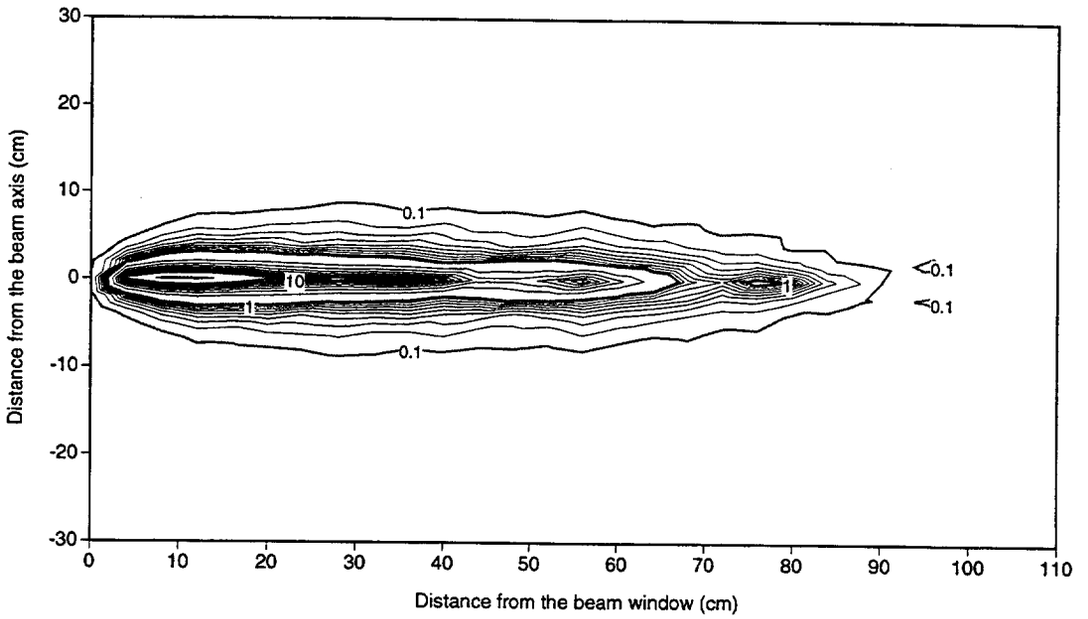

Figure 12. Power generated by a 24 GeV proton beam in a thick Lead target. Units are W/cm^3/μA.

Given the asymmetry of the target set-up, a full 3D model was developed, composed of more than 110,000 cells and 4000 boundaries. A temperature of 20 °C on the external surface of the lead was taken as a boundary condition. Calculations were made by considering average values of the heat release and not the real thermal cycle, which is highly peaked in very short pulses.

The temperature map of the Lead target under proton irradiation in steady state conditions is shown in Figure 13. The maximum temperature, reached at about 10 cm from the beam window, is 167 °C, well below the melting temperature of Lead (324 °C). The temperature of the beam window is about 110 °C.

In Figure 14 we give the dependence of the maximum Lead temperature on the beam intensity. The Lead starts melting at a beam current of about 0.64 μA, which is about twice the nominal current value.

The configuration envisaged for the target, i.e. a block of Lead naturally cooled in ambient air, is therefore feasible at the actual nominal value of the beam current of the CERN PS. Such target will remain solid in all its parts up

to an average current of 0.64 μA, about the double of the current maximum value of the PS.

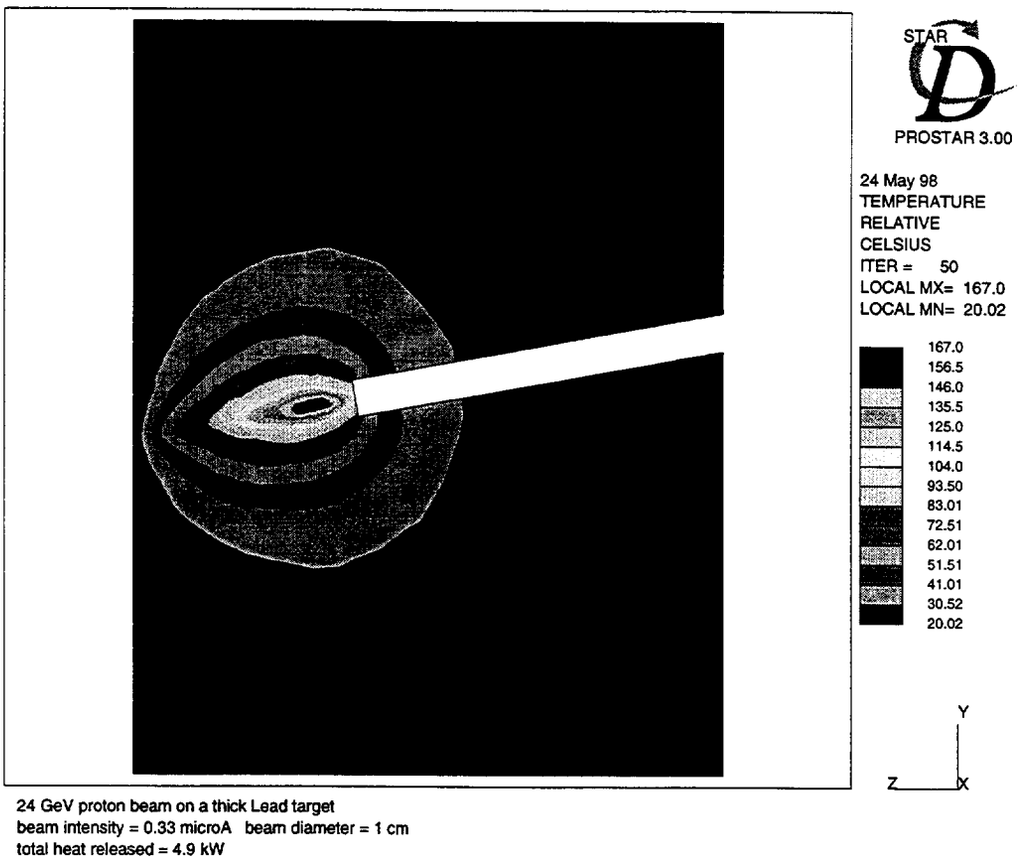

Figure 13. *Temperature map of the Lead target on the x=0 plane.*

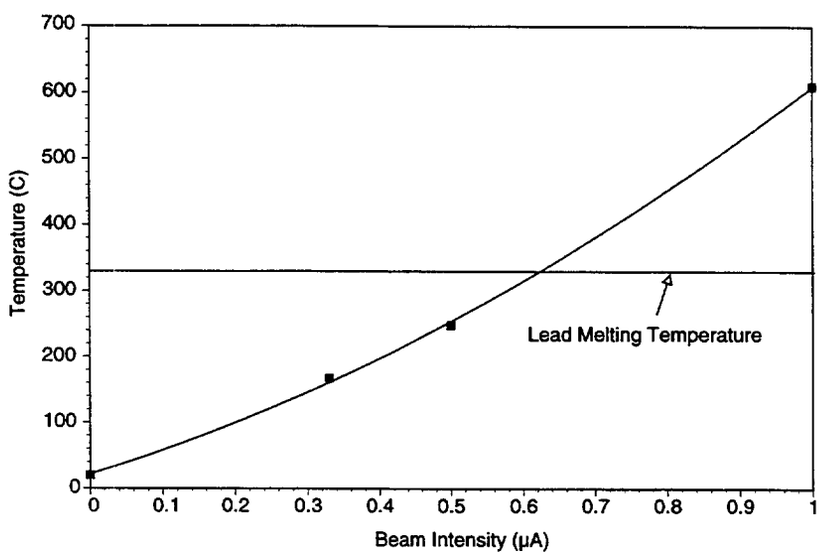

Figure 14. *Lead maximum temperature vs. beam intensity.*

2.5.- The TOF tunnel. The large majority (> 80%) of the neutron flux exits the Lead target within a radius of 80 cm. Since the neutron mean free path in air amounts to 25 m, a beam pipe evacuated to 10^{-3} bar allows the interaction-free neutron transmission for TOF distances up to ~ 1000 m. This beam pipe of a diameter of 1.6 m, equipped with a series of primary vacuum pumps, represents the TOF tube to be installed in the TT2A ISR tunnel. The TOF tube is inclined by 10° relative to the proton beam axis in order to avoid the forward shower of particles and photons at 0°.

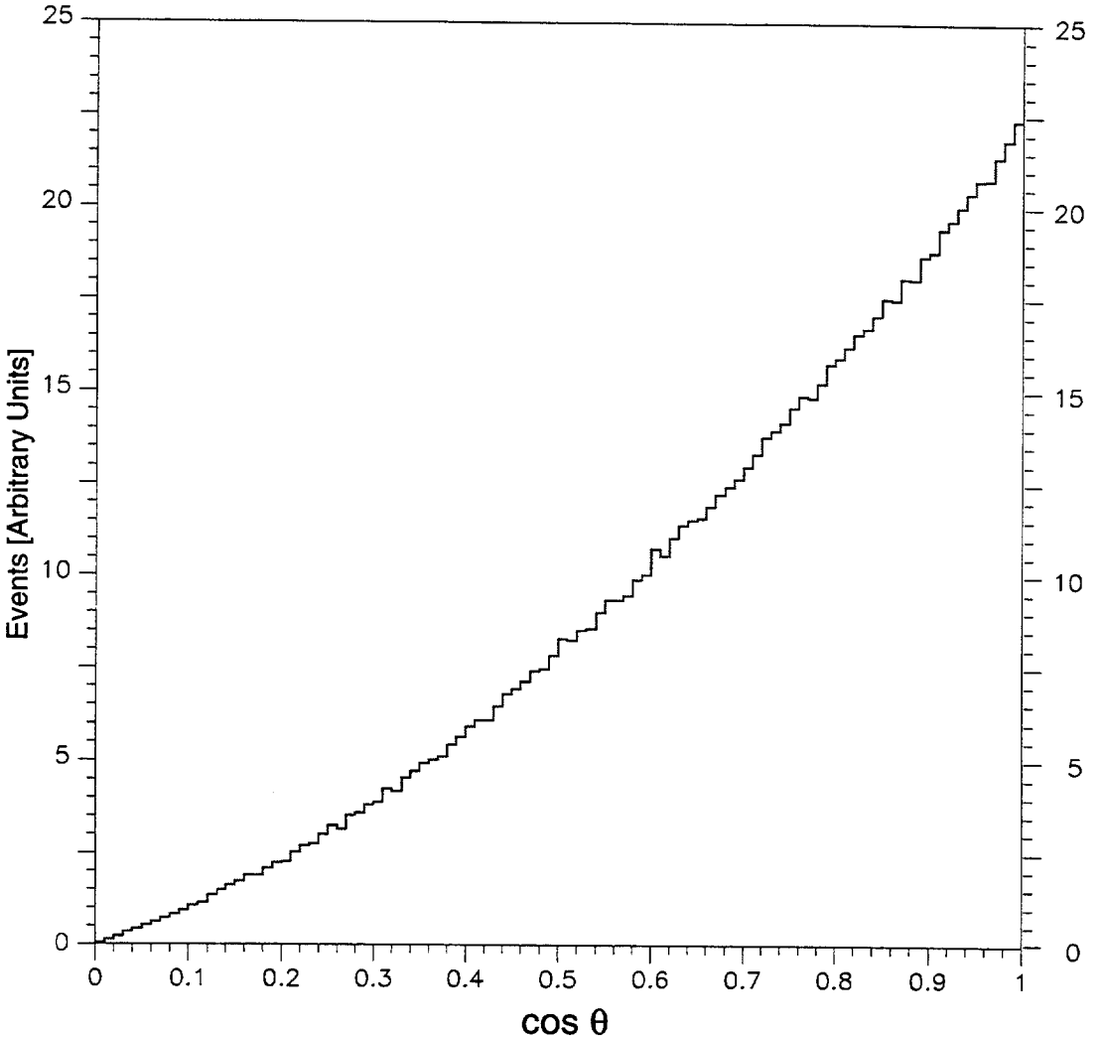

Figure 15. *Cosine of the angle between the neutron direction at the exit surface and the direction of the TOF pipe.*

Assuming an isotropic neutron distribution entering the TOF tube, the neutron flux at the experimental target will be:

$$\Phi_{\exp}^{ISOTR.} = \Phi_{source} \times \frac{\pi R^2}{2\pi L^2} = \Phi_{source} \times \left(8 \times 10^{-6}\right) = 2.8 \times 10^{6} \;\; n / cm^2 \; / \; pulse$$

where R = 80 cm and L = 200 m are the radius and the length of the TOF tube respectively. The more elaborate Montecarlo simulation gives a significantly forward peaked neutron flux (Figure 15), which corresponds to an additional multiplicative factor 2.5 in the neutron flux at the experimental area:

$$\Phi_{exp}^{MC} = \Phi_{source} \times 2.5 \times \left(8 \times 10^{-6}\right) = 7.0 \times 10^{6} \;\; n \,/\, cm^2 \,/\, pulse$$

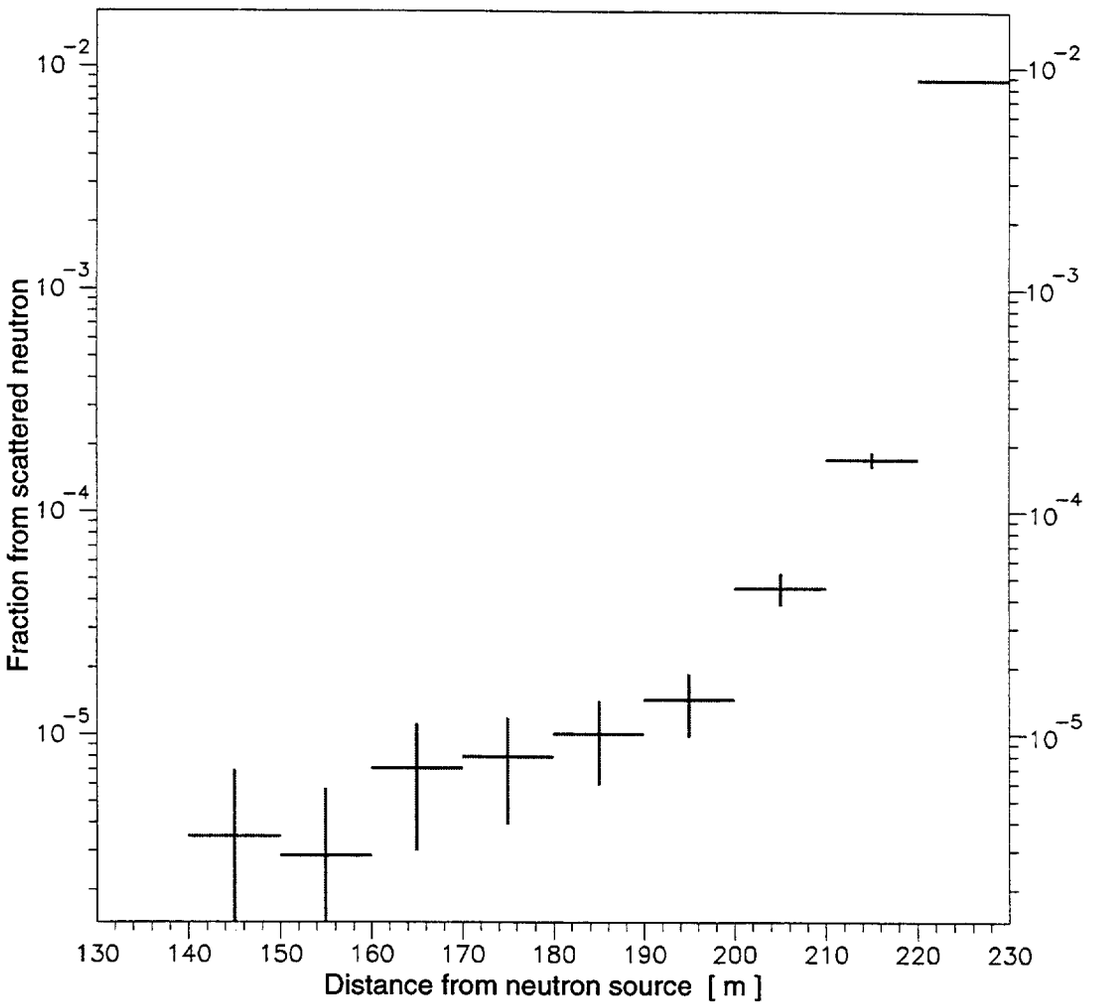

Figure 16. *The fraction of scattered neutrons as a function of the distance between the first scattering point and the source. The enlargement of the TOF tube in the last 30 m (see text) excludes the contributions of the last three points in the figure.*

The diameter of the TOF tube is decreased by 30 cm every 70 m in order to provide a neutron beam diameter of 1 m at the experimental area. Neutrons hitting the walls of the TOF tube may, in principle, reach the experimental sample after several scattering. Such neutrons will obviously not undergo the energy—time relation of the direct neutrons and will contaminate the measurements as background.

We studied by means of the TARC Montecarlo programme the effect of these neutrons scattered on the wall of the TOF tube and evaluated their contribution to the neutron flux. The geometry used in the simulation was a stainless steel tube of thickness of ≈ 1 cm surrounded by a concrete tunnel. We divided the TOF tube into several equally sized sections and generated mono-energetic neutron events hitting the tube wall inside each section. For every section runs were performed with different energies and the neutrons which crossed the downstream end of the TOF tube were recorded. Figure 16 shows the contribution to the main flux of such scattered neutrons at the experimental area as function of the distance of their first collision from the source. We remark that only those coming from the last sections may give a potentially relevant contribution.

In order to eliminate the effect, the radius of the TOF tube must be substantially increased over the last 30 m before the experimental area. With such a geometry, the scattered neutron background contribution to the main flux is reduced for all neutron energies to a negligible level ($\leq 10^{-4}$).

2.6.- Other particle contamination of the beam. The high energy (24 GeV) proton beam from the CERN-PS interacting with the target is not only an intense source of spallation neutrons but also a source of many other charged and neutral elementary particles. Fortunately most of them are unstable, with a lifetime which is much shorter than the TOF range and therefore they do not reach the measuring station. Gamma rays are "prompt" and provide a convenient t = 0 calibration for the TOF system.

Predicted (FLUKA) fluxes are listed in Table 1. The contribution of the charged particles reaching the end of the TOF tube amounts to ≈ 1.1×10^{-3} protons/neutron with a mean energy of ~ 50 MeV.Electrons ($\langle E_e \rangle \approx 2.6$ MeV) and pions ($\langle E_\pi \rangle \approx 160$ MeV) contribute about equally, with ≈ 1.4×10^{-3} per neutron. As already pointed out, charged particles are removed completely by the use of a simple sweeping magnet. The photon contamination of the beam, 8×10^{-2} γ/neutron ($\langle E_\gamma \rangle \approx 1.2$ MeV), is very reduced, since Lead in contrast with neutrons, is strongly absorbing them. Any background interaction from these photons (apriori small since associated to smaller cross sections) belongs to the t = 0 bin. The fastest neutrons, having an energy of 250 (100) MeV are delayed by TOF by as much as 484 (1029) ns at the close station (230 m) and

even more when further away. Therefore photon induced events are completely eliminated by the TOF measurement (>30σ).

In conclusion the contributions of other particles to the detected signals are either negligibly small or can be eliminated by the experimental method. Therefore the neutron beam can be considered as essentially free of contamination of other particles.

Table 1. Predicted particle fluxes at the near (230 m) measuring station.

Particle (at station)	Aver. Energy (MeV)	Integrated flux/neut.	Comments
gamma's	1.2	8.0×10^{-2}	separated by TOF
K_L's		2.5×10^{-5}	decay life 5 10-8 s
anti-neutrons	—	—	neglegible
Electrons	2.6	6×10^{-4}	swept by magnet
Muons, Pions, $K^{\pm}$	160.	1.4×10^{-3}	swept by magnet
Protons	50	1.1×10^{-3}	swept by magnet

2.7.- The detection station. The close by (230 m) detection station will be located at the end of the neutron beam tube in the ISR experimental area. A similar station is foreseen for the 1000 m TOF. Such a station will be of course dependent on the specific experiment to be performed. In general, measurements are based on coincidences between prompt events generated by the sample under test (Fission Fragments, γ-rays, secondary neutrons, protons and so on) and the TOF information with a resolution better than 10 ns. We give here only some exemplificative considerations. The main characteristics of the detectors are in general :

(1) highly segmented structure in order to detect the high event rate during the neutron pulse;
(2) fast rise-time of the order of 10 ns or less;
(3) high efficiency;
(4) good energy resolution.

The performance of the detectors should not be deteriorated by the high neutron flux in the vicinity of the target, making the use of a Germanium detector more difficult.

An indicative layout, limited to a Fission cross section measurement, is shown in Figure 6. It consists of a Detector Chamber located at the end of the vacuum tube with dimensions sufficient to house the sample under test and the associated detectors. The Detector Chamber will be lined with a neutron absorber like Boron loaded Polyethylene to minimise the parasitic effects due to back scattering. A shutter is used to separate the Detector Chamber from the vacuum tube to allow access without loosing the vacuum in the whole line.

Our first priority is the measurement of the cross section for Fission and neutron capture. Fission cross sections will be measured by the direct counting of Fission Fragments, for instance with the same type of gas detector already used for the FEAT Experiment [15].

The capture cross section will be measured through the detection of the prompt γ's of the nucleus produced. The measurement of cross sections requires the precise knowledge of their yield and energy distribution. For many elements of interest they are both poorly known and they will have to be determined from the experiment. We consider to use initially three types of γ-detectors:

(1) A liquid Xenon detector for gamma rays in the range 0.1 - 1 MeV with an energy resolution of ~ 56 keV at 1 MeV [16]. Liquid Xenon offers excellent stopping power, given its high density (3 g/cm^3) and high atomic number (Z = 54). The average energy to create an ion pair (W = 15.6 eV) is sufficient to produce a charge of ~ 64 e/keV. A detector thickness of less than 10 cm will be sufficient to fully absorb events in excess of 1 MeV. Xenon scintillates at 175 nm with a sufficient light yield and a fast time response (< 5 ns). The light signal is used to define the neutron arrival time, t_n, and therefore its energy. In a Liquid Xe Time Projection Chamber (LXeTPC) the ionisation electrons are free to drift under a uniform electric field at a velocity of 2 mm/μs, inducing a current signal on the anode X-Y wire chambers. The electron drift time, t_d, gives the third Z coordinate. The charge collected on the anode is proportional to the energy deposited by the interaction. For gamma-rays with complex histories, the advantages of self triggering, 3D images are apparent.

(2) For the minor Actinides of interest showing an X-ray signature in the range of 10 to 100 keV, another type of detector based on a Xe gas chamber operating in the proportional mode, is envisaged. In such a

detector, called Proportional Scintillation Chamber (PSC), the prompt scintillation is used for triggering purposes (t_n). The primary ionisation is multiplied in a high field and the secondary scintillation, produced by electro-luminescence, is precisely measured. An energy resolution of 2.7% at 122 keV could be achieved [17].
Other possible detectors for X-ray measurements, can be based on Cadmium Telluride and Mercuric Iodite compounds working at room temperature.

(3) Additionally the use of a well-shielded Ge γ-detector, showing a higher energy resolution (~2 keV FWHM at 1 MeV), could allow to distinguish the different components of certain samples by measuring directly the prompt γ spectrum.

The measurement of cross-sections requires the simultaneous, precise determination of the neutron flux. This will be achieved with monitor detectors based on the well-known cross-section of the (n,p) reaction in ^{3}He. A gas scintillation counter [18] seems to be an appropriate choice.

It should be pointed out that the absorption of the flux through the measuring sample is generally very small and therefore several measuring stations can be cascaded in the beam line, thus increasing considerably the data taking rate.

3. — NEUTRON FLUXES AND EVENT RATES.

3.1.- Rate estimates for different elements. The facility being proposed will allow precise measurements of essentially all neutron-induced reaction cross sections, which in addition to their practical relevance for ADS, will also provide new inputs to fundamental Nuclear Physics. The experimental determination of cross sections for a large number of relevant elements must be generally performed with small mass targets. This is so for three main reasons:

(1) the isotopically pure elements, especially when it comes to Actinides beyond Plutonium — one of the main thrusts of the measurements — are often extremely expensive and hence available only in very small amounts. It is not uncommon that targets may be available only at the level of a few milligrams.

(2) Many of the elements which are relevant to the transmutation programme for Fission Fragments from ordinary LWR's are radioactive and therefore the target mass is limited by the associated background counting rates in the detectors.

(3) Target layers must be very thin (few mg/cm^2) in order to remove self shielding of the narrow resonances and to permit a comprehensive detection of fission fragments and of low energy γ-rays. For a typical target thickness of 2 mg/cm^2 and a target area of 500 cm^2, this corresponds to 1 gram target.

It is a fortunate feature of our experiment that the limited target extent can be effectively compensated by the high intensity of the neutron flux. Therefore we have assumed a standard target mass of 1 gr. As we shall see, significant measurements can be performed in a reasonable exposure time already for a few milligrams of exposed material. These qualitative results, which are approximate, have to be confirmed with more detailed computer simulations and the actual detection geometry.

Event rates have been estimated on the basis of the neutron flux at the reference flight path of 200 m which, as discussed in Paragraph 2.3, amounts to about 7×10^6 n/cm^2/pulse in the close position and scales as the inverse of the square of the distance. They are reported per one gram of sample material

and per pulse (i.e. 3×10^{13} protons at 24 GeV PS-operation). The sample is assumed to be at room temperature (293 °K).

As already pointed out the energy spectrum is dependent on the Lead thickness d in the direction of the beam (Paragraph 2.3). For large values of d the spectrum becomes flat in lethargy, namely if plotted in terms of $d(\ln(E))$. However cross sections have the general tendency of decreasing with increasing neutron energy. A more uniform "illumination" of the energy range is therefore achieved with a spectrum which is peaked at higher energies as it is the case for the optimised choice d = 60 cm (Figure 3). The maximum of the spectrum, expressed in $d(\ln(E))$ is at about 450 keV with a mean energy of about 485 keV.

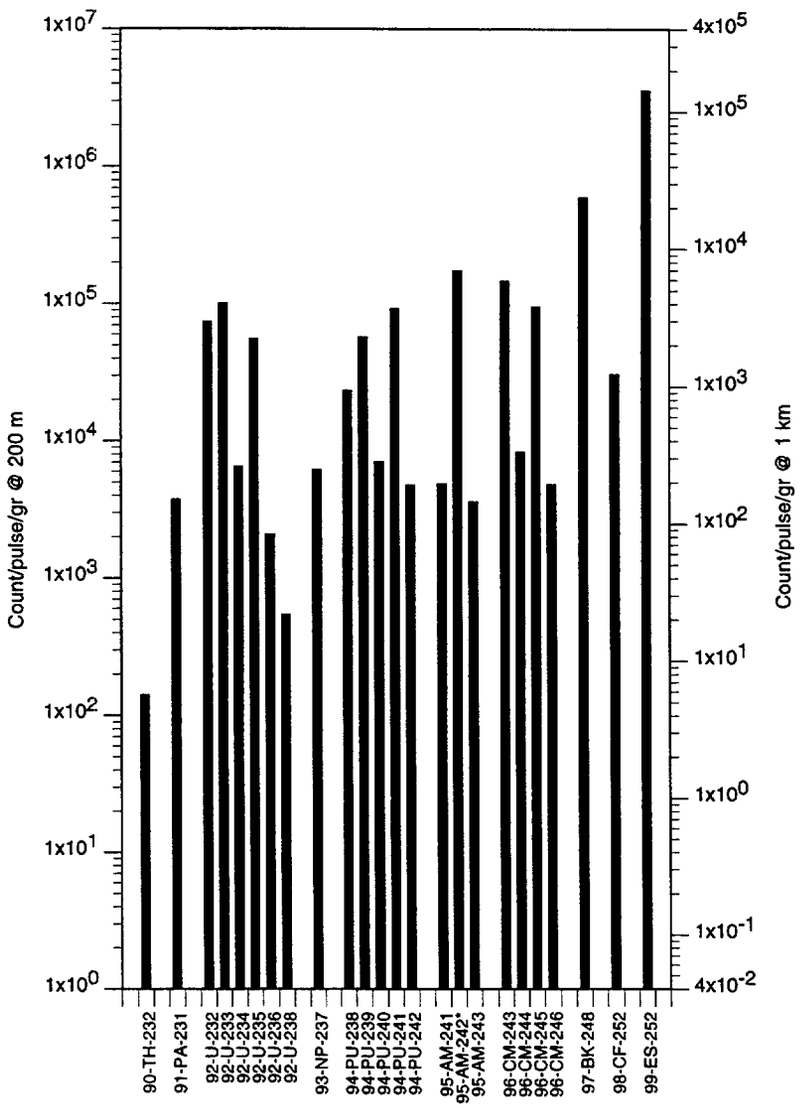

Figure 17. *Total fission event rates per gram per pulse (3×10^{13} protons at 24 GeV) for Actinides with 1/e life time > 1 year*

These parameters are very close to the ones of a sub-critical device and Lead environment. The neutron spectrum is arbitrarily cut off at 1 eV and extends with a measurable rate to about 250 MeV. However our rate estimates are limited to the energy interval available in the current Databases [5], namely up to 20 MeV.

Capture and fission event rates estimates for an exhaustive list of stable elements and of radio nuclides with a 1/e life time greater than 1 year are given in Appendix II, to which we refer for details. An inspection of such list shows that one can ensure rates which are well above the minimal value required for an extensive exploration for almost all known elements.

We shall consider in more details some specific strategies related to the application of our measuring method to ADS. One area in which the information is generally lacking and often contradictory is the one of Transuranics, especially Np, Pu, Am and Cm, which are all produced in substantial amounts during the incineration process. As shown in Figure 17, a total fission event rate between 10^3 and 10^4 per gram of material and per pulse (L_{ref} = 200 m) is expected for most Minor Actinides of interest (^{237}Np, ^{241}Am, ^{243}Am and ^{244}Cm) and up to 10^5 fission/g/pulse for the readily fissile nuclides such as ^{233}U, ^{239}Pu, ^{242m}Am and ^{243,245}Cm. Even with samples of 10 mg — which is more realistic for the majority of such elements— one can collect over a run of 10^4 pulses (slightly more than one day) over 10^7 Fission for the more readily fissionable elements and still something like $10^5 \div 10^6$ counts for the more resilient elements. It should also be remarked that several targets can be cascaded and therefore in specific instances one could envisage at least one order of magnitude longer exposure time.

Likewise, capture event rates of the order of 10^4 ev/g/pulse are expected for fissile nuclides and up to 10^5 ev/g/pulse for the more fission resilient elements (Appendix II). Considering that a reasonable exposure could consist in about $10^4 \div 10^5$ pulses, there is no doubt that a comprehensive exploration of all the relevant nuclear species can be performed already with a target mass of a few milligrams.

In order to verify the correct matching between the spectrum and the cross section behaviour we have reported in Appendix II also the rates subdivided for each energy decade. This is exemplified in Figure 18 in the case of few representative, fissionable elements. Indeed, the full energy spectrum is covered with comparable statistics.

As expected, the main contribution to capture events is concentrated at relatively low energies (see Appendix II).

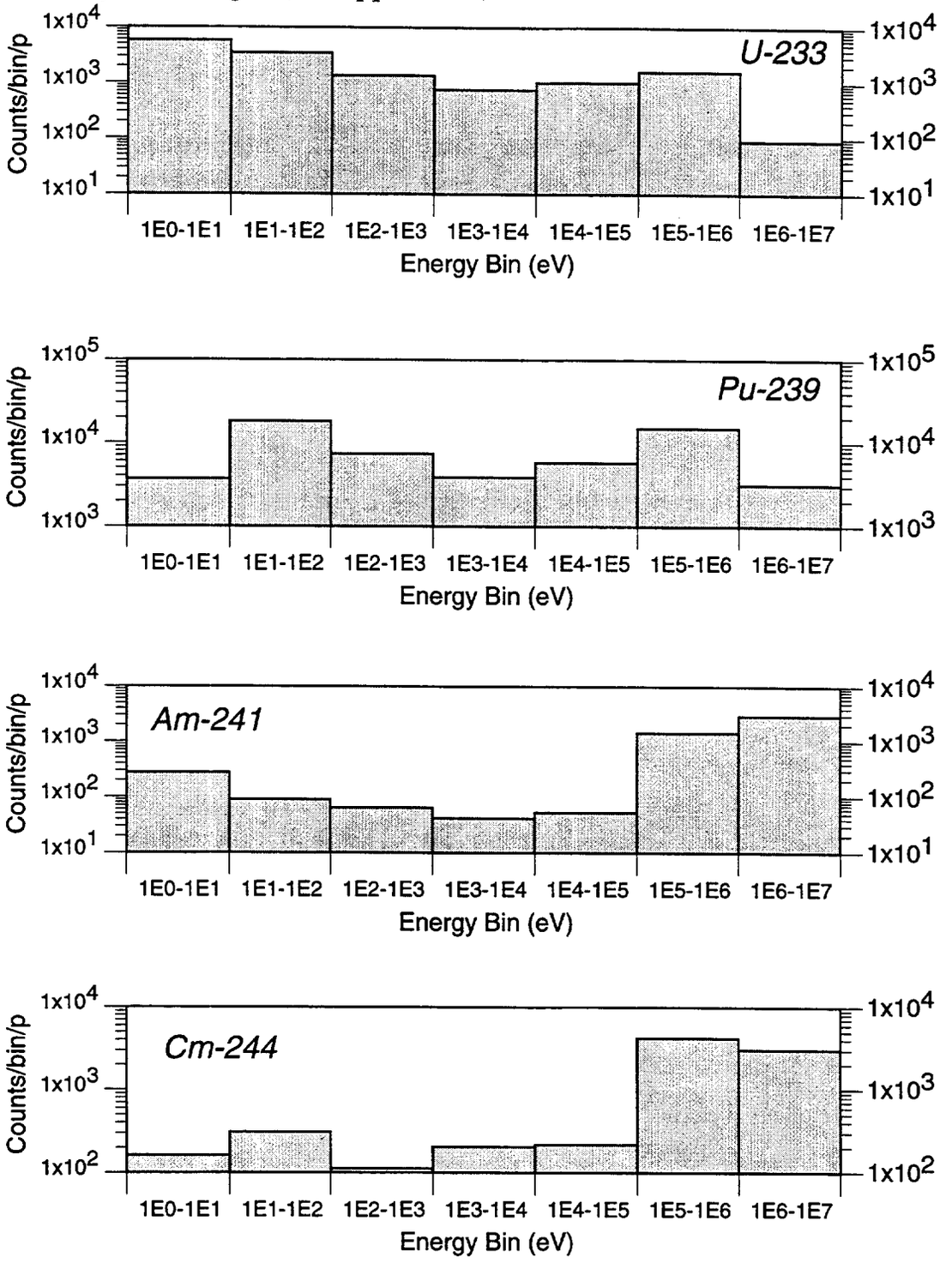

Figure 18. *Fission event rate spectra (per gram per pulse) for representative Actinides with 1/e life time > 1 year.*

Another important domain in which better cross section are needed is the one of Fission Fragments (FF) which one would like to transmute into stable species [3] because of their important radio-toxicity. If we limit

ourselves with those FFs which have a half-life larger than 30 years, the most relevant offending elements are the medium-lived ($\approx$ 30 years) elements ^{90}Sr and ^{137}Cs and the very long-lived ones, namely ^{79}Se, ^{93}Zr, ^{99}Tc, ^{129}I and ^{135}Cs. Unfortunately little or no information exists on their resonance spectrum, essential in order to ensure an effective transmutation with the method of Ref. [3]. A recent experimental exploration [8] has proven the feasibility of the method and given very encouraging results for ^{99}Tc and ^{129}I. These results need to be extended to other elements.

In the case of the very long lived FFs, the scarce experimental data available in the literature predict capture event rates between 10^4 and 10^5 ev/g/pulse (see Figure 19). In absence of a more precise knowledge of resonances, ^{126}Sn exhibits very few events, of the order of 10^2 ev/g/pulse. Such element would therefore not be immediately suitable for this technique. The possibility of transmutation at higher energies in which other channels are open must be explored as well.

Most capture events are expected to occur in the resonance region (1 eV to 10 keV) as shown in Figure 20, where the energy resolution of our method is very good.

Medium-lived Fission Fragments such as ^{90}Sr and ^{137}Cs are at present totally "terra incognita". Assuming the validity of the phenomenological predictions in [5] the capture rates are relatively small, though no information exists on the presence of resonances which could greatly enhance the capture rate and therefore the speed of transmutation. Also for these elements high energy channels must be explored as an alternative method of transmutation. Some of the expected rates as a function of the neutron energy bin are shown in Figure 20. For more detail we refer to Appendix II.

In the case of the stable elements we expect total capture event rates between 10^3 and 10^5 ev/g/pulse, except for closed shell nuclides for which the neutron capture cross section is relatively small (see Table 4, Appendix II).

Finally, such high event rates allow to study systematically the neutron induced reactions in the energy interval between 1 eV and 250 MeV, of almost any nuclide using targets of very modest mass (few milligrams), as needed for unstable or otherwise expensive materials, like for instance transuranics and medium to long-lived Fission Fragments.

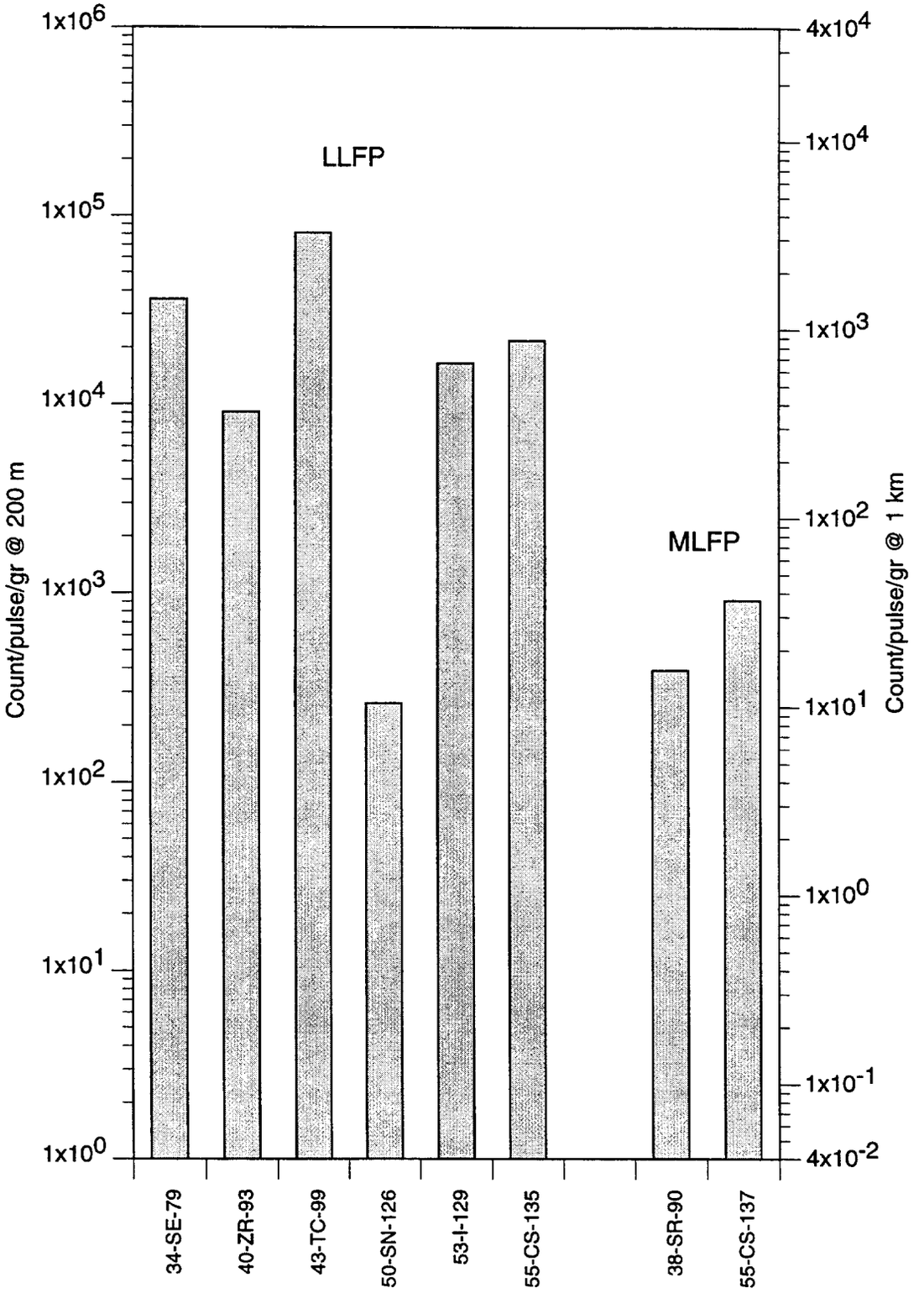

Figure 19. *Total capture event rates per gram per pulse (3×10^{13} protons at 24 GeV) for long-lived (LLFP) and medium-lived (MLFP) Fission Products.*

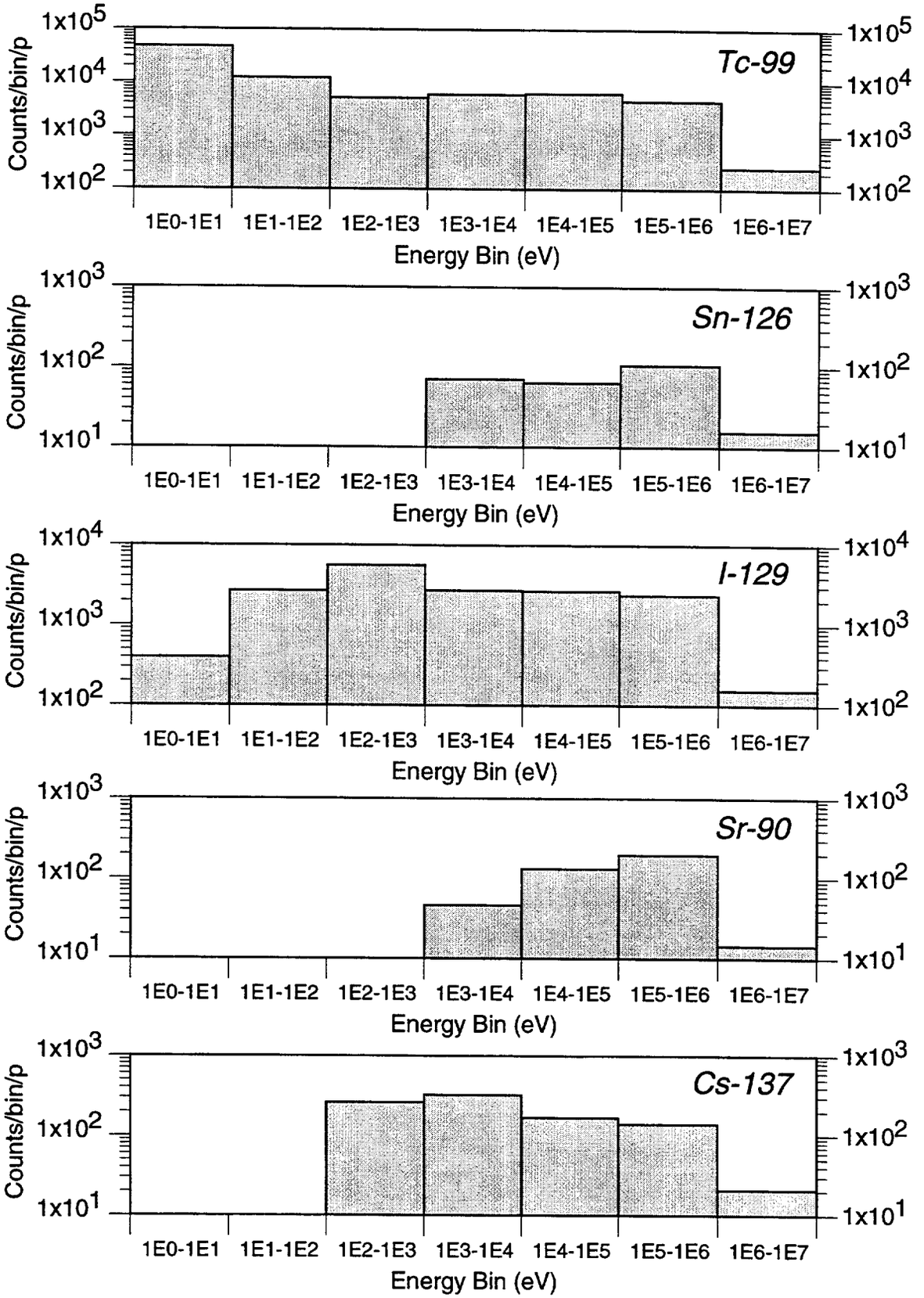

Figure 20. *Capture event rate spectra (per gram per pulse) at the reference distance L_{ref} = 200 m for representative medium and long-lived Fission Fragments*

3.2.- The experimental programme. The installation of the infrastructure for the initial set up with the 230 m long vacuum pipe requires the following actions:

(1) Modification of the present TT2A tunnel over a length of 20 metres to achieve a linear development of 230 m.
(2) Replacement of the present beam dump and the concrete shielding blocks obstructing the TT2A tunnel in the direction of the ISR.
(3) Installation of the Lead target and the associated shielding.
(4) Installation of the vacuum pipe and its equipment.
(5) Installation of the instrumentation of the beam line to monitor the position and the beam intensity.
(6) Survey of the whole set-up.

All of these tasks can easily take place during one standard 3 month winter shut-down of the accelerator complex. In addition, some preparation work could be done for the next stage of the project, extending the time of flight path to 1000 m.

Depending on which solution is ultimately chosen between an extension of the 230 m line in the same direction or a completely new line, the civil engineering work impact on the present tunnel infrastructure may be different, but small in all cases. If the solution of a totally new line is accepted, the impact on the TT2 tunnel is limited to the place where this new line is branching off the present tunnel, and therefore, the corresponding civil engineering work could be arranged to take place during one shut-down period. The main part of the civil engineering (most of the new gallery and installation of the vacuum pipe) can be done if necessary outside an accelerator shut down period.

The beam line is already equipped with most of the instrumentation needed. The only minor addition would be a beam position monitoring device at the entrance of the Lead target hole (either a scintillating screen at the input of the lead target hole, or pick up electrodes). Beam transformers already exist which can provide a measurement of the proton beam intensity. A beam pulse timing signal with fluctuations of only a few nanoseconds can be obtained from the PS-RF system.

The construction and installation of the detectors described in section 2.6 does not interfere with the preparation of the beam line and the setting up of the neutron vacuum pipe, and can be planned independently, so as to be

ready when the neutron beam becomes operational. All the installation will take place in the existing ISR tunnel.

The development of the associated electronics and Data Acquisition could be similar to the one used for the TARC experiment, based on the CERN CASCADE code.

The test of the performance and the energy calibration of the detector could be performed in CEN-Bordeaux's small 4 MVolt Van de Graff. Where a special line can be used for a production of mono-energetic fast neutrons from 30 keV to 3 MeV [19]. Neutrons are produced from the well known reactions $^{7}Li(p,n)^{7}Be$ and $T(p,n)^{3}He$.

The general strategy consists in measuring systematically poorly known neutron induced cross-sections for the elements of interest, in the energy range from 1 eV to 250 MeV.

We will start by using a few elements with relatively well known cross-sections (^{181}Ta, ^{197}Au, ^{235}U and ^{238}U) though even for these elements the knowledge at high energies is still limited. In particular it will be important to verify the energy resolution and the separation power for near resonances. Natural silver (51.84% of ^{107}Ag et 48.16% of ^{109}Ag) will provide a test of the separation of data for non-isotopically pure elements.

The nuclides of interest in the framework of ADS which we propose to measure with priority are the Minor Actinides (typical examples are ^{241}Am, ^{242}Am, ^{243}Am, ^{244}Cm and ^{237}Np) and specific fission fragments (like for instance ^{99}Tc, ^{129}I, ^{90}Sr and ^{137}Cs). Obviously also the ^{232}Th, ^{233}Pa, ^{233}U elements, important to the EA system, will be studied carefully.

There is no principle limitation in the choice of elements to be studied, since the flux allows high quality measurements even with very small quantities of element. This is a unique feature which comes from the unprecedented flux ($7 \times 10^{6}/n/cm^{2}/pulse$ at 200 m and 2.8×10^{5} at 1000 m) as a result very thin samples can be used (mg/cm^{2}) which minimises absorption effects.

There exist simple methods to test in detail the properties (width and amplitude) of a given resonance, for instance by varying the thickness of the sample, which can be achieved by rotating the sample around an axis perpendicular to the beam direction.

As is shown in paragraph 1.5, the high resolution $\Delta E/E \approx 3 \times 10^{-3}$ for 230 m and $\Delta E/E \approx 6.6 \times 10^{-4}$ for 1000 m distances allows not only the observation of a multitude of resonances without any ambiguity in the possible interference with other resonances, but also for instance the determination with very good precision of the energy of the fission threshold for the elements for which the fission is possible (close to the resonance at 1.6 MeV for the ^{232}Th fission for instance). It will be particularly interesting and easy to look for giant resonances in the $10 \div 15$ MeV range for the Actinides. The experiment performed with the presently described facility can also give a good, additional information of the level structure of the daughter nuclei. We are clearly covering new ground in the field of Nuclear Physics and we believe that this new facility will trigger new ideas and improve tremendously our general knowledge.

3.3.- The experiment operated as a Facility. The uniqueness of the proposed neutron source lies in the availability of a high neutron flux in the broad energy range between 1 eV and 250 MeV (exceeding eight orders of magnitude) and in the high energy resolution limited only by the thermal motion of the target. These novel features provide a great potential for modern Nuclear Physics experiments, for exploiting new ideas in nuclear technology with emphasis to ADS but also for providing data relevant to other domains of physics.

The experimental area will be equipped with all necessary infrastructure to provide flexible operation in the running of individual experiments. Different targets and different detectors may be used in a variety of configurations according to the requirements of each specific measurement. Technical services would ensure the operation of the target and detection stations, the high performance data acquisition system, the neutron flux monitors and could provide consultancy to the users for the standard analysis and simulation software.

The proposed neutron source would be compatible with the normal operation of the PS complex within the foreseen CERN program and should attract many physicists from a broader community with different scientific interests. The results obtained will allow to compile the most reliable and accurate nuclear level data and neutron induced cross section evaluation.

4.— CONCLUSIONS.

We have studied in detail the new concept of an intense neutron source based on the spallation of Lead nuclei by high energy protons concentrated in short time pulses, as presented in Ref. [20]. The conclusions of this paper confirm fully the early expectations of the proposed method, namely that such a neutron source is characterised by three main, practically unique features:

1) High neutron flux exceeding 2.8×10^5 /L^2(km) n/cm^2/pulse for the standard CERN-PS intensity, allowing very modest mass targets, normally less than 1 gram and whenever necessary, down to a few milligrams.
2) An excellent energy resolution in the neutron energy determination by TOF, namely $\Delta E/E = 6.6 \times 10^{-4}$/L(km).
3) A very wide energy spectrum, covering simultaneously the whole energy domain of interest, from 1 eV to 250 MeV.

The CERN-PS accelerator complex appears to be the most suitable and immediate host to operate such a source. It is foreseen that in the future such accelerator is capable of delivering protons in excess of the needs of the CERN programme. The facility could be therefore operated parasitically, out of the existing PS beam dump, though suitably modified. We propose a graded strategy for the implementation namely the early installation of a TOF tube of 230 m in the available ISR tunnel, followed by a second phase for which an adequate pipe has to be constructed.

The measuring station should have several different detectors to study the majority of the reaction channels. Practically all the elements of the Mendeleiev Table (stable and with accessibly long lifetime) can be studied with adequate statistics and only small mass targets are required.

The source and the detector station will run as a highly standardised facility with different targets and detectors, which may be eventually cascaded in order to improve the beam time utilisation. The extension to a 1 km long TOF tube for the subsequent phase is presently under study. Some highlights of the potential scientific program prove the potentials and the uniqueness of the facility, which may be later extended to the SPS beam with more than one order of magnitude gain in the flux.

Some of these measurements are essential for elements relevant to ADS energy production (EA), nuclear waste incineration and similar Nuclear Physics applications. But such high energy spallation facility, combining prolific rates with high resolution, due to the unique properties of the CERN-PS and of the neutron behaviour in Lead, will undoubtedly open up also novel avenues in Nuclear Physics with a careful and systematic study of many neutron driven reactions over an energy domain of over eight orders of magnitude, from thermal energies up to 250 MeV.

5.— REFERENCES.

[1] C. Rubbia et al., "A Realistic Plutonium Elimination Scheme with Fast Energy Amplifiers and Thorium-Plutonium Fuel", CERN/AT/95-53 (ET); C. Rubbia et al., "Fast Neutron Incineration in the Energy Amplifier as Alternative to Geological Storage: the Case of Spain", CERN/LHC/97-01 (EET).

[2] C. Rubbia, J-A. Rubio, S. Buono, F. Carminati, N. Fiétier, J. Galvez, C. Gelès, Y. Kadi, R. Klapisch, P. Mandrillon, J.P. Revol and Ch. Roche, "Conceptual Design of a fast Neutron Operated High Power Energy Amplifier", CERN/AT/95-44 (ET); see also C. Rubbia, "A High Gain Energy Amplifier Operated with fast Neutrons", AIP Conference Proceedings 346, International Conference on Accelerator-Driven Transmutation Technologies and Applications, Las Vegas, 1994.

[3] Carlo Rubbia, "Resonance Enhanced Neutron Captures for Element Activation and Waste Transmutation", CERN/LHC/97-04 (EET).

[4] Carlo Rubbia, Paper in preparation.

[5] Data from the following nuclear data libraries have been compared:
JENDL-3.2, OECD NEA Data bank (1996);
JEF-2.2, OECD NEA Data bank (1996);
ENDF/B-VI, OECD NEA Data bank (1996);
BROND-2, OECD NEA Data bank (1996).
See also J. Cobo et al, "Notes on the Study of the Most Reliable Neutron Cross Section Data", CERN/AT/95-035 (ET).

[6] C. Rubbia and J.A. Rubio, "A Tentative Programme Towards a Full Scale Energy Amplifier", CERN/LHC/96-11 (EET).

[7] For the thermal neutron capture cross-section of ^{90}Sr, the Atomic data and Nuclear data Tables, Vol. 29, Number 2, Sept. 1983, give a capture cross-section of 0.9 barns, while M.A. Lone et al, NIM A332 (1993)232-238 find 9.7 ± 0.7mb. There is essentially no data at other energies.

[8] S. Andriamonje et al., TARC Proposal, "Experimental Study of the Phenomenology of Spallation Neutrons in a Large Lead Block", CERN/SPSLC 95-17, SPSLC/P291, 5th May, 1995.

[9] First study on the deceleration of neutrons presented by E.L. Feinberg at a seminar at the Academy of Sciences, USSR, 1944.

[10] C. Rubbia, "Relation between time and kinetic energy in a constant lethargy system", CERN/AT/ET/Internal Note 95-010, 2nd May, 1995.

[11] A.A. Bergman, A.I. Isakov, I.D. Murin, F.L. Shapiro, I.V. Chtranikh and M.V. Kazarnovsky, "Lead Slowing-Down Neutron Spectrometry", in Proc. 1st Inst. Conf Peaceful Uses At. Energy", vol. 4, 1955, p. 135.

[12] A. Fassó et al, in "Intermediate Energy Nuclear Data: Models and Codes", Proceedings of a Specialists' Meeting, Issy les Moulineaux (France) 30 May-1-June 1994, p. 271, published by OECD, 1994, and references therein.
A. Fassó, A. Ferrari, J. Ranft, P.R. Sala, G.R. Stevenson and J.M. Zazula, Nuclear Instruments and Methods A, 332, 459 (1993), also, CERN Divisional Report CERN/TIS-RP/93-2/PP (1993).

[13] F. Carminati et al., "TARC General Purpose MonteCarlo", CERN/ET/Internal Note 96-11.

[14] "STAR-CD Version 3.0 Manuals", Computational Dynamics, 1997.

[15] F. Casagrande et al, "The Argon Gas Detectors for the Fission Measurement in the FEAT", NIM-A 372 (1996) 307-310.

[16] E. Aprile et al, "Performance of a liquid Xenon Ionisation Chamber irradiated with Electrons and gamma-rays", NIM-A 302 (1991) 177-185.

[17] A. Bolozdynya et al, "A high pressure Xenon self-triggered scintillation drift chamber with 3D sensitivity in the range 20-140 keV deposited energy", NIM-A 385 (1997) 225-238.

[18] D. Brozzi et al, "Neutron flux measurements in the TARC experiment with ^{3}He scintillation chamber", CERN/ET/Internal Note 97-27.

[19] S. Andriamonje, "Mesure entre 30 keV et 2 MeV à Bordeaux", Atelier Gestion des Déchets par des Options Nouvelles", Cadarache-France (1997).

[20] C. Rubbia, "A spallation driven experimental campaign to measure the relevant cross sections for the EA", CERN/ET/ Internal Note 97-19.

6.— ACKNOWLEDGEMENTS.

We would like to thank D. Brozzi and F. Saldaña for their technical support, all CERN staff and in particular the PS Group, especially J.L. Baldy and J.P. Quesnels, for the useful help given for studying the possibility to use the TT2A tunnel for this project. We do not forget the interesting discussions with A. Ferrari, R. Klapisch and G. Barreau.

Finally we would like to thank A.M. Fornasaro and S. Lilliu for help in the preparation of the manuscript.

7.— APPENDIX I: A CONSISTENCY COMPARISON OF EXISTING DATA.

We have compared, for neutron energies from 0.1 eV up to 1 MeV and for all the elements and their isotopes, the cross sections compiled in the four known Nuclear Databases [5]. We build for each nuclear Database the mean cross section for each energy bin, spanning between E_i (eV) and E_{i+1} (eV),where $\log_{10} E_{i+1}/E_i = 0.1$ according to:

$$\sigma_i = \frac{\int_{E_i}^{E_{i+1}} \sigma(E)dE}{E_{i+1} - E_i}$$

We calculated the r.m.s. of the difference of the capture and fission reaction cross sections of BROND-2, ENDF/B-VI and JEF-2.2 relative to JENDL-3.2 [5]. For each cross section we present in Table 1 the three r.m.s. values corresponding to BROND-2, ENDF/B-VI and JEF-2.2 with respect to JENDL-3.2. A mark "-" means that the cross sections were not found in the selected Nuclear Database.

This comparison leads clearly to the conclusion that the cross sections are not sufficiently well known or not measured at all, in particular in the unresolved resonance domain of the epithermal and fast energies.

To illustrate this graphically, we present in Figures 1 to 4, a comparison of the neutron-induced capture and fission cross sections, between the different Nuclear Databases mentioned in ref. [5], for a selection of Minor Actinides, namely: ^{237}Np, ^{242,243}Am and ^{244}Cm.

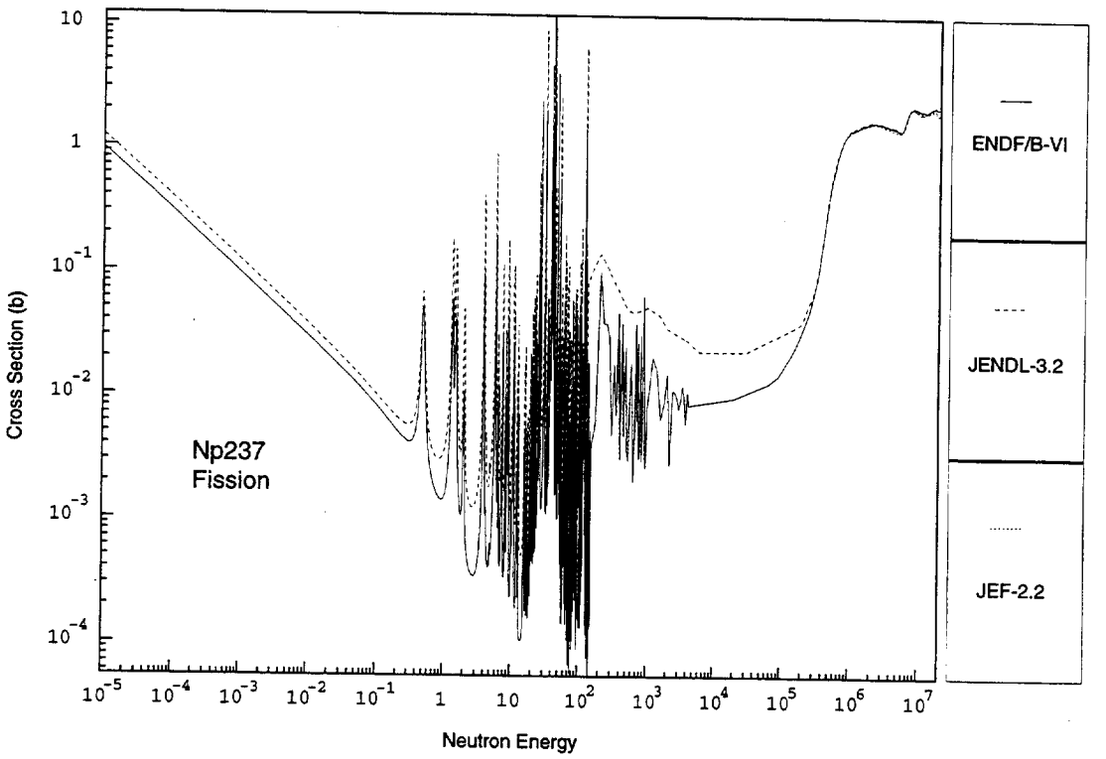

Figure 1. *Comparison of the fission cross section of ^{237}Np between the American (ENDF/B-VI), Japanese (JENDL-3.2) and European (JEF-2.2) Nuclear Databases.*

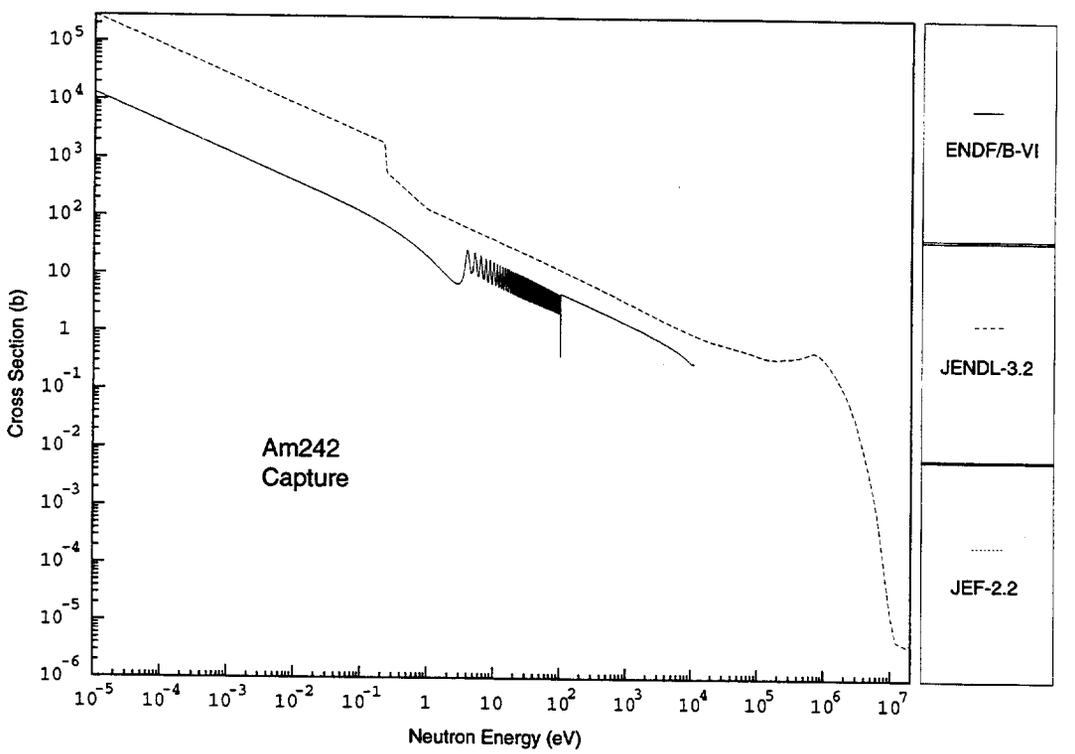

Figure 2. *Comparison of the capture cross section of ^{242}Am between the American (ENDF/B-VI), Japanese (JENDL-3.2) and European (JEF-2.2) Nuclear Databases.*

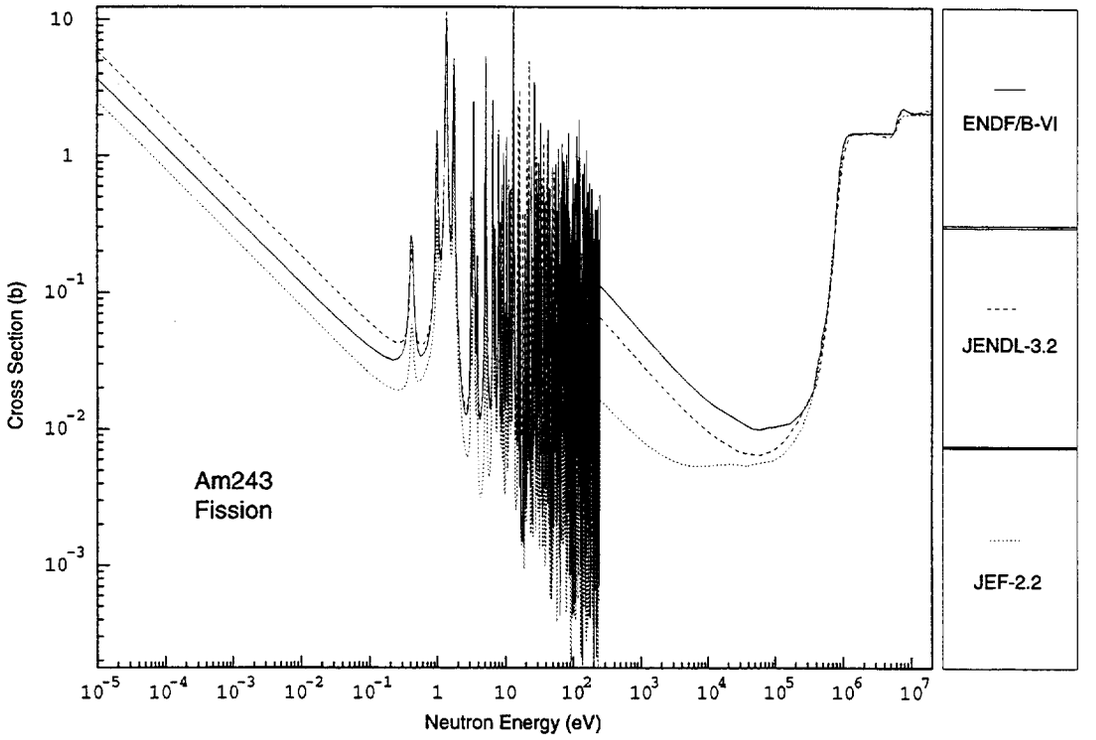

Figure 3. *Comparison of the fission cross section of ^{243}Am between the American (ENDF/B-VI), Japanese (JENDL-3.2) and European (JEF-2.2) Nuclear Databases.*

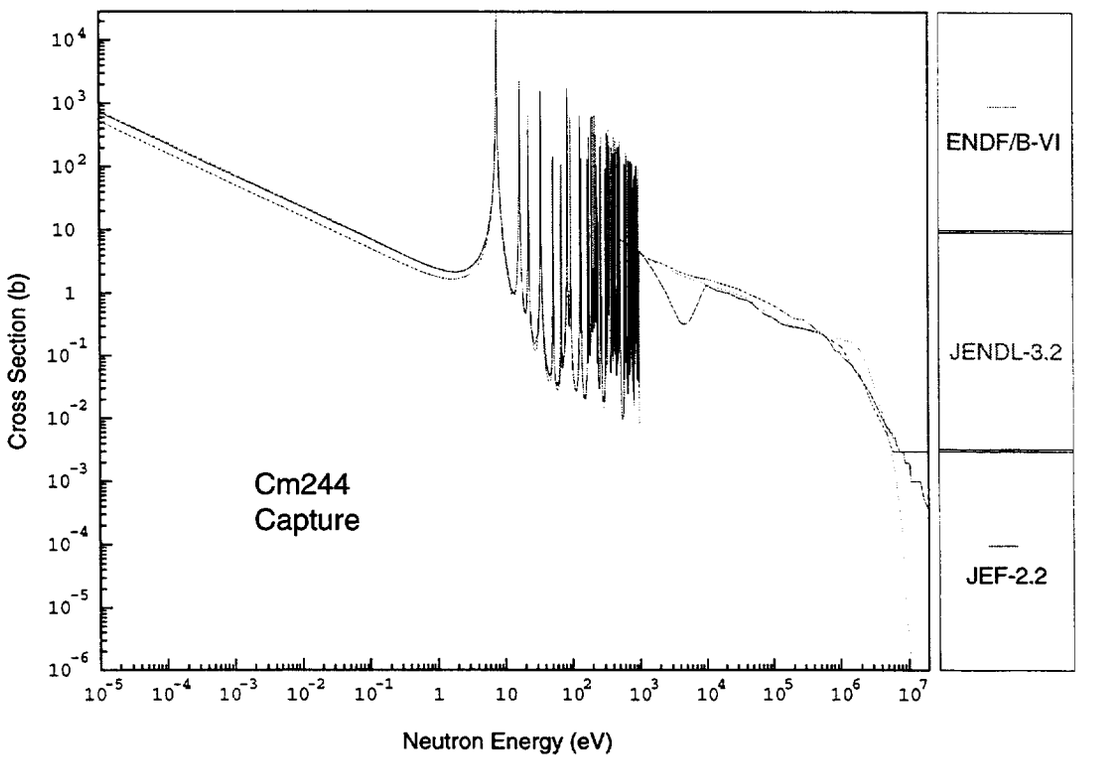

Figure 4. *Comparison of the capture cross section of ^{244}Cm between the American (ENDF/B-VI), Japanese (JENDL-3.2) and European (JEF-2.2) Nuclear Databases.*

Table 1. *R.M.S. of the ratio of capture and fission cross sections for the three Databases BROND-2 (A), ENDF/B-VI (B) and JEF-2.2 (C), relative to JENDL-3.2 for incident neutron energies from 0.1 eV up to 1 MeV and for all Actinides. A mark "–" means that the cross sections are not available.*

Element	Reaction	A	B	C
90-Th-230	n,γ	-	0.24	0.24
	n,f	-	0.63	0.63
90-Th-232	n,γ	0.17	0.26	0.14
	n,f	0.18	0.19	0.00
91-Pa-231	n,γ	-	0.53	0.53
	n,f	-	13.87	13.87
91-Pa-233	n,γ	-	0.28	0.28
	n,f	-	0.23	0.23
92-U-232	n,γ	-	9.88	9.88
	n,f	-	9.56	9.56
92-U-233	n,γ	0.20	0.23	0.21
	n,f	0.08	0.04	0.07
92-U-234	n,γ	-	0.18	0.18
	n,f	-	17.75	17.75
92-U-235	n,γ	0.14	0.10	0.11
	n,f	0.08	0.02	0.02
92-U-236	n,γ	0.16	0.10	0.31
	n,f	7.48	0.55	0.55
92-U-237	n,γ	-	1.07	1.05
	n,f	-	0.44	0.44
92-U-238	n,γ	0.05	0.01	0.01
	n,f	0.21	1.28	1.79
93-Np-237	n,γ	-	0.08	0.08
	n,f	-	0.25	0.26
93-Np-238	n,γ	-	0.24	0.19
	n,f	-	0.13	0.62
93-Np-239	n,γ	-	0.45	0.00
	n,f	-	0.00	0.00
94-Pu-236	n,γ	-	31.81	31.79
	n,f	-	99.35	99.29

Element	Reaction	A	B	C
94-Pu-238	n,γ	0.18	0.28	0.14
	n,f	0.49	0.51	0.30
94-Pu-239	n,γ	0.12	0.08	0.05
	n,f	0.13	0.02	0.03
94-Pu-240	n,γ	0.09	0.10	0.05
	n,f	6.03	1.03	8.48
94-Pu-241	n,γ	0.36	0.12	0.22
	n,f	0.10	0.03	0.03
94-Pu-242	n,γ	0.37	0.08	0.06
	n,f	161.54	2.87	3.47
95-Am-241	n,γ	0.14	0.19	0.20
	n,f	0.24	0.26	0.29
95-Am-242	n,γ	0.89	0.34	0.00
	n,f	0.09	0.22	0.00
95-Am-243	n,γ	0.03	0.09	0.11
	n,f	0.11	0.41	0.29
96-Cm-241	n,γ	-	0.51	0.51
	n,f	-	0.96	0.96
96-Cm-242	n,γ	72.87	0.27	0.21
	n,f	6.89	0.39	1.28
96-Cm-243	n,γ	-	0.68	0.70
	n,f	-	0.47	0.38
96-Cm-244	n,γ	0.21	0.26	0.20
	n,f	0.76	0.63	1.28
96-Cm-245	n,γ	-	0.23	0.25
	n,f	-	0.20	0.21
96-Cm-246	n,γ	-	0.21	0.21
	n,f	-	0.48	0.48
96-Cm-247	n,γ	-	11.02	11.04
	n,f	-	7.88	7.89
96-Cm-248	n,γ	-	0.12	0.12
	n,f	-	0.39	0.39
97-Bk-249	n,γ	-	0.04	32.09
	n,f	-	0.55	0.94
98-Cf-249	n,γ	-	0.30	0.45
	n,f	-	0.04	0.16

Element	Reaction	A	B	C
98-Cf-250	n,γ	-	23.98	23.98
	n,f	-	40.27	40.27
98-Cf-251	n,γ	-	4.69	4.51
	n,f	-	8.95	8.58
98-Cf-252	n,γ	-	136.04	136.01
	n,f	-	165.26	165.28

8.— APPENDIX II: EVENT RATES FOR 1 GRAM TARGET.

An exhaustive estimate of some neutron induced reaction rates per gram of sample material is given. This includes mainly an evaluation of the neutron capture event rates for most of the stable nuclides present in our nuclear Databases [5], as well as unstable nuclides with a 1/e life time greater than 1 year (Tables 2 & 4). In the case of Actinides, neutron fission events have also been computed (Table 3). Rates are given for 1 gram of target at the reference distance L_{ref} = 200 m. For different distances, rates can be scaled according to the inverse of the square of the distance.

Table 2. Total capture event rates per gram (3 x10^{13} protons at 24 GeV) for unstable nuclides with a 1/e life time > 1 year

Nuclide	1/e Life Time (Years)	Capture Event Rate per gram per 3 x 10^{13} protons Energy bins in eV							
		1 to 10	10 to 10^2	10^2 to 10^3	10^3 to 10^4	10^4 to 10^5	10^5 to 10^6	10^6 to 10^7	Total
4-BE-10	2.18E+6	3.35E-1	2.34E-1	1.76E-1	3.31E-1	9.98E-1	5.03E+0	2.65E+0	9.76E+0
11-NA-22	3.76E+0	3.84E+4	4.13E+4	2.67E+4	7.11E+1	2.61E+2	2.14E+2	7.73E+0	1.07E+5
13-AL-26	1.07E+6	1.93E+1	1.35E+1	7.11E+0	4.88E+0	4.14E+0	1.85E+0	3.48E-1	5.11E+1
14-SI-32	2.49E+2	5.62E-1	3.93E-1	2.01E-1	1.40E-1	2.56E-1	7.29E-1	2.19E-1	2.50E+0
17-CL-36	4.35E+5	8.93E+2	6.24E+2	3.30E+2	2.27E+2	2.62E+2	1.40E+2	5.98E+0	2.48E+3
18-AR-39	3.89E+2	4.95E+4	3.46E+4	1.83E+4	1.26E+4	3.74E+1	1.95E+1	1.88E+0	1.15E+5
18-AR-42	4.76E+1	1.12E+1	7.81E+0	4.13E+0	2.83E+0	2.44E+0	1.08E+0	1.63E-1	2.97E+1
19-K-40	1.85E+9	2.42E+3	1.69E+3	8.90E+2	5.76E+2	3.90E+2	1.93E+2	1.01E+1	6.17E+3
20-CA-41	1.49E+5	3.14E+2	2.19E+2	1.16E+2	2.36E+2	3.00E+2	1.62E+2	1.46E+1	1.36E+3
22-TI-44	7.09E+1	7.11E+1	4.96E+1	2.62E+1	1.81E+1	7.47E+1	7.68E+1	4.52E+0	3.21E+2
23-V-49	1.34E+0	2.67E+2	1.86E+2	2.32E+3	2.24E+3	1.18E+3	6.22E+2	4.87E+1	6.86E+3
23-V-50	2.02E+17	1.97E+3	1.11E+3	3.63E+4	1.23E+3	4.17E+2	4.11E+2	1.94E+1	4.14E+4
25-MN-53	5.41E+6	4.25E+3	2.97E+3	4.94E+3	2.87E+3	1.56E+3	9.98E+2	7.83E+1	1.77E+4
25-MN-54	1.24E+0	5.96E+2	4.16E+2	6.17E+3	3.23E+3	1.77E+3	6.84E+2	2.61E+1	1.29E+4
26-FE-55	3.95E+0	3.80E+2	2.66E+2	1.25E+3	1.15E+3	6.45E+2	4.74E+2	2.61E+1	4.19E+3
26-FE-60	2.17E+6	3.94E+1	2.75E+1	1.46E+1	1.00E+1	3.27E+1	4.00E+1	2.59E+0	1.67E+2
27-CO-57	1.08E+0	3.20E+2	2.24E+2	6.09E+3	2.60E+3	1.47E+3	1.10E+3	9.16E+1	1.19E+4
27-CO-60	7.62E+0	1.07E+2	7.49E+1	6.75E+2	2.09E+2	1.18E+2	7.22E+1	3.85E+0	1.26E+3
28-NI-59	1.10E+5	4.58E+3	4.86E+3	7.60E+4	1.39E+3	8.15E+2	4.61E+2	1.97E+1	8.81E+4
28-NI-63	1.45E+2	1.25E+3	8.70E+2	5.99E+2	4.91E+2	3.15E+2	9.20E+1	6.20E+0	3.62E+3
32-GE-68	1.07E+0	2.60E+2	1.82E+2	9.61E+1	6.68E+2	5.07E+2	5.92E+2	4.91E+1	2.35E+3
34-SE-79	9.40E+5	2.04E+3	1.08E+4	1.13E+4	5.28E+3	4.10E+3	2.33E+3	9.02E+1	3.60E+4
34-SE-82	2.02E+20	1.73E+0	1.20E+0	4.36E+2	2.49E+2	2.65E+2	4.98E+2	4.15E+1	1.49E+3
36-KR-81	3.31E+5	7.96E+2	2.90E+4	9.93E+3	3.65E+3	2.07E+3	1.51E+3	9.42E+1	4.71E+4
36-KR-85	1.56E+1	6.31E+1	4.40E+1	2.33E+1	1.18E+3	6.22E+2	4.34E+2	4.31E+1	2.41E+3
37-RB-87	6.87E+10	4.51E+0	3.71E+0	1.71E+3	7.30E+1	2.14E+2	1.74E+2	1.10E+1	2.20E+3
38-SR-90	4.16E+1	5.38E-1	3.75E-1	1.98E-1	4.59E+1	1.31E+2	1.97E+2	1.44E+1	3.89E+2
40-ZR-93	2.21E+6	2.36E+1	7.43E+1	6.48E+3	1.13E+3	6.93E+2	6.00E+2	9.08E+1	9.09E+3
41-NB-91	9.83E+2	2.28E+2	1.59E+2	4.28E+3	1.97E+3	1.09E+3	7.72E+2	7.23E+1	8.58E+3
41-NB-92	5.02E+7	4.12E+2	1.03E+4	1.11E+4	3.57E+3	2.11E+3	1.60E+3	1.20E+2	2.91E+4

Nuclide	1/e Life Time (Years)	Capture Event Rate per gram per 3 x 10^{13} protons (continued) Energy bins in eV							
		1 to 10	10 to 10^2	10^2 to 10^3	10^3 to 10^4	10^4 to 10^5	10^5 to 10^6	10^6 to 10^7	Total
41-NB-93*	2.33E+1	3.94E+1	1.77E+2	2.93E+3	3.53E+3	1.87E+3	1.60E+3	6.42E+1	1.02E+4
41-NB-94	2.94E+4	8.37E+2	3.04E+4	6.33E+3	3.72E+3	2.70E+3	9.48E+2	5.23E+1	4.50E+4
42-MO-93	5.78E+3	3.37E+2	1.57E+3	3.88E+3	1.27E+3	7.45E+2	6.11E+2	5.31E+1	8.46E+3
43-TC-97	3.76E+6	6.12E+2	5.06E+4	1.55E+4	5.40E+3	3.33E+3	2.82E+3	1.80E+2	7.85E+4
43-TC-98	6.07E+6	4.92E+4	6.12E+4	2.21E+4	8.64E+3	5.14E+3	3.09E+3	7.30E+1	1.49E+5
43-TC-99	3.05E+5	4.68E+4	1.20E+4	5.10E+3	5.96E+3	6.20E+3	4.50E+3	2.53E+2	8.09E+4
44-RU-106	1.48E+0	4.45E+0	3.10E+0	3.85E+2	1.13E+3	7.19E+2	6.31E+2	4.24E+1	2.91E+3
45-RH-101	4.77E+0	6.51E+3	6.66E+4	2.16E+4	7.91E+3	5.52E+3	5.17E+3	2.92E+2	1.14E+5
45-RH-102*	4.19E+0	9.87E+4	6.42E+4	2.86E+4	1.42E+4	9.77E+3	8.27E+3	2.20E+2	2.24E+5
46-PD-107	9.40E+6	8.18E+2	2.26E+4	1.62E+4	9.90E+3	9.27E+3	7.66E+3	2.71E+2	6.67E+4
47-AG-108*	6.04E+2	1.14E+5	7.14E+4	3.01E+4	1.39E+4	9.70E+3	6.43E+3	1.72E+2	2.45E+5
48-CD-109	1.83E+0	3.66E+4	2.88E+4	1.16E+4	5.10E+3	3.46E+3	3.11E+3	1.66E+2	8.88E+4
48-CD-113	1.35E+16	5.00E+3	6.72E+3	3.46E+3	4.47E+3	4.59E+3	4.19E+3	1.71E+2	2.86E+4
48-CD-113*	2.04E+1	4.98E+3	6.62E+3	5.51E+3	4.32E+3	2.88E+3	2.57E+3	1.48E+2	2.70E+4
49-IN-115	6.38E+14	3.24E+5	4.86E+3	5.29E+3	5.45E+3	5.19E+3	5.41E+3	5.48E+2	3.51E+5
50-SN-119*	1.16E+0	9.47E+1	4.80E+1	5.81E+2	7.44E+2	3.85E+2	2.60E+2	2.26E+1	2.13E+3
50-SN-121*	7.95E+1	4.47E+2	1.11E+4	5.16E+3	1.80E+3	1.11E+3	8.02E+2	5.85E+1	2.05E+4
50-SN-126	1.45E+5	2.31E+0	1.61E+0	8.51E-1	7.05E+1	6.39E+1	1.06E+2	1.56E+1	2.61E+2
51-SB-125	3.99E+0	1.29E+2	1.01E+4	5.41E+3	3.30E+3	3.28E+3	3.23E+3	3.70E+2	2.58E+4
52-TE-123	1.45E+13	5.92E+5	2.81E+4	1.28E+4	6.18E+3	4.98E+3	5.08E+3	2.73E+2	6.49E+5
52-TE-130	1.81E+21	6.21E+0	2.63E+0	2.12E-1	7.25E+1	6.47E+1	1.47E+2	1.58E+1	3.09E+2
53-I-129	2.27E+7	3.97E+2	2.68E+3	5.58E+3	2.71E+3	2.65E+3	2.37E+3	1.55E+2	1.65E+4
55-CS-134	2.98E+0	2.26E+3	2.87E+3	1.64E+4	1.08E+4	6.52E+3	3.42E+3	9.41E+1	4.23E+4
55-CS-135	3.33E+6	1.73E+2	1.15E+4	5.89E+3	1.85E+3	1.23E+3	1.06E+3	5.80E+1	2.17E+4
55-CS-137	4.35E+1	3.34E+0	2.40E+0	2.60E+2	3.21E+2	1.67E+2	1.40E+2	2.09E+1	9.15E+2
56-BA-133	1.52E+1	5.33E+2	1.13E+4	7.61E+3	2.75E+3	1.49E+3	9.47E+2	8.19E+1	2.47E+4
57-LA-137	8.68E+4	4.51E+2	3.45E+4	1.28E+4	4.54E+3	2.51E+3	1.99E+3	1.10E+2	5.69E+4
57-LA-138	1.52E+11	3.23E+4	7.13E+3	6.82E+3	2.31E+3	1.74E+3	1.41E+3	6.46E+1	5.18E+4
58-CE-144	1.13E+0	2.53E+1	1.76E+1	7.30E+2	2.57E+2	2.64E+2	3.36E+2	1.45E+1	1.64E+3
60-ND-144	3.31E+15	7.98E+1	5.31E+1	7.49E+2	5.36E+2	3.65E+2	6.62E+2	7.53E+1	2.52E+3
61-PM-143	1.05E+0	3.39E+2	1.29E+4	8.44E+3	2.98E+3	1.81E+3	1.33E+3	1.12E+2	2.80E+4
61-PM-144	1.44E+0	4.82E+4	4.55E+4	1.67E+4	6.86E+3	4.65E+3	3.12E+3	1.54E+2	1.25E+5
61-PM-145	2.56E+1	2.60E+4	4.76E+4	1.51E+4	5.58E+3	3.64E+3	2.63E+3	2.23E+2	1.01E+5

Nuclide	1/e Life Time (Years)	Capture Event Rate per gram per 3 x 10^{13} protons (continued) Energy bins in eV							
		1 to 10	10 to 10^2	10^2 to 10^3	10^3 to 10^4	10^4 to 10^5	10^5 to 10^6	10^6 to 10^7	Total
61-PM-146	8.00E+0	8.45E+4	5.29E+4	2.19E+4	1.01E+4	7.31E+3	5.86E+3	1.60E+2	1.83E+5
61-PM-147	3.79E+0	2.36E+5	4.11E+4	2.42E+4	1.14E+4	5.83E+3	6.55E+3	3.64E+2	3.26E+5
62-SM-145	1.35E+0	1.74E+4	2.07E+4	6.20E+3	2.24E+3	1.48E+3	1.52E+3	1.87E+2	4.97E+4
62-SM-146	1.49E+8	3.23E+2	2.26E+2	1.75E+3	1.04E+3	8.20E+2	1.09E+3	1.01E+2	5.35E+3
62-SM-147	1.53E+11	2.24E+4	1.07E+5	3.23E+4	9.17E+3	5.20E+3	4.56E+3	2.26E+2	1.80E+5
62-SM-148	1.01E+16	5.00E+1	7.22E+3	3.73E+3	1.84E+3	1.23E+3	2.10E+3	2.24E+2	1.64E+4
62-SM-151	1.30E+2	1.82E+5	1.49E+5	4.24E+4	1.67E+4	1.00E+4	5.27E+3	1.66E+2	4.06E+5
63-EU-150	5.18E+1	9.17E+4	5.97E+4	2.67E+4	1.35E+4	1.28E+4	1.14E+4	3.17E+2	2.16E+5
63-EU-152	1.96E+1	9.81E+4	1.02E+5	5.48E+4	3.51E+4	2.67E+4	2.17E+4	4.75E+2	3.39E+5
63-EU-154	1.24E+1	7.07E+4	6.32E+4	4.35E+4	2.34E+4	1.50E+4	1.17E+4	1.93E+2	2.28E+5
63-EU-155	6.77E+0	2.61E+4	6.78E+4	4.90E+4	2.27E+4	1.09E+4	1.02E+4	2.58E+3	1.89E+5
64-GD-148	1.08E+2	5.39E+2	7.56E+3	4.92E+3	1.82E+3	1.52E+3	2.22E+3	2.47E+2	1.88E+4
64-GD-150	2.59E+6	6.72E+2	1.34E+4	6.59E+3	2.39E+3	2.00E+3	2.93E+3	2.85E+2	2.83E+4
64-GD-152	1.56E+14	5.75E+4	7.50E+4	1.62E+4	5.55E+3	4.85E+3	7.29E+3	7.23E+2	1.67E+5
65-TB-157	1.43E+2	8.53E+4	5.73E+4	2.74E+4	1.53E+4	1.20E+4	1.38E+4	6.81E+2	2.12E+5
65-TB-158	2.60E+2	8.09E+4	5.57E+4	2.83E+4	1.78E+4	1.56E+4	1.65E+4	3.66E+2	2.15E+5
66-DY-154	4.34E+6	3.89E+4	3.74E+4	1.44E+4	6.16E+3	4.85E+3	7.41E+3	8.76E+2	1.10E+5
67-HO-163	6.61E+3	6.57E+4	4.27E+4	1.91E+4	9.54E+3	7.09E+3	6.90E+3	2.53E+2	1.51E+5
67-HO-166*	1.74E+3	2.92E+4	5.61E+4	1.95E+4	7.65E+3	5.83E+3	3.55E+3	1.25E+2	1.22E+5
69-TM-171	2.78E+0	1.49E+4	4.11E+4	2.19E+4	7.82E+3	4.36E+3	3.19E+3	2.69E+2	9.35E+4
71-LU-173	1.98E+0	6.91E+4	4.28E+4	1.75E+4	7.88E+3	5.56E+3	4.08E+3	2.07E+2	1.47E+5
71-LU-174	4.79E+0	9.58E+4	5.74E+4	2.22E+4	9.49E+3	6.48E+3	4.74E+3	1.76E+2	1.96E+5
71-LU-176	5.47E+10	4.42E+4	4.79E+4	2.04E+4	9.16E+3	9.90E+3	5.09E+3	1.33E+2	1.37E+5
72-HF-172	2.70E+0	7.39E+2	2.54E+4	7.87E+3	2.89E+3	2.34E+3	2.34E+3	2.52E+2	4.19E+4
72-HF-174	2.89E+15	1.36E+3	3.13E+4	1.43E+4	6.57E+3	4.26E+3	5.89E+3	8.95E+2	6.46E+4
72-HF-178**	4.48E+1	1.83E+5	8.56E+2	3.62E+3	1.60E+3	1.14E+3	1.08E+3	1.64E+2	1.91E+5
72-HF-182	1.30E+7	2.49E+2	1.74E+2	1.27E+3	8.11E+2	6.18E+2	3.21E+2	4.28E+1	3.48E+3
73-TA-179	2.59E+0	7.84E+4	4.65E+4	1.78E+4	7.46E+3	4.78E+3	3.11E+3	1.30E+2	1.58E+5
75-RE-186*	2.89E+5	6.86E+4	1.24E+5	3.75E+4	1.36E+4	9.13E+3	4.03E+3	1.53E+2	2.57E+5
75-RE-187	6.29E+10	4.10E+3	2.91E+4	2.40E+4	6.28E+3	3.61E+3	3.73E+3	1.60E+2	7.11E+4
76-OS-186	2.89E+15	7.99E+2	4.62E+4	9.70E+3	2.48E+3	1.78E+3	1.33E+3	1.18E+2	6.24E+4
76-OS-194	8.68E+0	7.50E+1	5.24E+1	2.77E+1	1.28E+2	1.37E+2	4.58E+1	6.56E+0	4.72E+2
77-IR-192**	3.49E+2	1.68E+5	1.74E+5	5.51E+4	2.02E+4	1.34E+4	1.12E+4	2.25E+2	4.41E+5

Nuclide	1/e Life Time (Years)	Capture Event Rate per gram per 3 x 10^{13} protons (continued) Energy bins in eV							
		1 to 10	10 to 10^2	10^2 to 10^3	10^3 to 10^4	10^4 to 10^5	10^5 to 10^6	10^6 to 10^7	Total
78-PT-190	9.40E+11	1.52E+3	9.05E+3	3.74E+3	1.42E+3	1.21E+3	1.26E+3	7.45E+1	1.83E+4
78-PT-193	7.23E+1	5.03E+2	2.80E+4	9.83E+3	2.94E+3	1.48E+3	7.37E+2	8.40E+1	4.36E+4
80-HG-194	7.52E+2	3.86E+2	1.75E+3	3.37E+3	1.30E+3	1.10E+3	1.30E+3	1.41E+2	9.34E+3
81-TL-204	5.47E+0	3.40E+2	2.38E+2	1.16E+3	7.68E+2	5.03E+2	4.34E+2	1.92E+1	3.46E+3
82-PB-202	7.59E+4	1.26E+2	8.78E+1	6.52E+1	3.49E+2	2.76E+2	3.26E+2	2.76E+1	1.26E+3
82-PB-205	2.21E+7	7.86E+1	5.50E+1	3.51E+2	3.27E+2	2.02E+2	1.70E+2	8.51E+0	1.19E+3
82-PB-210	3.23E+1	7.65E+0	5.34E+0	2.82E+0	1.95E+0	1.67E+0	1.25E+0	6.86E-2	2.08E+1
83-BI-207	4.56E+1	9.52E+1	6.65E+1	7.86E+2	6.74E+2	4.44E+2	4.34E+2	2.51E+1	2.53E+3
83-BI-208	5.32E+5	8.70E+1	6.08E+1	6.22E+2	6.06E+2	3.94E+2	3.05E+2	1.69E+1	2.09E+3
83-BI-210*	4.40E+6	8.26E-1	5.78E-1	3.05E-1	2.12E-1	1.05E+1	1.21E+1	2.80E-1	2.47E+1
84-PO-208	4.19E+0	6.10E+1	4.26E+1	2.25E+1	5.06E+1	1.10E+2	1.38E+2	8.72E+0	4.33E+2
84-PO-209	1.48E+2	6.05E+1	4.23E+1	2.23E+1	9.36E+1	1.08E+2	1.17E+2	6.79E+0	4.50E+2
88-RA-226	2.31E+3	3.45E+1	3.38E+3	2.07E+3	1.90E+3	1.50E+3	1.27E+3	1.99E+2	1.04E+4
88-RA-228	8.31E+0	5.07E+2	3.54E+2	1.87E+2	1.13E+2	1.51E+1	3.55E+0	7.58E-1	1.18E+3
89-AC-227	3.15E+1	6.24E+4	5.09E+4	1.71E+3	6.20E+2	2.99E+2	6.90E+1	3.98E+0	1.16E+5
90-TH-228	2.77E+0	6.07E+4	1.61E+4	4.63E+3	1.71E+3	1.44E+3	1.28E+3	1.40E+2	8.60E+4
90-TH-229	1.06E+4	2.15E+4	2.91E+4	1.36E+4	7.09E+3	4.64E+3	4.33E+3	3.01E+2	8.06E+4
90-TH-230	1.09E+5	3.95E+4	3.13E+4	3.73E+3	1.68E+3	1.44E+3	1.46E+3	1.49E+2	7.93E+4
90-TH-232	2.03E+10	5.23E+1	6.92E+3	3.95E+3	1.32E+3	1.49E+3	1.46E+3	1.39E+2	1.53E+4
91-PA-231	4.74E+4	1.84E+4	2.39E+4	1.07E+4	6.74E+3	6.98E+3	6.61E+3	3.34E+2	7.36E+4
92-U-232	9.96E+1	8.76E+3	5.61E+3	2.97E+3	2.25E+3	9.07E+2	3.79E+2	5.13E+1	2.09E+4
92-U-233	2.30E+5	5.79E+3	3.46E+3	1.36E+3	7.51E+2	1.03E+3	1.63E+3	9.00E+1	1.41E+4
92-U-234	3.54E+5	4.09E+4	9.81E+3	5.58E+3	2.07E+3	1.83E+3	2.26E+3	4.23E+2	6.29E+4
92-U-235	1.02E+9	3.20E+3	8.34E+3	3.36E+3	2.37E+3	2.23E+3	2.21E+3	1.20E+2	2.18E+4
92-U-236	3.39E+7	2.13E+4	1.03E+4	5.33E+3	1.94E+3	2.05E+3	2.88E+3	3.02E+2	4.42E+4
92-U-238	6.46E+9	1.10E+4	2.01E+4	7.31E+3	1.25E+3	1.33E+3	1.20E+3	1.11E+2	4.23E+4
93-NP-235	1.57E+0	2.05E+3	1.70E+4	8.91E+3	3.33E+3	1.63E+3	3.73E+2	3.96E+1	3.33E+4
93-NP-236	2.23E+5	7.36E+3	6.05E+3	3.20E+3	2.20E+3	2.05E+3	3.60E+3	2.99E+2	2.48E+4
93-NP-237	3.09E+6	1.81E+4	2.49E+4	1.11E+4	6.92E+3	6.72E+3	5.92E+3	1.48E+2	7.37E+4
94-PU-236	4.13E+0	1.29E+4	1.23E+4	4.56E+3	1.85E+3	1.50E+3	1.14E+3	4.75E+1	3.43E+4
94-PU-238	1.27E+2	3.02E+3	7.84E+3	7.08E+3	2.37E+3	2.30E+3	2.00E+3	6.76E+1	2.47E+4
94-PU-239	3.49E+4	2.00E+3	1.34E+4	6.12E+3	2.85E+3	1.78E+3	1.59E+3	7.17E+1	2.78E+4
94-PU-240	9.49E+3	3.45E+5	1.89E+4	6.32E+3	1.93E+3	2.22E+3	1.71E+3	1.01E+2	3.77E+5

Nuclide	1/e Life Time (Years)	Capture Event Rate per gram per 3×10^{13} protons (continued) Energy bins in eV							
		1 to 10	10 to 10^2	10^2 to 10^3	10^3 to 10^4	10^4 to 10^5	10^5 to 10^6	10^6 to 10^7	Total
94-PU-241	2.08E+1	5.65E+3	8.26E+3	2.50E+3	1.74E+3	1.58E+3	1.54E+3	1.24E+2	2.14E+4
94-PU-242	5.40E+5	6.25E+4	6.49E+3	2.63E+3	2.14E+3	2.09E+3	1.49E+3	1.24E+2	7.75E+4
94-PU-244	1.17E+8	1.60E+1	1.06E+4	4.16E+3	1.28E+3	5.97E+2	3.90E+2	1.67E+1	1.70E+4
95-AM-241	6.26E+2	3.60E+4	1.83E+4	1.21E+4	7.69E+3	7.16E+3	6.65E+3	1.98E+2	8.80E+4
95-AM-242*	2.04E+2	6.89E+3	7.82E+3	3.97E+3	2.46E+3	1.51E+3	5.40E+2	1.31E+1	2.32E+4
95-AM-243	1.07E+4	7.94E+4	2.15E+4	1.07E+4	6.35E+3	6.47E+3	4.54E+3	1.13E+2	1.29E+5
96-CM-243	4.21E+1	8.14E+3	4.03E+3	2.32E+3	1.62E+3	1.47E+3	1.49E+3	1.54E+2	1.92E+4
96-CM-244	2.62E+1	4.94E+4	5.99E+3	4.93E+3	2.76E+3	2.82E+3	2.60E+3	2.12E+2	6.88E+4
96-CM-245	1.23E+4	4.18E+3	3.50E+3	1.83E+3	1.07E+3	1.45E+3	1.82E+3	6.80E+1	1.39E+4
96-CM-246	6.84E+3	5.20E+3	5.05E+3	1.25E+3	1.57E+3	1.35E+3	1.06E+3	7.93E+1	1.56E+4
96-CM-247	2.26E+7	2.35E+4	4.19E+3	1.31E+3	1.13E+3	2.51E+3	2.04E+3	7.12E+1	3.47E+4
96-CM-248	4.92E+5	9.98E+3	1.55E+4	8.49E+2	9.61E+2	9.76E+2	7.88E+2	7.45E+1	2.91E+4
96-CM-250	1.40E+4	5.16E+0	1.04E+2	1.22E+3	6.65E+2	4.34E+2	2.36E+2	1.63E+1	2.68E+3
97-BK-247	2.00E+3	1.03E+4	1.43E+4	3.49E+3	1.26E+3	6.90E+2	2.09E+2	2.18E+1	3.03E+4
97-BK-248	1.30E+1	3.38E+3	1.02E+4	2.34E+3	9.36E+2	5.21E+2	4.14E+2	3.46E+1	1.78E+4
97-BK-249	1.27E+0	4.55E+4	2.31E+4	1.07E+4	6.01E+3	5.59E+3	3.49E+3	2.02E+2	9.46E+4
98-CF-248	1.32E+0	3.38E+3	1.02E+4	2.34E+3	9.36E+2	5.21E+2	4.14E+2	3.46E+1	1.78E+4
98-CF-249	5.08E+2	3.41E+3	4.30E+3	2.65E+3	1.51E+3	2.48E+3	4.16E+3	3.06E+2	1.88E+4
98-CF-250	1.89E+1	1.88E+5	1.61E+4	5.88E+3	2.57E+3	2.47E+3	2.05E+3	1.11E+2	2.17E+5
98-CF-251	1.30E+3	8.09E+3	7.30E+3	3.18E+3	1.53E+3	1.33E+3	6.55E+2	2.79E+1	2.21E+4
98-CF-252	3.83E+0	4.54E+2	3.30E+3	7.07E+2	1.48E+3	1.38E+3	1.02E+3	6.06E+1	8.40E+3
99-ES-252	1.87E+0	3.33E+3	10.00E+3	2.30E+3	9.21E+2	5.12E+2	4.07E+2	3.41E+1	1.75E+4
99-ES-254	1.09E+0	2.63E+2	5.39E+2	6.64E+2	1.13E+3	1.97E+3	2.50E+3	1.60E+1	7.08E+3

Table 3. Total fission event rates per gram (3 x10^{13} protons at 24 GeV) for Actinides with a 1/e life time > 1 year

Nuclide	1/e Life Time (Years)	Fission Event Rate per gram per 3 x 10^{13} protons Energy bins in eV							
		1 to 10	10 to 10^2	10^2 to 10^3	10^3 to 10^4	10^4 to 10^5	10^5 to 10^6	10^6 to 10^7	Total
88-RA-228	8.31E+0	4.62E-6	9.66E-6	9.65E-6	6.25E-7	1.71E-6	4.88E-6	8.75E+2	8.75E+2
89-AC-227	3.15E+1	4.12E-3	3.18E-3	4.45E-3	1.01E-2	2.77E-2	5.88E-1	1.96E+1	2.02E+1
90-TH-228	2.77E+0	4.24E+0	2.96E+0	1.56E+0	4.54E-1	0.00E+0	5.31E+1	2.20E+2	2.82E+2
90-TH-229	1.06E+4	2.14E+4	3.46E+3	1.94E+3	2.01E+3	3.26E+3	6.23E+3	7.84E+2	3.91E+4
90-TH-230	1.09E+5	0.00E+0	0.00E+0	0.00E+0	0.00E+0	0.00E+0	5.24E+1	4.11E+2	4.63E+2
90-TH-232	2.03E+10	0.00E+0	0.00E+0	0.00E+0	0.00E+0	0.00E+0	1.08E+0	1.40E+2	1.41E+2
91-PA-231	4.74E+4	1.11E+0	2.54E+0	4.48E-1	3.88E-1	1.52E+0	2.00E+3	1.72E+3	3.73E+3
92-U-232	9.96E+1	5.82E+3	2.99E+4	5.21E+3	2.41E+3	6.86E+3	2.01E+4	3.47E+3	7.38E+4
92-U-233	2.30E+5	2.68E+4	2.25E+4	1.03E+4	7.77E+3	9.47E+3	2.06E+4	3.31E+3	1.01E+5
92-U-234	3.54E+5	3.14E+1	3.57E+0	1.28E+2	1.29E+1	5.86E+1	3.86E+3	2.38E+3	6.47E+3
92-U-235	1.02E+9	5.58E+3	1.39E+4	8.54E+3	5.86E+3	7.00E+3	1.24E+4	2.08E+3	5.54E+4
92-U-236	3.39E+7	2.52E+2	1.64E+2	9.31E+1	2.72E+1	2.32E+1	2.84E+2	1.23E+3	2.08E+3
92-U-238	6.46E+9	5.52E-3	3.46E-2	4.29E-2	4.60E-1	2.42E-1	1.13E+1	5.28E+2	5.40E+2
93-NP-235	1.57E+0	1.15E+2	1.03E+2	6.97E+1	1.01E+2	2.77E+2	7.88E+2	3.39E+3	4.85E+3
93-NP-236	2.23E+5	2.91E+4	2.39E+4	1.27E+4	8.70E+3	8.93E+3	1.98E+4	3.25E+3	1.06E+5
93-NP-237	3.09E+6	1.10E+0	1.46E+1	1.20E+1	1.22E+1	4.00E+1	3.46E+3	2.65E+3	6.19E+3
94-PU-236	4.13E+0	1.29E+4	1.23E+4	4.21E+3	2.68E+3	3.72E+3	1.42E+4	4.18E+3	5.42E+4
94-PU-238	1.27E+2	2.26E+2	6.08E+2	3.26E+3	1.40E+3	2.44E+3	1.16E+4	3.65E+3	2.32E+4
94-PU-239	3.49E+4	3.67E+3	1.81E+4	7.31E+3	3.88E+3	5.74E+3	1.51E+4	3.15E+3	5.70E+4
94-PU-240	9.49E+3	6.78E+1	3.80E+1	1.48E+2	1.20E+2	3.09E+2	3.66E+3	2.70E+3	7.04E+3
94-PU-241	2.08E+1	2.25E+4	2.40E+4	1.05E+4	7.50E+3	8.83E+3	1.64E+4	2.68E+3	9.24E+4
94-PU-242	5.40E+5	5.01E+0	1.22E+0	2.49E+1	1.43E+1	4.21E+1	2.30E+3	2.38E+3	4.77E+3
94-PU-244	1.17E+8	0.00E+0	0.00E+0	5.08E-1	1.56E+1	5.16E+1	1.65E+3	2.14E+3	3.85E+3
95-AM-241	6.26E+2	2.73E+2	8.97E+1	6.38E+1	4.15E+1	5.26E+1	1.45E+3	2.92E+3	4.89E+3
95-AM-242*	2.04E+2	5.04E+4	4.51E+4	2.33E+4	1.50E+4	1.31E+4	2.34E+4	3.61E+3	1.74E+5
95-AM-243	1.07E+4	7.17E+1	5.57E+1	4.93E+1	3.30E+1	3.83E+1	9.51E+2	2.42E+3	3.62E+3
96-CM-243	4.21E+1	6.84E+4	2.36E+4	1.14E+4	9.22E+3	1.04E+4	1.98E+4	3.21E+3	1.46E+5
96-CM-244	2.62E+1	1.62E+2	3.07E+2	1.12E+2	2.05E+2	2.17E+2	4.24E+3	3.04E+3	8.29E+3
96-CM-245	1.23E+4	3.01E+4	1.73E+4	1.04E+4	7.44E+3	9.14E+3	1.77E+4	2.80E+3	9.48E+4

Nuclide	1/e Life Time (Years)	Fission Event Rate per gram per 3 x 10^{13} protons (continued) Energy bins in eV							
		1 to 10	10 to 10^2	10^2 to 10^3	10^3 to 10^4	10^4 to 10^5	10^5 to 10^6	10^6 to 10^7	Total
96-CM-246	6.84E+3	2.03E+2	5.70E+1	6.65E+1	1.02E+2	1.20E+2	1.66E+3	2.59E+3	4.80E+3
96-CM-247	2.26E+7	2.43E+4	9.11E+3	7.89E+3	4.91E+3	6.95E+3	1.85E+4	3.05E+3	7.46E+4
96-CM-248	4.92E+5	3.43E+2	5.73E+2	2.63E+1	3.09E+1	1.14E+2	2.09E+3	2.81E+3	5.98E+3
96-CM-250	1.40E+4	2.58E-2	4.93E+0	7.81E+1	7.16E+1	1.27E+2	2.08E+3	2.62E+3	4.98E+3
97-BK-247	2.00E+3	5.15E+2	1.08E+3	1.07E+3	2.13E+1	5.83E+1	1.66E+2	3.23E+3	6.13E+3
97-BK-248	1.30E+1	1.05E+5	2.19E+5	2.17E+5	4.33E+3	1.19E+4	3.38E+4	3.22E+3	5.93E+5
97-BK-249	1.27E+0	2.63E+2	1.28E+2	5.98E+1	3.37E+1	3.31E+1	4.11E+2	1.95E+3	2.88E+3
98-CF-248	1.32E+0	7.32E+3	1.53E+4	1.52E+4	3.03E+2	8.30E+2	2.36E+3	3.22E+3	4.45E+4
98-CF-249	5.08E+2	1.19E+4	1.96E+4	1.06E+4	6.73E+3	9.05E+3	1.74E+4	2.74E+3	7.81E+4
98-CF-250	1.89E+1	4.33E+2	3.71E+1	1.50E+1	6.96E+0	1.02E+1	4.02E+3	3.70E+3	8.23E+3
98-CF-251	1.30E+3	1.39E+4	1.25E+4	6.39E+3	4.03E+3	7.96E+3	2.26E+4	3.86E+3	7.13E+4
98-CF-252	3.83E+0	1.50E+3	6.23E+3	7.78E+2	1.80E+3	2.93E+3	1.33E+4	3.89E+3	3.04E+4
99-ES-252	1.87E+0	6.92E+5	1.45E+6	1.43E+6	5.96E+2	1.63E+3	4.65E+3	3.17E+3	3.57E+6
99-ES-254	1.09E+0	4.57E+4	2.63E+4	5.10E+3	3.62E+3	7.07E+3	2.01E+4	3.42E+3	1.11E+5

Table 4. *Total capture event rates per gram (3 x10^{13} protons at 24 GeV) for stable nuclides*

Nuclide	1/e Life Time (Years)	Capture Event Rate per gram per 3 x 10^{13} protons Energy bins in eV							
		1 to 10	10 to 10^2	10^2 to 10^3	10^3 to 10^4	10^4 to 10^5	10^5 to 10^6	10^6 to 10^7	Total
1-H-1	Stable	1.06E+3	7.42E+2	3.91E+2	2.68E+2	1.87E+2	1.19E+2	1.37E+1	2.78E+3
1-H-2	Stable	8.09E-1	5.63E-1	2.96E-1	2.13E-1	5.45E-1	4.24E+0	1.47E+0	8.14E+0
2-HE-3	Stable	3.31E-2	2.84E-2	4.35E-2	9.88E-2	2.70E-1	7.56E-1	1.18E-1	1.35E+0
2-HE-4	Stable	0.00E+0	0.00E+0	0.00E+0	0.00E+0	0.00E+0	0.00E+0	0.00E+0	0.00E+0
3-LI-6	Stable	2.07E+1	1.44E+1	7.61E+0	5.24E+0	4.50E+0	6.99E+0	1.77E+0	6.12E+1
3-LI-7	Stable	2.09E+1	1.46E+1	7.26E+0	5.84E+0	5.52E+0	5.46E+0	2.75E-1	5.98E+1
4-BE-9	Stable	2.72E+0	1.90E+0	1.60E+0	3.31E+0	9.08E+0	2.58E+1	4.43E+0	4.89E+1
5-B-10	Stable	1.60E+2	1.11E+2	5.87E+1	4.02E+1	3.45E+1	3.07E+1	0.00E+0	4.36E+2
5-B-11	Stable	1.61E+0	1.13E+0	5.94E-1	4.18E-1	2.95E+0	9.30E-1	6.45E-2	7.70E+0
6-C-12	Stable	9.50E-1	6.63E-1	3.63E-1	3.22E-1	8.89E-1	4.11E+0	7.86E-1	8.08E+0
6-C-13	Stable	3.37E+0	2.36E+0	1.26E+0	1.02E+0	4.75E+0	6.60E+2	2.42E+0	6.75E+2
7-N-14	Stable	1.72E+1	1.20E+1	6.37E+0	4.39E+0	3.79E+0	8.26E+0	7.64E+0	5.97E+1
7-N-15	Stable	5.22E-3	3.64E-3	1.93E-3	1.34E-3	1.30E-3	4.59E-2	4.10E-2	1.00E-1
8-O-16	Stable	3.91E-2	3.12E-2	3.51E-2	1.65E-1	1.35E+0	1.08E+1	2.49E+0	1.50E+1
8-O-17	Stable	7.24E-1	5.04E-1	2.66E-1	1.82E-1	1.56E-1	1.11E+1	4.93E+0	1.79E+1
8-O-18	Stable	3.41E-2	2.38E-2	1.26E-2	8.65E-3	7.45E-3	7.04E-3	1.59E-1	2.52E-1
9-F-19	Stable	1.62E+0	1.14E+0	6.54E-1	8.84E-1	3.13E+2	4.28E+1	1.96E+0	3.63E+2
10-NE-20	Stable	5.94E+0	4.14E+0	2.18E+0	1.41E+0	7.74E-1	2.29E+0	1.74E+0	1.85E+1
10-NE-21	Stable	1.02E+2	7.10E+1	3.63E+1	1.84E+1	3.92E+0	1.44E+1	1.47E+0	2.48E+2
10-NE-22	Stable	6.66E+0	4.64E+0	2.45E+0	1.63E+0	1.10E+0	4.49E+0	3.46E-1	2.13E+1
11-NA-23	Stable	7.47E+1	5.32E+1	3.68E+1	3.46E+2	1.82E+1	6.20E+1	2.85E+0	5.94E+2
12-MG-24	Stable	6.77E+0	4.73E+0	2.51E+0	1.88E+0	1.04E+2	4.80E+1	3.96E+0	1.72E+2
12-MG-25	Stable	2.45E+1	1.71E+1	9.07E+0	6.97E+0	1.55E+2	4.60E+1	3.34E+0	2.62E+2
12-MG-26	Stable	4.74E+0	3.30E+0	1.72E+0	1.04E+0	4.70E-1	5.15E+1	4.76E+0	6.75E+1
13-AL-27	Stable	2.57E+1	1.81E+1	9.72E+0	1.18E+2	6.01E+1	1.04E+2	1.92E+0	3.38E+2
14-SI-28	Stable	2.04E+1	1.42E+1	7.51E+0	5.14E+0	3.82E+1	3.40E+1	7.32E+0	1.27E+2
14-SI-29	Stable	1.16E+1	8.19E+0	4.33E+0	3.04E+0	2.85E+1	3.78E+1	3.28E+0	9.68E+1
14-SI-30	Stable	1.26E+1	9.18E+0	5.44E+0	1.84E+3	5.38E+0	6.72E+1	8.08E+0	1.94E+3
15-P-31	Stable	1.88E+1	1.30E+1	6.28E+0	2.30E+0	2.00E+0	8.57E+1	1.63E+1	1.44E+2
16-S-32	Stable	5.31E+1	3.69E+1	1.87E+1	9.70E+0	8.76E+1	6.93E+1	3.08E+0	2.78E+2
16-S-33	Stable	3.42E+1	2.36E+1	1.11E+1	3.56E+0	4.36E+1	1.96E+1	2.07E+0	1.38E+2

Nuclide	1/e Life Time (Years)	Capture Event Rate per gram per 3 x 10^{13} protons (continued) Energy bins in eV							
		1 to 10	10 to 10^2	10^2 to 10^3	10^3 to 10^4	10^4 to 10^5	10^5 to 10^6	10^6 to 10^7	Total
16-S-34	Stable	2.12E+1	1.47E+1	7.31E+0	3.10E+0	4.80E-1	2.95E+1	2.97E+0	7.92E+1
16-S-36	Stable	2.29E+1	2.06E+1	1.40E+1	1.26E+1	1.36E+1	1.57E+1	2.50E+0	1.02E+2
17-CL-35	Stable	3.80E+3	1.80E+3	1.07E+3	1.05E+1	2.16E+2	1.48E+2	1.07E+1	7.05E+3
17-CL-37	Stable	0.00E+0	0.00E+0	0.00E+0	0.00E+0	0.00E+0	4.24E+1	5.12E+0	4.75E+1
18-AR-36	Stable	4.54E+2	3.14E+2	1.55E+2	6.42E+1	1.87E+2	2.55E+2	4.05E+1	1.47E+3
18-AR-38	Stable	6.80E+1	4.69E+1	2.21E+1	6.89E+0	5.58E-1	4.91E+1	8.87E+0	2.02E+2
18-AR-40	Stable	5.30E+1	3.48E+1	1.19E+1	1.62E+0	1.73E+1	2.78E+1	7.88E+0	1.54E+2
19-K-39	Stable	1.73E+2	1.19E+2	5.50E+1	3.30E+2	1.42E+2	1.77E+2	2.53E+1	1.02E+3
19-K-41	Stable	1.15E+2	7.98E+1	4.07E+1	1.07E+3	4.38E+2	5.88E+2	5.44E+1	2.38E+3
20-CA-40	Stable	3.29E+1	2.29E+1	1.20E+1	7.65E+0	5.31E+2	8.32E+1	1.06E+1	7.01E+2
20-CA-42	Stable	5.23E+1	3.60E+1	1.69E+1	1.85E+2	1.22E+2	2.82E+2	2.46E+1	7.19E+2
20-CA-43	Stable	8.71E+2	5.76E+2	2.18E+2	2.43E+3	6.28E+2	2.99E+2	1.09E+1	5.03E+3
20-CA-44	Stable	6.50E+1	4.52E+1	2.26E+1	9.93E+0	4.33E+1	7.07E+1	9.52E+0	2.66E+2
20-CA-46	Stable	5.19E+1	3.63E+1	1.92E+1	2.54E+1	1.58E+1	1.40E+1	1.46E+0	1.64E+2
20-CA-48	Stable	7.33E+1	5.08E+1	2.53E+1	1.06E+1	1.34E+0	6.03E+0	1.48E+0	1.69E+2
21-SC-45	Stable	1.91E+3	1.14E+3	3.12E+2	1.03E+3	1.68E+3	7.65E+2	3.82E+1	6.87E+3
22-TI-46	Stable	4.18E+1	2.90E+1	1.49E+1	1.01E+1	3.48E+2	5.09E+2	2.94E+1	9.82E+2
22-TI-47	Stable	1.17E+2	8.20E+1	1.57E+2	1.56E+3	6.72E+2	5.51E+2	4.48E+1	3.19E+3
22-TI-48	Stable	5.27E+2	3.69E+2	2.02E+2	2.36E+2	6.78E+2	1.94E+2	1.41E+1	2.22E+3
22-TI-49	Stable	1.44E+2	8.71E+1	2.54E+1	2.50E+2	1.95E+2	2.27E+2	2.65E+1	9.54E+2
22-TI-50	Stable	1.15E+1	8.00E+0	4.09E+0	2.08E+0	2.22E+1	2.67E+1	3.44E+0	7.80E+1
23-V-51	Stable	3.11E+2	2.17E+2	1.21E+2	7.52E+2	6.76E+2	1.90E+2	1.26E+1	2.28E+3
24-CR-50	Stable	1.02E+3	6.87E+2	3.26E+2	1.38E+3	4.30E+2	3.58E+2	2.15E+1	4.22E+3
24-CR-52	Stable	4.61E+1	3.19E+1	1.56E+1	2.09E+1	1.04E+2	1.17E+2	1.21E+1	3.47E+2
24-CR-53	Stable	1.09E+3	7.46E+2	3.60E+2	1.34E+3	4.65E+2	1.63E+2	9.60E+0	4.18E+3
24-CR-54	Stable	2.15E+1	1.49E+1	7.36E+0	3.29E+0	1.20E+2	7.01E+1	7.42E+0	2.44E+2
25-MN-55	Stable	7.94E+2	6.11E+2	5.05E+3	1.44E+3	3.65E+2	2.54E+2	1.47E+1	8.53E+3
26-FE-54	Stable	1.54E+2	1.07E+2	5.51E+1	4.32E+2	1.53E+2	2.59E+2	3.96E+1	1.20E+3
26-FE-56	Stable	1.49E+2	1.02E+2	4.39E+1	7.35E+1	1.27E+2	1.52E+2	1.39E+1	6.61E+2
26-FE-57	Stable	1.36E+2	8.88E+1	3.58E+1	5.76E+2	1.81E+2	1.54E+2	1.40E+1	1.19E+3
26-FE-58	Stable	6.45E+1	4.52E+1	5.49E+2	4.45E+1	2.73E+2	2.37E+2	1.54E+1	1.23E+3
27-CO-59	Stable	2.12E+3	3.12E+3	4.52E+4	5.36E+2	2.36E+2	3.89E+2	2.83E+1	5.16E+4
28-NI-58	Stable	2.56E+2	1.78E+2	9.01E+1	1.03E+2	5.50E+2	4.43E+2	3.60E+1	1.66E+3

Nuclide	1/e Life Time (Years)	Capture Event Rate per gram per 3 x 10^{13} protons (continued) Energy bins in eV							
		1 to 10	10 to 10^2	10^2 to 10^3	10^3 to 10^4	10^4 to 10^5	10^5 to 10^6	10^6 to 10^7	Total
28-NI-60	Stable	1.47E+2	9.66E+1	4.58E+1	5.09E+2	5.29E+2	3.34E+2	2.20E+1	1.68E+3
28-NI-61	Stable	1.32E+2	9.12E+1	4.51E+1	5.68E+2	1.01E+3	4.57E+2	1.87E+1	2.32E+3
28-NI-62	Stable	7.06E+2	3.52E+2	1.12E+2	3.58E+2	6.76E+2	4.77E+2	3.38E+1	2.71E+3
28-NI-64	Stable	7.65E+1	5.37E+1	2.94E+1	3.75E+1	3.12E+2	2.57E+2	2.83E+1	7.95E+2
29-CU-63	Stable	2.25E+2	1.36E+2	3.41E+3	2.23E+3	8.33E+2	7.30E+2	5.62E+1	7.62E+3
29-CU-65	Stable	1.06E+2	7.13E+1	8.17E+2	5.46E+2	5.08E+2	4.02E+2	4.00E+1	2.49E+3
30-ZN-64	Stable	3.86E+1	2.74E+1	4.40E+2	7.88E+2	6.99E+2	1.28E+3	1.09E+2	3.39E+3
30-ZN-66	Stable	4.16E+1	2.85E+1	4.91E+2	4.64E+1	2.66E+2	4.62E+2	3.64E+1	1.37E+3
30-ZN-67	Stable	3.30E+2	2.57E+2	1.63E+4	3.30E+3	1.54E+3	1.23E+3	8.08E+1	2.30E+4
30-ZN-68	Stable	4.72E+1	3.21E+1	1.63E+3	1.32E+2	3.03E+2	2.35E+2	1.83E+1	2.40E+3
30-ZN-70	Stable	4.19E+0	2.77E+0	9.98E-1	2.83E-1	1.19E+2	1.09E+2	5.98E+0	2.41E+2
31-GA-69	Stable	1.03E+2	1.15E+2	1.34E+4	2.03E+3	1.32E+3	1.26E+3	7.38E+1	1.83E+4
31-GA-71	Stable	1.74E+2	1.39E+4	7.35E+3	2.24E+3	1.08E+3	9.76E+2	4.36E+1	2.58E+4
32-GE-70	Stable	1.32E+2	7.83E+1	2.15E+1	8.67E+2	9.43E+2	1.46E+3	1.60E+2	3.67E+3
32-GE-72	Stable	3.59E+1	2.28E+1	7.37E+1	1.89E+2	4.25E+2	1.31E+3	1.05E+2	2.16E+3
32-GE-73	Stable	6.50E+2	2.98E+3	3.16E+4	2.94E+3	2.18E+3	1.27E+3	3.38E+1	4.16E+4
32-GE-74	Stable	1.83E+1	1.25E+1	5.58E+0	1.63E+2	1.02E+2	4.51E+2	2.35E+1	7.77E+2
32-GE-76	Stable	6.39E+0	4.51E+0	2.77E+3	2.43E+1	6.95E+1	2.08E+2	9.99E+0	3.09E+3
33-AS-75	Stable	2.06E+2	2.11E+4	1.38E+4	7.88E+3	4.55E+3	2.89E+3	8.63E+1	5.05E+4
34-SE-74	Stable	2.92E+3	2.43E+5	1.16E+4	2.61E+3	2.16E+3	2.40E+3	1.66E+2	2.64E+5
34-SE-76	Stable	3.53E+3	2.05E+3	2.85E+3	1.50E+3	9.82E+2	1.13E+3	7.10E+1	1.21E+4
34-SE-77	Stable	1.46E+3	4.31E+2	9.92E+3	6.40E+3	4.46E+3	2.65E+3	5.65E+1	2.54E+4
34-SE-78	Stable	1.78E+1	1.28E+1	3.04E+3	5.63E+2	9.17E+2	1.15E+3	8.15E+1	5.79E+3
34-SE-80	Stable	2.46E+1	1.73E+1	1.12E+1	9.51E+2	3.43E+2	4.51E+2	3.04E+1	1.83E+3
35-BR-79	Stable	4.59E+2	4.15E+4	1.72E+4	1.20E+4	6.58E+3	4.38E+3	1.37E+2	8.22E+4
35-BR-81	Stable	1.10E+2	7.77E+2	2.46E+4	2.76E+3	2.31E+3	1.65E+3	6.12E+1	3.23E+4
36-KR-78	Stable	2.45E+2	1.75E+2	1.24E+4	3.99E+3	3.78E+3	3.86E+3	2.93E+2	2.48E+4
36-KR-80	Stable	4.54E+2	7.83E+2	2.97E+4	3.15E+3	2.86E+3	3.25E+3	3.61E+2	4.06E+4
36-KR-82	Stable	1.18E+3	9.72E+4	7.24E+2	1.32E+3	9.62E+2	1.27E+3	1.25E+2	1.03E+5
36-KR-83	Stable	2.62E+3	4.07E+4	5.23E+3	4.06E+3	2.50E+3	1.61E+3	8.37E+1	5.68E+4
36-KR-84	Stable	3.22E+0	2.51E+0	1.81E+3	2.88E+2	3.18E+2	3.44E+2	2.56E+1	2.79E+3
36-KR-86	Stable	1.12E-1	7.84E-2	4.19E-2	2.97E-1	1.96E+1	3.69E+1	8.55E+0	6.56E+1
37-RB-85	Stable	1.83E+1	1.36E+1	2.20E+3	3.72E+3	2.63E+3	1.78E+3	8.14E+1	1.04E+4

Nuclide	1/e Life Time (Years)	Capture Event Rate per gram per 3 x 10^{13} protons (continued) Energy bins in eV							
		1 to 10	10 to 10^2	10^2 to 10^3	10^3 to 10^4	10^4 to 10^5	10^5 to 10^6	10^6 to 10^7	Total
38-SR-84	Stable	3.16E+1	2.49E+1	6.07E+3	1.76E+3	2.12E+3	2.89E+3	2.63E+2	1.32E+4
38-SR-86	Stable	3.96E+1	3.10E+1	2.71E+3	8.45E+2	5.42E+2	8.86E+2	1.06E+2	5.16E+3
38-SR-87	Stable	2.05E+4	9.54E+1	1.78E+2	8.53E+2	7.56E+2	5.15E+2	4.56E+1	2.30E+4
38-SR-88	Stable	2.12E-1	1.49E-1	8.43E-2	2.66E+2	3.74E+1	5.00E+1	1.15E+1	3.65E+2
39-Y-89	Stable	4.67E+1	3.26E+1	1.72E+1	2.58E+2	1.84E+2	1.77E+2	1.84E+1	7.33E+2
40-ZR-90	Stable	4.00E-1	2.81E-1	1.64E-1	6.69E+1	1.40E+2	2.14E+2	3.88E+1	4.61E+2
40-ZR-91	Stable	4.41E+1	2.98E+1	3.27E+3	9.68E+2	4.22E+2	4.19E+2	5.31E+1	5.21E+3
40-ZR-92	Stable	7.27E+0	3.91E+0	1.53E+0	1.19E+3	1.81E+2	7.49E+2	7.41E+1	2.20E+3
40-ZR-94	Stable	1.70E+0	1.14E+0	4.70E-1	1.79E+2	1.81E+2	4.81E+2	4.56E+1	8.90E+2
40-ZR-96	Stable	8.34E-1	1.21E+0	2.59E+3	5.48E+1	5.49E+1	1.71E+2	3.76E+1	2.91E+3
41-NB-93	Stable	4.50E+1	1.82E+2	2.93E+3	4.31E+3	2.22E+3	1.61E+3	7.50E+1	1.14E+4
42-MO-100	Stable	6.32E+0	5.63E+1	6.77E+2	1.12E+3	7.35E+2	9.12E+2	6.84E+1	3.57E+3
42-MO-92	Stable	7.31E-1	5.44E-1	3.65E+2	3.52E+2	4.61E+2	7.39E+2	1.37E+2	2.05E+3
42-MO-94	Stable	4.52E-1	4.11E-1	3.90E+1	1.45E+3	7.21E+2	1.27E+3	1.34E+2	3.62E+3
42-MO-95	Stable	4.36E+2	4.10E+4	2.83E+3	4.18E+3	3.20E+3	2.35E+3	1.38E+2	5.41E+4
42-MO-96	Stable	2.12E+1	3.57E+1	9.21E+3	1.03E+3	7.49E+2	1.09E+3	9.91E+1	1.22E+4
42-MO-97	Stable	5.36E+1	2.97E+3	1.87E+3	4.24E+3	3.15E+3	2.46E+3	1.12E+2	1.48E+4
42-MO-98	Stable	7.74E+0	4.28E+2	1.97E+3	1.53E+3	4.71E+2	1.08E+3	9.34E+1	5.58E+3
44-RU-100	Stable	1.56E+2	8.41E+1	3.55E+3	2.82E+3	1.52E+3	1.89E+3	2.08E+2	1.02E+4
44-RU-101	Stable	1.77E+2	2.27E+4	1.32E+4	6.45E+3	7.02E+3	5.20E+3	1.89E+2	5.49E+4
44-RU-102	Stable	1.21E+2	1.31E+2	6.04E+1	3.14E+3	1.30E+3	1.61E+3	1.35E+2	6.50E+3
44-RU-104	Stable	9.98E+0	2.21E+2	5.93E+2	2.33E+3	1.48E+3	1.25E+3	9.91E+1	5.98E+3
44-RU-96	Stable	9.75E+0	6.81E+0	2.53E+3	2.50E+3	2.15E+3	2.74E+3	3.90E+2	1.03E+4
44-RU-98	Stable	2.64E+2	1.84E+2	3.07E+3	2.25E+3	1.88E+3	2.34E+3	2.97E+2	1.03E+4
44-RU-99	Stable	9.37E+3	2.71E+4	1.30E+4	5.82E+3	5.64E+3	3.79E+3	1.89E+2	6.49E+4
45-RH-103	Stable	1.00E+5	7.39E+2	1.17E+4	5.86E+3	6.59E+3	5.27E+3	2.23E+2	1.31E+5
46-PD-102	Stable	6.57E+1	1.52E+1	1.01E+4	3.25E+3	2.90E+3	3.67E+3	4.14E+2	2.04E+4
46-PD-104	Stable	1.01E+1	1.10E+1	6.43E+3	1.70E+3	1.46E+3	1.71E+3	1.62E+2	1.15E+4
46-PD-105	Stable	5.56E+2	1.75E+4	1.26E+4	1.01E+4	8.74E+3	7.61E+3	2.43E+2	5.73E+4
46-PD-106	Stable	8.39E+0	4.57E+0	1.54E+3	1.64E+3	1.58E+3	1.90E+3	1.91E+2	6.86E+3
46-PD-108	Stable	1.60E+3	8.16E+4	2.41E+3	1.39E+3	1.74E+3	2.05E+3	1.66E+2	9.10E+4
46-PD-110	Stable	5.02E+0	1.28E+2	1.88E+2	1.03E+3	1.07E+3	1.22E+3	7.70E+1	3.71E+3
47-AG-107	Stable	7.94E+2	2.42E+4	6.43E+3	4.58E+3	6.07E+3	5.12E+3	3.09E+2	4.75E+4

Nuclide	1/e Life Time (Years)	Capture Event Rate per gram per 3 x 10^{13} protons (continued) Energy bins in eV							
		1 to 10	10 to 10^2	10^2 to 10^3	10^3 to 10^4	10^4 to 10^5	10^5 to 10^6	10^6 to 10^7	Total
47-AG-109	Stable	2.25E+5	2.30E+4	8.08E+3	6.51E+3	6.07E+3	4.80E+3	2.55E+2	2.74E+5
48-CD-106	Stable	2.76E+1	1.29E+1	1.41E+3	4.85E+3	4.15E+3	4.69E+3	6.38E+2	1.58E+4
48-CD-108	Stable	3.28E+1	1.86E+2	7.84E+3	3.66E+3	3.02E+3	3.40E+3	4.72E+2	1.86E+4
48-CD-110	Stable	2.47E+2	9.07E+3	7.70E+2	1.75E+3	1.63E+3	2.21E+3	2.62E+2	1.59E+4
48-CD-111	Stable	3.10E+2	7.65E+3	7.69E+3	5.19E+3	7.28E+3	7.32E+3	4.35E+2	3.59E+4
48-CD-112	Stable	6.02E+1	2.86E+3	5.61E+2	1.96E+3	1.45E+3	1.97E+3	2.12E+2	9.07E+3
48-CD-114	Stable	9.93E+0	5.02E+1	7.81E+3	1.21E+3	9.94E+2	1.35E+3	1.24E+2	1.16E+4
48-CD-116	Stable	2.08E+0	7.91E+1	5.99E+2	1.88E+2	6.07E+2	8.20E+2	6.50E+1	2.36E+3
49-IN-113	Stable	1.90E+4	3.58E+4	4.82E+3	7.19E+3	6.27E+3	6.75E+3	7.21E+2	8.06E+4
50-SN-112	Stable	2.65E+1	1.07E+4	2.13E+3	1.35E+3	1.34E+3	1.96E+3	4.45E+2	1.79E+4
50-SN-114	Stable	3.63E+0	3.28E+0	1.53E+3	1.52E+3	1.03E+3	1.55E+3	3.65E+2	6.00E+3
50-SN-115	Stable	4.90E+2	5.39E+1	1.04E+3	3.20E+3	2.63E+3	2.95E+3	2.33E+2	1.06E+4
50-SN-116	Stable	3.78E+0	1.09E+1	6.09E+3	1.09E+3	6.93E+2	1.06E+3	2.28E+2	9.18E+3
50-SN-117	Stable	8.93E+1	2.74E+3	3.09E+3	1.74E+3	2.06E+3	1.75E+3	1.64E+2	1.16E+4
50-SN-118	Stable	5.78E+0	4.35E+2	6.66E+2	5.07E+2	4.19E+2	6.55E+2	1.26E+2	2.81E+3
50-SN-119	Stable	6.71E+1	9.33E+0	4.94E+2	2.01E+3	1.50E+3	1.10E+3	9.68E+1	5.28E+3
50-SN-120	Stable	3.70E+0	1.59E+1	2.30E+2	4.20E+2	1.25E+2	3.87E+2	6.78E+1	1.25E+3
50-SN-122	Stable	3.03E+0	9.97E-1	2.56E+2	1.33E+2	1.21E+2	2.46E+2	3.69E+1	7.97E+2
50-SN-124	Stable	3.03E+0	2.37E+3	1.71E+1	4.10E+1	8.02E+1	1.40E+2	2.30E+1	2.68E+3
51-SB-121	Stable	1.88E+4	1.88E+4	7.21E+3	4.07E+3	3.40E+3	2.42E+3	2.54E+2	5.49E+4
51-SB-123	Stable	1.32E+2	2.76E+4	3.90E+3	2.53E+3	2.00E+3	1.68E+3	1.99E+2	3.80E+4
52-TE-120	Stable	6.29E+1	2.01E+3	5.60E+3	2.17E+3	1.84E+3	2.71E+3	3.14E+2	1.47E+4
52-TE-122	Stable	9.88E+1	2.39E+4	3.48E+3	1.19E+3	1.57E+3	2.49E+3	3.28E+2	3.31E+4
52-TE-124	Stable	1.14E+2	1.62E+1	1.28E+3	1.58E+3	9.83E+2	1.35E+3	1.66E+2	5.49E+3
52-TE-125	Stable	3.39E+1	8.36E+2	6.18E+3	2.91E+3	2.67E+3	2.10E+3	1.30E+2	1.49E+4
52-TE-126	Stable	2.27E+1	9.71E+0	4.64E+3	3.63E+2	6.95E+2	7.94E+2	9.74E+1	6.62E+3
52-TE-128	Stable	5.43E+0	3.81E+0	1.21E+3	2.49E+1	2.70E+2	2.63E+2	2.57E+1	1.80E+3
53-I-127	Stable	1.63E+2	3.26E+4	1.13E+4	4.76E+3	4.06E+3	2.81E+3	1.68E+2	5.58E+4
54-XE-124	Stable	4.41E+5	3.30E+4	1.09E+4	8.06E+3	6.92E+3	1.10E+4	1.82E+3	5.13E+5
54-XE-126	Stable	5.48E+1	8.01E+3	8.06E+3	2.07E+3	1.65E+3	2.03E+3	2.03E+2	2.21E+4
54-XE-128	Stable	8.21E+1	1.47E+1	4.58E+3	1.26E+3	1.16E+3	1.54E+3	1.32E+2	8.77E+3
54-XE-129	Stable	3.52E+4	4.88E+3	8.20E+3	3.69E+3	2.92E+3	2.10E+3	1.92E+2	5.72E+4
54-XE-130	Stable	6.34E+2	3.84E+2	5.91E+2	2.52E+3	1.61E+3	2.43E+3	3.00E+2	8.47E+3

Nuclide	1/e Life Time (Years)	Capture Event Rate per gram per 3 x 10^{13} protons (continued) Energy bins in eV							
		1 to 10	10 to 10^2	10^2 to 10^3	10^3 to 10^4	10^4 to 10^5	10^5 to 10^6	10^6 to 10^7	Total
54-XE-131	Stable	4.25E+3	1.75E+5	4.18E+3	3.26E+3	2.13E+3	1.69E+3	8.93E+1	1.90E+5
54-XE-132	Stable	1.11E+1	8.24E+0	1.31E+3	1.73E+2	2.69E+2	4.02E+2	3.56E+1	2.21E+3
54-XE-134	Stable	5.96E+0	2.68E+0	2.01E+0	1.35E+3	1.35E+2	2.26E+2	2.64E+1	1.75E+3
54-XE-136	Stable	6.12E+0	3.97E+0	1.24E+0	9.40E-1	7.56E+0	5.82E+0	2.16E+0	2.78E+1
55-CS-133	Stable	4.43E+4	1.13E+4	9.31E+3	4.20E+3	2.97E+3	2.31E+3	9.56E+1	7.45E+4
56-BA-130	Stable	2.88E+2	4.06E+4	1.12E+4	4.00E+3	4.23E+3	7.46E+3	1.66E+3	6.94E+4
56-BA-132	Stable	1.71E+2	2.13E+3	6.74E+3	2.99E+3	2.58E+3	4.40E+3	8.60E+2	1.99E+4
56-BA-134	Stable	4.68E+1	1.75E+2	5.75E+3	8.92E+2	1.31E+3	2.30E+3	4.27E+2	1.09E+4
56-BA-135	Stable	1.49E+2	2.95E+4	5.94E+3	5.73E+3	2.75E+3	2.94E+3	2.56E+2	4.72E+4
56-BA-136	Stable	9.27E+0	5.44E+0	6.39E+1	2.22E+2	3.28E+2	6.74E+2	1.16E+2	1.42E+3
56-BA-137	Stable	9.50E+1	2.23E+1	6.70E+2	5.13E+2	3.53E+2	3.79E+2	4.07E+1	2.07E+3
56-BA-138	Stable	8.39E+0	5.80E+0	3.12E+0	3.86E+0	4.77E+1	3.73E+1	1.10E+1	1.17E+2
57-LA-139	Stable	1.96E+2	3.26E+3	9.09E+1	3.41E+2	1.93E+2	1.75E+2	2.15E+1	4.28E+3
58-CE-136	Stable	1.31E+2	3.61E+3	9.82E+3	3.70E+3	2.95E+3	3.47E+3	2.41E+2	2.39E+4
58-CE-138	Stable	2.60E+1	1.82E+1	6.55E+2	7.91E+2	5.84E+2	6.86E+2	4.91E+1	2.81E+3
58-CE-140	Stable	1.18E+1	4.40E+0	3.03E-1	9.80E+0	2.25E+1	7.33E+1	2.18E+1	1.44E+2
58-CE-142	Stable	2.27E+1	1.52E+1	1.17E+1	1.70E+2	1.15E+2	1.66E+2	1.99E+1	5.21E+2
59-PR-141	Stable	2.17E+2	3.08E+2	4.89E+3	7.99E+2	6.75E+2	4.70E+2	5.36E+1	7.41E+3
60-ND-142	Stable	4.21E+2	2.77E+2	1.64E+2	1.83E+2	2.86E+2	6.22E+2	1.91E+2	2.15E+3
60-ND-143	Stable	3.37E+3	5.15E+3	1.40E+4	2.27E+3	1.51E+3	1.63E+3	2.07E+2	2.82E+4
60-ND-145	Stable	1.25E+4	1.52E+4	1.12E+4	4.15E+3	2.74E+3	2.56E+3	1.59E+2	4.86E+4
60-ND-146	Stable	2.99E+1	1.67E+1	1.17E+2	3.44E+2	6.31E+2	1.01E+3	9.33E+1	2.25E+3
60-ND-148	Stable	5.55E+1	8.39E+1	4.10E+3	6.71E+2	6.26E+2	8.69E+2	6.13E+1	6.46E+3
60-ND-150	Stable	1.78E+1	2.20E+3	7.49E+2	1.12E+3	8.39E+2	7.24E+2	6.65E+1	5.72E+3
62-SM-144	Stable	3.45E+1	1.59E+1	2.93E+0	7.18E+2	4.67E+2	8.67E+2	2.88E+2	2.39E+3
62-SM-149	Stable	8.55E+4	1.23E+5	3.92E+4	1.91E+4	9.00E+3	8.75E+3	3.83E+2	2.85E+5
62-SM-150	Stable	9.30E+2	5.91E+4	7.43E+3	2.88E+3	2.07E+3	3.18E+3	2.85E+2	7.58E+4
62-SM-152	Stable	3.75E+5	1.06E+4	9.92E+3	2.58E+3	2.38E+3	2.53E+3	2.32E+2	4.03E+5
62-SM-154	Stable	1.49E+2	6.55E+3	8.06E+2	1.46E+3	1.27E+3	9.77E+2	1.10E+2	1.13E+4
63-EU-151	Stable	1.13E+5	1.03E+5	6.80E+4	3.54E+4	2.20E+4	1.59E+4	9.19E+2	3.58E+5
63-EU-153	Stable	9.13E+4	7.08E+4	4.00E+4	1.97E+4	1.25E+4	9.41E+3	4.83E+2	2.44E+5
64-GD-154	Stable	5.96E+2	2.37E+4	2.76E+4	5.39E+3	4.14E+3	5.70E+3	6.63E+2	6.78E+4
64-GD-155	Stable	9.71E+4	6.54E+4	3.17E+4	1.94E+4	1.39E+4	9.07E+3	3.40E+2	2.37E+5

Nuclide	1/e Life Time (Years)	Capture Event Rate per gram per 3 x 10^{13} protons (continued) Energy bins in eV							
		1 to 10	10 to 10^2	10^2 to 10^3	10^3 to 10^4	10^4 to 10^5	10^5 to 10^6	10^6 to 10^7	Total
64-GD-156	Stable	5.12E+1	1.67E+4	1.58E+4	4.30E+3	2.91E+3	3.31E+3	4.27E+2	4.36E+4
64-GD-157	Stable	1.43E+4	5.41E+4	3.37E+4	9.99E+3	6.12E+3	3.99E+3	1.90E+2	1.22E+5
64-GD-158	Stable	5.95E+1	9.34E+3	3.23E+3	1.09E+3	1.49E+3	1.29E+3	1.31E+2	1.66E+4
64-GD-160	Stable	1.53E+1	1.11E+1	1.62E+3	6.47E+2	7.08E+2	9.58E+2	1.36E+2	4.09E+3
65-TB-159	Stable	1.13E+4	4.77E+4	2.24E+4	1.30E+4	9.99E+3	7.01E+3	2.96E+2	1.12E+5
66-DY-156	Stable	5.05E+4	7.80E+4	2.07E+4	9.38E+3	7.35E+3	1.01E+4	9.78E+2	1.77E+5
66-DY-158	Stable	2.21E+2	4.14E+4	1.34E+4	5.47E+3	4.33E+3	5.17E+3	5.88E+2	7.05E+4
66-DY-160	Stable	3.88E+4	1.90E+5	4.13E+4	1.53E+4	7.14E+3	1.08E+4	2.01E+3	3.06E+5
66-DY-161	Stable	5.96E+4	7.36E+4	5.21E+4	2.11E+4	9.23E+3	5.06E+3	1.54E+2	2.21E+5
66-DY-162	Stable	2.93E+5	3.03E+4	8.60E+3	6.52E+3	3.22E+3	4.77E+3	7.28E+2	3.47E+5
66-DY-163	Stable	8.68E+4	4.07E+4	2.06E+4	8.98E+3	3.75E+3	2.56E+3	1.43E+2	1.64E+5
66-DY-164	Stable	9.44E+3	2.87E+2	8.20E+3	1.41E+3	1.05E+3	2.17E+3	2.30E+2	2.28E+4
67-HO-165	Stable	3.88E+4	5.11E+4	3.00E+4	1.37E+4	5.98E+3	5.19E+3	2.31E+2	1.45E+5
68-ER-162	Stable	1.13E+4	7.25E+4	2.84E+4	1.12E+4	7.35E+3	1.07E+4	1.39E+3	1.43E+5
68-ER-164	Stable	5.81E+3	6.66E+3	2.03E+4	5.01E+3	4.14E+3	4.41E+3	5.01E+2	4.68E+4
68-ER-166	Stable	3.65E+2	1.58E+4	7.36E+3	3.86E+3	3.02E+3	2.99E+3	3.47E+2	3.37E+4
68-ER-167	Stable	1.18E+5	5.81E+4	2.26E+4	1.02E+4	6.75E+3	4.63E+3	1.51E+2	2.21E+5
68-ER-168	Stable	1.48E+2	6.35E+3	6.35E+3	1.67E+3	1.53E+3	1.23E+3	1.31E+2	1.74E+4
68-ER-170	Stable	1.83E+2	1.15E+4	3.18E+3	1.31E+3	1.25E+3	7.97E+2	7.81E+1	1.83E+4
69-TM-169	Stable	1.45E+5	2.30E+4	1.91E+4	1.20E+4	5.07E+3	3.71E+3	2.25E+2	2.08E+5
70-YB-168	Stable	1.24E+4	2.03E+4	7.95E+3	5.27E+3	4.27E+3	4.16E+3	4.76E+2	5.48E+4
70-YB-170	Stable	1.19E+4	4.64E+4	7.79E+3	3.93E+3	3.29E+3	4.69E+3	4.24E+2	7.84E+4
70-YB-171	Stable	1.42E+4	2.49E+4	1.50E+4	6.80E+3	6.18E+3	3.62E+3	2.93E+2	7.11E+4
70-YB-172	Stable	1.54E+1	1.52E+1	1.40E+4	1.57E+3	1.80E+3	1.34E+3	1.64E+2	1.89E+4
70-YB-173	Stable	2.44E+3	6.15E+4	1.13E+4	6.84E+3	3.79E+3	2.46E+3	1.12E+2	8.85E+4
70-YB-174	Stable	9.95E+2	2.20E+2	1.56E+3	1.50E+3	7.70E+2	4.66E+2	6.64E+1	5.58E+3
70-YB-176	Stable	5.02E+1	3.31E+1	1.57E+3	5.28E+2	4.85E+2	2.64E+2	3.49E+1	2.97E+3
71-LU-175	Stable	2.05E+4	6.36E+4	1.72E+4	7.25E+3	6.32E+3	3.28E+3	8.44E+1	1.18E+5
72-HF-176	Stable	5.94E+4	1.75E+4	7.92E+3	4.12E+3	3.43E+3	4.58E+3	7.95E+2	9.78E+4
72-HF-177	Stable	4.92E+5	4.25E+4	1.88E+4	1.27E+4	8.60E+3	9.52E+3	6.55E+2	5.84E+5
72-HF-178	Stable	2.25E+5	9.66E+2	4.98E+3	2.62E+3	1.29E+3	1.21E+3	1.85E+2	2.36E+5
72-HF-179	Stable	3.22E+4	3.09E+4	2.01E+4	6.55E+3	4.18E+3	3.49E+3	2.25E+2	9.77E+4
72-HF-180	Stable	1.43E+2	6.98E+3	3.53E+3	5.56E+2	7.09E+2	5.70E+2	8.35E+1	1.26E+4

Nuclide	1/e Life Time (Years)	Capture Event Rate per gram per 3×10^{13} protons (continued) Energy bins in eV							
		1 to 10	10 to 10^2	10^2 to 10^3	10^3 to 10^4	10^4 to 10^5	10^5 to 10^6	10^6 to 10^7	Total
73-TA-180*	Stable	3.90E+3	7.77E+1	2.75E+1	1.09E+1	7.73E+0	8.97E+0	5.42E-1	4.03E+3
73-TA-181	Stable	3.60E+4	3.57E+4	1.62E+4	6.68E+3	3.07E+3	2.37E+3	1.57E+2	1.00E+5
74-W-180	Stable	4.23E+2	4.15E+4	9.39E+3	3.39E+3	2.87E+3	2.36E+3	2.53E+2	6.02E+4
74-W-182	Stable	3.31E+4	3.84E+4	1.10E+4	1.93E+3	1.08E+3	1.18E+3	1.62E+2	8.69E+4
74-W-183	Stable	1.02E+4	3.39E+4	1.24E+4	2.94E+3	1.87E+3	1.35E+3	8.51E+1	6.27E+4
74-W-184	Stable	3.00E+1	2.65E+1	2.95E+3	2.54E+3	7.85E+2	8.15E+2	7.74E+1	7.22E+3
74-W-186	Stable	9.18E+2	5.05E+4	4.61E+3	8.20E+2	7.02E+2	7.82E+2	6.69E+1	5.84E+4
75-RE-185	Stable	1.07E+5	3.18E+4	1.69E+4	7.01E+3	4.25E+3	4.72E+3	3.14E+2	1.72E+5
76-OS-184	Stable	5.24E+4	3.11E+4	8.01E+3	2.88E+3	2.46E+3	2.01E+3	2.27E+2	9.91E+4
76-OS-187	Stable	8.25E+3	4.65E+4	3.65E+4	6.61E+3	3.60E+3	1.55E+3	1.55E+2	1.03E+5
76-OS-188	Stable	9.15E+1	1.66E+4	1.77E+4	1.98E+3	1.65E+3	1.86E+3	2.44E+2	4.00E+4
76-OS-189	Stable	4.73E+4	5.62E+4	3.08E+4	1.17E+4	6.02E+3	3.63E+3	1.86E+2	1.56E+5
76-OS-190	Stable	1.31E+2	7.31E+2	7.10E+2	1.17E+3	1.69E+3	1.94E+3	1.78E+2	6.55E+3
76-OS-192	Stable	3.12E+1	5.46E+1	9.56E+2	5.56E+2	4.58E+2	4.11E+2	2.85E+1	2.50E+3
77-IR-191	Stable	8.66E+4	3.73E+4	2.28E+4	8.25E+3	5.41E+3	3.47E+3	2.95E+2	1.64E+5
77-IR-193	Stable	7.15E+4	3.00E+4	1.32E+4	5.56E+3	3.51E+3	2.42E+3	1.62E+2	1.26E+5
78-PT-192	Stable	1.67E+2	3.05E+4	1.03E+4	4.24E+3	2.83E+3	5.14E+3	4.61E+2	5.37E+4
78-PT-194	Stable	2.33E+1	1.36E+1	1.51E+3	1.68E+3	1.30E+3	1.17E+3	4.65E+1	5.75E+3
78-PT-195	Stable	7.19E+2	3.53E+4	1.07E+4	5.95E+3	4.26E+3	1.36E+3	8.62E+1	5.83E+4
78-PT-196	Stable	1.15E+1	7.20E+1	1.62E+2	6.92E+2	7.17E+2	5.91E+2	2.61E+1	2.27E+3
78-PT-198	Stable	6.02E+1	1.04E+4	1.03E+3	3.76E+2	2.48E+2	1.94E+2	9.69E+0	1.23E+4
79-AU-197	Stable	1.31E+5	9.96E+3	1.01E+4	3.61E+3	2.25E+3	2.13E+3	1.15E+2	1.59E+5
80-HG-196	Stable	9.66E+3	1.10E+4	5.12E+3	3.24E+3	2.66E+3	2.89E+3	2.15E+2	3.48E+4
80-HG-198	Stable	4.39E+1	1.01E+4	2.86E+3	9.02E+2	7.02E+2	6.70E+2	3.64E+1	1.53E+4
80-HG-199	Stable	7.45E+3	2.09E+4	1.02E+4	2.11E+3	1.50E+3	7.59E+2	3.25E+1	4.30E+4
80-HG-200	Stable	2.31E+1	1.53E+1	8.23E+0	7.95E+2	4.57E+2	3.79E+2	1.81E+1	1.70E+3
80-HG-201	Stable	1.15E+2	2.01E+3	4.65E+3	9.38E+2	4.69E+2	2.08E+2	2.08E+1	8.41E+3
80-HG-202	Stable	7.71E+1	4.49E+1	9.48E+0	3.48E+2	2.92E+2	2.57E+2	1.41E+1	1.04E+3
80-HG-204	Stable	6.77E+0	4.73E+0	2.50E+0	1.72E+0	1.34E+2	1.54E+2	1.07E+1	3.15E+2
81-TL-203	Stable	1.86E+2	1.88E+2	8.58E+3	1.46E+3	3.86E+2	4.26E+2	2.43E+1	1.13E+4
81-TL-205	Stable	1.64E+0	1.07E+1	6.71E-1	3.75E+2	8.44E+1	1.34E+2	6.98E+0	6.13E+2
82-PB-204	Stable	1.06E+1	7.33E+0	3.94E+0	1.27E+3	8.91E+1	2.00E+1	3.67E+0	1.40E+3
82-PB-206	Stable	4.63E-1	3.11E-1	1.26E-1	3.90E+0	9.24E+1	9.85E+1	8.73E+0	2.04E+2

Nuclide	1/e Life Time (Years)	Capture Event Rate per gram per 3 x 10^{13} protons (continued) Energy bins in eV							
		1 to 10	10 to 10^2	10^2 to 10^3	10^3 to 10^4	10^4 to 10^5	10^5 to 10^6	10^6 to 10^7	Total
82-PB-207	Stable	1.11E+1	7.74E+0	4.08E+0	3.20E+0	2.07E+1	6.06E+1	1.04E+1	1.18E+2
82-PB-208	Stable	7.64E-3	5.35E-3	2.93E-3	2.84E-3	1.88E+0	1.19E+1	1.05E+0	1.48E+1
83-BI-209	Stable	5.25E-1	3.89E-1	3.49E+1	1.72E+1	4.72E+0	3.85E+1	5.16E+0	1.01E+2